Mechanical behaviour of masonry assemblages built with mortar containing anti-freeze admixtures subject to sub-freezing curing temperatures

A Thesis Submitted to the College of

Graduate and Postdoctoral Studies

In Partial Fulfilment of the Requirements

For the Degree of

Master of Science

In the Department of Civil, Geological and Environmental Engineering

University of Saskatchewan

Saskatoon

By

JAWDAT ALFARRA

PERMISSION TO USE

In presenting this thesis in partial fulfilment of the requirements for a Postgraduate degree from the University of Saskatchewan, I agree that the Libraries of this University may make it freely available for inspection. I further agree that permission for copying of this thesis/dissertation in any manner, in whole or in part, for scholarly purposes may be granted by the professor or professors who supervised my thesis/dissertation work or, in their absence, by the Head of the Department or the Dean of the College in which my thesis/dissertation work was done. It is understood that any copying or publication or use of this thesis/dissertation or parts thereof for financial gain shall not be allowed without my written permission. It is also understood that due recognition shall be given to me and to the University of Saskatchewan in any scholarly use which may be made of any material in my thesis/dissertation.

Requests for permission to copy or to make other use of material in this thesis/dissertation in whole or part should be addressed to:

Head of the Department of Civil, Geological and Environmental Engineering

University of Saskatchewan

Engineering Building, 57 Campus Drive

Saskatoon, Saskatchewan S7N 5A9 Canada

OR

Dean

College of Graduate and Postdoctoral Studies

University of Saskatchewan

116 Thorvaldson Building, 110 Science Place

Saskatoon, Saskatchewan S7N 5C9 Canada

ABSTRACT

Cold weather masonry construction is a major concern for contractors in North America as well as other geographic locations. When exposed to cold conditions during construction and curing, the performance of masonry assemblies may be affected. Because of the vulnerability of mortar joints to considerable delay in setting time and low strength development rate in cold temperatures, the construction industry has been forced to follow extraordinary building methods. These methods focused primarily on protecting the freshly mixed and placed mortar from freezing for a suitable curing time. This can lead to loss of productivity rate and postponements in construction plans with related additional costs.

This research evaluates the performance of mortars that contain nanocellulose and sodium nitrite and as a cold-weather admixture in masonry assemblages under sub-freezing curing temperatures. The effect of sodium nitrite with a dosage of 12% by mass of mixing water and nanocellulose with a dosage of 0.3% by mass of cement on Type S masonry mortars cured at -10°C and room temperatures was investigated. Flowability, air content, and setting time of fresh mixtures were determined. Moreover, for the hardened mortar state, the 28-day compressive strength of mortar cubes and the air content of mortar cylinders were determined. For the purpose of this study, two types of experiments were performed on masonry prisms constructed with four different kinds of mortars and cured under both sub-freezing and room temperatures. The first test was the compressive test to assess the design compressive strength and failure behaviour of the assemblies. A total of 72 prisms of six hollow concrete bricks stacked vertically with full bedding were built and tested in eight separate sets of nine prisms each. The second test was the flexural bond strength test using the bond wrench method described in CSA A3004-C9. For this test, 40 prisms were built, each one six units in height with five mortar joints for a total of 200 joints. These were divided into eight groups based on the kind of mortar used and the curing temperature.

Test results indicated that the addition of sodium nitrite and cellulose nanocrystals affected the properties of the fresh and hardened mortar mixtures. The admixtures generally increased the flowability, reduced the air content, and sped up the hydration of cement. The mechanical property tests on masonry prisms showed that the compressive and flexural bond strengths of

the prisms were affected considerably by the addition of these admixtures when cured at room temperature. At room temperature, the incorporation of nanocellulose in the mortar resulted in an increase in the compressive strength of the brick prisms by 15% compared to the control sample, while the use of sodium nitrite in the mortar resulted in an 11% increase in the compressive strength compared to the control prisms. For the flexural bond strength, the average results for prisms cured at room temperature indicate that the addition of sodium nitrite lowered the flexural bond strength by 14%, while incorporating nanocellulose separately or in combination with sodium nitrite improved the flexural bond strength by 13% and 14%, respectively. However, at -10°C, only samples with sodium nitrite reached acceptable compressive and flexural bond strengths (21.2 MPa and 0.404 MPa, respectively), as defined by the relevant Canadian standards.

Generally, test results showed that sodium nitrite can be used successfully to minimize the adverse effects of freezing temperatures as low as -10°C on strength development of Type S mortar joints by lowering the freezing point of the mixing water, which opens a new approach in mitigating the problems associated with cold weather masonry construction. On the other hand, the use of nanocellulose at normal curing temperatures (22±2°C) resulted in a considerable improvement in the mechanical properties of masonry prisms. In order to improve the mechanical properties of the masonry assemblages, the incorporation of nanocellulose with sodium nitrite resulted in the highest compressive and flexural bond strengths at both normal and subfreezing curing temperatures.

From the results discussed in this work, it is shown that the addition of sodium nitrite in masonry mortar mixtures can speed up masonry construction during the winter, with the need for only 4-8 hours of pre-curing at room temperature before being exposed to subfreezing temperatures, which is much relaxed compared to the 48 hours of protection currently required by the Canadian CSA A371 standard.

ACKNOWLEDGMENTS

I want to start by thanking God the almighty for giving me the force and courage to start and finish this work.

My profound gratitude and deepest regards go to my supervisors, Prof. Moh Boulfiza and Prof. Leon Wegner for their continuous support, encouragement, and their valuable advice throughout my M.Sc. program, the foundation of this work would have not been shaped without them. I would also like to thank them for the time and effort they dedicated to solve the research problems and revise the research work that improved my academic performance. They were always reinforcing my research ideas and helping me to implement my knowledge in practical applications. They were and will remain a valuable source of inspiration for me.

My thanks also go to my Advisory committee members Prof. Bruce Sparling, and Dr. Lisa Feldman for their valuable comments and orientations during my study and research.

Countless thanks to our Structural Laboratory Technician Brennan Pokoyoway, and all the fellow grad students who assisted and discussed this work.

I would like to acknowledge Saskatchewan Masonry Institute (SMI), the Saskatchewan Centre for Masonry Design (SCMD), the Canada Masonry Design Centre (CMDC), and the Department of Civil, Geological, and Environmental Engineering of the University of Saskatchewan for their financial support to this project.

At last, but not least, my deepest gratitude goes to my beloved parents, Khalid and Ayda, for their endless love, prayers, and support. Their love provided my inspiration and was my driving force. I would like to appreciate the support of my friends who backed me in every step of my life and my studies.

DEDICATION

To my family and friends

A special feeling of gratitude to my loving parents, Khalid and Ayda Alfarra,

whose words of encouragement and insistence on perseverance still echo in my ears

TABLE OF CONTENTS

PERMISSION TO USE ii

ABSTRACT iii

ACKNOWLEDGMENTS v

DEDICATION vi

TABLE OF CONTENTS vi

LIST OF FIGURES xiv

LIST OF ABBREVIATIONS AND SYMBOLS xvi

1 INTRODUCTION 1

1.1 Background 1

1.2 Objectives 4

1.3 Scope and Methodology 4

2 LITERATURE REVIEW 6

2.1 Overview 6

2.2 Mechanisms of Cement Hydration 7

2.3 Problems Associated with Masonry Construction in Cold Weather 9

2.4 Application of Chemical Admixtures in Cold Weather Construction 12

2.4.1 Accelerators 12

2.4.2 Water-Reducing Admixtures 12

2.4.3 Antifreeze Admixtures 12

2.5 Earlier Studies on Bond Strength of Brick Masonry 17

2.6 Reinforcing Mortar with Cellulose Nano-fibres 19

2.7 Masonry Assemblage Strengths and Properties 22

2.7.1 Overview 22

2.7.2 Construction of Prisms 23
2.7.3 Factors Affecting Masonry Compressive Strength of Ungrouted Masonry 23
2.7.4 Flexural Tensile Strength 27
2.8 Summary 31
3 EXPERIMENTAL PROGRAM 32
3.1 Overview 32
3.2 Mortar Materials and Properties 32
3.2.1 Materials and Preparation 32
3.2.2 Flowability of Fresh Mortar 33
3.2.3 Air Content of Fresh Mortar 34
3.2.4 Air Content of Hardened Mortar 35
3.2.5 Setting Time Test 37
3.2.6 Compressive Strength of Mortar Cubes 38
3.3 Brick Properties 39
3.4 Number of Specimens 42
3.5 Prism Construction Process 44
3.6 Compressive Strength Test 48
3.7 Flexural Bond Strength Test 50
4 RESULTS AND DISCUSSION 54
4.1 Mortar Properties 54
4.1.1 Flow Test Results 54
4.1.2 Air Content 56
4.1.3 Setting Time 58
4.1.4 Mortar Compressive Strength 61
4.2 Brick Properties 65
4.2.1 Water Absorption 65
4.2.2 Initial Rate of Absorption 66

4.2.3 Compressive Strength of Masonry Bricks 66

4.3 Mechanical Properties of Masonry Assemblages 67

4.3.1 Compressive Strength of Masonry Prisms 67

4.3.2 Flexural Bond Test Results 77

5 CONCLUSIONS AND RECOMMENDATIONS 81

5.1 Summary 81

5.2 Conclusions 82

5.3 Recommendations 85

REFERENCES 86

APPENDICES 96

APPENDIX A – COMPRESSIVE STRENGTH VALUES WITH PAIRED SAMPLE T-TEST ANALYSIS FOR COMPRESSION TEST RESULTS BETWEEN DIFFERENT GROUPS 97

APPENDIX B – LINEAR REGRESSION ANALYSIS FOR THE PROPOSED MODEL TO ESTIMATE THE COMPRESSIVE STRENGTH OF MASONRY BRICK PRISM 112

APPENDIX C – FLEXURAL BOND TEST RESULTS WITH PAIRED SAMPLE T-TEST ANALYSIS FOR COMPRESSION TEST RESULTS BETWEEN DIFFERENT GROUPS 113

APPENDIX D – ASTM C140 ABSORPTION TEST RESULTS 127

APPENDIX E – INITIAL RATE OF ABSORPTION TEST RESULTS 128

APPENDIX F – COMPRESSIVE STRENGTH OF STANDARD CONCRETE MASONRY BRICKS 129

LIST OF TABLES

Table 2.1 Portland cement major constituents 7
Table 2.2 Setting time of mortar containing SN at +20℃ (Ratinove and Rozenberg 1996) 15
Table 2.3 Prediction models for masonry compressive strength 24
Table 2.4 Correction Factors for the Compressive Strength of Masonry Prisms (CSA S304-14) 26
Table 2.5 Specified flexural tensile strength, ft (CSA S304-14) 27
Table 3.1 Mortar ingredients, mix proportions and curing conditions 33
Table 3.2 Prism labelling system 48
Table 3.3 Prism labelling system used for flexural bond strength tests 51
Table 4.1 Air content of fresh and hardened mortar mixtures 57
Table 4.2 Average setting time results for samples cured at room temperature 59
Table 4.3 Average setting time results for samples cured at -7°C 60
Table 4.4 28-day compressive strengths of mortar cubes cured at room temperature 62
Table 4.5 28-day compressive strengths of mortar cubes cured at -10°C 63
Table 4.6 Average compressive strength of prisms cured at room temperature and at -10°C 68
Table 4.7 Solid brick masonry specified compressive strength normal to bed joint (reproduced from CSA S304-14 (CSA 2014)) 71
Table 4.8 Average compressive strengths of different prism groups with their corresponding mortar compressive strength 74
Table 4.9 Flexural bond strength test results for all prisms cured at room temperature and at -10°C 77
Table A.1 Compressive strengths of control prisms cured at room temperature 97
Table A.2 Compressive strengths of control prisms cured at -10°C 97
Table A.3 Compressive strengths of sodium nitrite prisms cured at room temperature 98
Table A.4 Compressive strengths of sodium nitrite prisms cured at -10°C 98
Table A.5 Compressive strengths of nanocellulose prisms cured at room temperature 98

Table A.6 Compressive strengths of nanocellulose prisms cured at -10°C 99
Table A.7 Compressive strengths of sodium nitrite and nanocellulose prisms cured at room temperature.....99
Table A.8 Compressive strengths of sodium nitrite and nanocellulose prisms cured at -10°C.....100
Table A.9 Paired samples statistics for the control groups 100
Table A.10 Paired samples correlations for the control groups 100
Table A.11 Paired samples test for the control groups 100
Table A.12 Paired samples statistics for the sodium nitrite groups 101
Table A.13 Paired samples correlations for the sodium nitrite groups 101
Table A.14 Paired samples test for the sodium nitrite groups 101
Table A.15 Paired samples statistics for the nanocellulose groups.....102
Table A.16 Paired samples correlations for the nanocellulose groups 102
Table A.17 Paired samples test for the nanocellulose groups.....102
Table A.18 Paired samples statistics for the sodium nitrite with nanocellulose groups ..103
Table A.19 Paired samples correlations for the sodium nitrite with nanocellulose groups 103
Table A.20 Paired samples test for the sodium nitrite with nanocellulose groups 103
Table A.21 Paired samples statistics for the control and sodium nitrite samples cured at room temperature 104
Table A.22 Paired samples correlations for the control and sodium nitrite samples cured at room temperature 104
Table A.23 Paired samples test for the control and sodium nitrite samples cured at room temperature.....104
Table A.24 Paired samples statistics for the control and nanocellulose samples cured at room temperature 105
Table A.25 Paired samples correlations for the control and nanocellulose samples cured at room temperature 105
Table A.26 Paired samples test for the control and nanocellulose samples cured at room temperature.....105
Table A.27 Paired samples statistics for the control and sodium nitrite with nanocellulose samples cured at room temperature.....106
Table A.28 Paired samples correlations for the control and sodium nitrite with nanocellulose samples cured at room temperature.....106

Table A.29 Paired samples test for the control and sodium nitrite with nanocellulose samples cured at room temperature 106
Table A.30 Paired samples statistics for the control and sodium nitrite samples cured at freezing temperature 107
Table A.31 Paired samples correlations for the control and sodium nitrite samples cured at freezing temperature 107
Table A.32 Paired samples test for the control and sodium nitrite samples cured at freezing temperature 107
Table A.33 Paired samples statistics for the control and nanocellulose samples cured at freezing temperature 108
Table A.34 Paired samples correlations for the control and nanocellulose samples cured at freezing temperature 108
Table A.35 Paired samples test for the control and nanocellulose samples cured at freezing temperature 108
Table A.36 Paired samples statistics for the control and sodium nitrite with nanocellulose samples cured at freezing temperature 109
Table A.37 Paired samples correlations for the control and sodium nitrite with nanocellulose samples cured at freezing temperature 109
Table A.38 Paired samples test for the control and sodium nitrite with nanocellulose samples cured at freezing temperature 109
Table A.39 Paired samples statistics for control samples cured at room temperature and sodium nitrite samples cured at freezing temperature 110
Table A.40 Paired samples correlations for control samples cured at room temperature and sodium nitrite samples cured at freezing temperature 110
Table A.41 Paired samples test for control samples cured at room temperature and sodium nitrite samples cured at freezing temperature 110
Table A.42 Paired samples statistics for control samples cured at room temperature and sodium nitrite with nanocellulose samples cured at freezing temperature 111
Table A.43 Paired samples correlations for control samples cured at room temperature and sodium nitrite with nanocellulose samples cured at freezing temperature 111
Table A.44 Paired samples test for control samples cured at room temperature and sodium nitrite with nanocellulose samples cured at freezing temperature 111
Table B.1 Model summary 112

Table B.2 ANOVA....112
Table B.3 Coefficients....112
Table C.1 Flexural bond strength test results for control samples cured at the room temperature....113
Table C.2 Flexural bond strength test results for control samples cured at the freezing temperature....114
Table C.3 Flexural bond strength test results for sodium nitrite samples cured at the room temperature....115
Table C.4 Flexural bond strength test results for sodium nitrite samples cured at the freezing temperature....116
Table C.5 Flexural bond strength test results for nanocellulose samples cured at the room temperature....117
Table C.6 Flexural bond strength test results for nanocellulose samples cured at the freezing temperature....118
Table C.7 Flexural bond strength test results for sodium nitrite with nanocellulose samples cured at the room temperature....119
Table C.8 Flexural bond strength test results for sodium nitrite with nanocellulose samples cured at the freezing temperature....120
Table C.9 Paired samples statistics for the control groups....121
Table C.10 Paired samples correlations for the control groups....121
Table C.11 Paired samples test for the control groups....121
Table C.12 Paired samples statistics for the sodium nitrite groups....122
Table C.13 Paired samples correlations for the sodium nitrite groups....122
Table C.14 Paired samples test for the sodium nitrite groups....122
Table C.15 Paired samples statistics for the nanocellulose groups....123
Table C.16 Paired samples correlations for the nanocellulose groups....123
Table C.17 Paired samples test for the nanocellulose groups....123
Table C.18 Paired samples statistics for the sodium nitrite with nanocellulose groups....124
Table C.19 Paired samples correlations for the sodium nitrite with nanocellulose groups....124
Table C.20 Paired samples test for the sodium nitrite with nanocellulose groups....124
Table C.21 Paired samples statistics for control samples cured at room temperature and sodium nitrite samples cured at freezing temperature....125

Table C.22 Paired samples correlations for control samples cured at room temperature and sodium nitrite samples cured at freezing temperature.....125
Table C.23 Paired samples test for control samples cured at room temperature and sodium nitrite samples cured at freezing temperature 125
Table C.24 Paired samples statistics for control samples cured at room temperature and sodium nitrite with nanocellulose samples cured at freezing temperature.....126
Table C.25 Paired samples correlations for control samples cured at room temperature and sodium nitrite with nanocellulose samples cured at freezing temperature.....126
Table C.26 Paired samples test for control samples cured at room temperature and sodium nitrite with nanocellulose samples cured at freezing temperature 126
Table D.1 ASTM C140 absorption test results 127
Table E.1 Initial rate of absorption test results.....128
Table F.1 Compressive strength of standard concrete masonry bricks.....129

LIST OF FIGURES

Figure 2.1 Masonry assemblies: (a) Prisms, and (b) Wallettes 22
Figure 2.2 Testing arrangement of four-point loading on wallettes: (a) plain of failure parallel to bed joints, and (b) plain of failure normal to bed joints 28
Figure 2.3 Third-point loading 29
Figure 2.4 Bond wrench testing apparatus (CAN/CSA A3005-13) 30
Figure 3.1 Flow of masonry mortar mixture 34
Figure 3.2 Air content for hardened concrete test set up 35
Figure 3.3 Water-cooled diamond saw 36
Figure 3.4 Vibrating-polishing table 36
Figure 3.5 Scanned image of the sample after the contrast enhancement 37
Figure 3.6 Vicat apparatus 38
Figure 3.7 Mortar cube for compression testing 39
Figure 3.8 Bricks immersed in water, suspended by wires 40
Figure 3.9 Brick being soaked in 3 mm of water 41
Figure 3.10 Capped brick for the compression testing using Amsler Beam Bender machine 42
Figure 3.11 The six-brick prisms used for compression tests 44
Figure 3.12 A partially constructed prism showing the use of alignment jig and mortar template to build the prisms 45
Figure 3.13 Clamped prism for transportation 46
Figure 3.14 Embedded thermocouple in the mortar joint 47
Figure 3.15 Evolution of mortar temperature after removal from freezing chamber 47
Figure 3.16 Compressive strength test setup for brick prisms 49
Figure 3.17 Bond wrench test set up with various components labelled 52
Figure 3.18 Schematic diagram of bond wrench apparatus, showing the variables used to calculate the flexural strength 52
Figure 4.1 Mass of water required to achieve the specified flowability of mortar mixtures for samples of different batch sizes 55
Figure 4.2 Flowability of mortar mixtures with the same w/c ratio of 0.51 56

Figure 4.3 Setting time results for representative samples of mortar mixtures at room temperature 58
Figure 4.4 Setting time results for representative samples of mortar mixtures at -7°C 60
Figure 4.5 Failure of the control sample cured at -10°C 64
Figure 4.6 Representative failure of mortar cubes of different mixtures cured at room temperature and those containing sodium nitrite cured at -10°C 64
Figure 4.7 Average compressive strengths of different prism groups cured at room temperature and at -10°C 68
Figure 4.8 Progressive failure of a prism with the control mortar cured at room temperature: (a) vertical splitting cracks, (b) followed by crushing of the bricks, and (c) another prism followed the same progressive failure 72
Figure 4.9 Failure of a prism with sodium nitrite cured at the subfreezing temperature, showing vertical splitting cracks 73
Figure 4.10 Failure due to mortar joint crushing in a control specimen cured at -10°C 73
Figure 4.11 Failure mode associated with crushing of bricks followed by splitting failure 73
Figure 4.12 Graphical representation of the variation of the average compressive strength of different prism groups with their average mortar compressive strength 75
Figure 4.13 Graphical representation of the developed model 76
Figure 4.14 Average flexural bond strengths of different prism groups cured at room temperature and at -10°C 77
Figure 4.15 Failure at the brick-mortar interface, as demonstrated in prisms cured at room temperature 79
Figure 4.16 Flexural failure in the bed joint, illustrated for control and nanocellulose prisms cured at -10°C: (a) and (b) are control joints, and (c) nanocellulose joint 79

LIST OF ABBREVIATIONS AND SYMBOLS

ACI	American Concrete Institute
AS	Australian Standard
ASCE	American Society of Civil Engineers
ASTM	American Standard for Testing and Materials
BS	British Standard
C_2S	Dicalcium Silicate
C_3A	Tricalcium Aluminate
C_3S	Tricalcium Silicate
$C_3S_2H_3$	Calcium Silicate Hydrate
C_4AF	Tetracalcium Aluminoferrite
$C_6AS_3H_{32}$	Ettringite
$CaCl_2$	Calcium Chloride
CEM	Concrete Equivalent Mortar
CH	Calcium Hydroxide
CMDC	Canada Masonry Design Centre
CNFs	Cellulose nano-fibres
CRREL	Cold Region Research and Engineering Laboratory
CSA	Canadian Standard Association
C-S-H	Calcium Silicate Hydrate
Ctr	Control samples
CWAS	Cold Weather Admixture System
f_{bl}	Unit Compressive Strength
f'_m	Compressive strength of the assembly
f_{mr}	Mortar Compressive Strength
f_t	Flexural tensile strength
h/t	The ratio of the height of a prism to its thickness

IRA	Initial Rate of Absorption of masonry units
K_2CO_3	Potassium Carbonate
L	Length
MC	Masonry cement
Na_2SO_4	Sodium Sulphate
$NaNO_2$	Sodium Nitrite
NC	Mortar with nanocellulose
NN	Mortar with sodium nitrite and nanocellulose
PCL	Portland cement/lime mortars
SN	Mortar with sodium nitrite
T	Thickness
TDR	Time Domain Reflectometry
TMS	The Masonry Society
UHP	Ultra-high-performance mortar
W	Width
w/c	Water to Cement ratio
Δt	Setting Period

1 INTRODUCTION

1.1 Background

Masonry is considered to be one of the oldest and most commonly used building materials in human history. Over the past few thousand years, masonry has been used as the basic building material for public and residential buildings; from the great wall of China to the pyramids of Egypt, from the ancient fortress of Machu Pichu to the beautiful Taj Mahal, all these masonry structures serve as a witness of time. However, due to its composite nature, the process of masonry construction is greatly affected by some major aspects such as material availability, environmental conditions, and associated costs.

When exposed to cold conditions during construction and curing in autumn, winter, and spring, the performance of masonry assemblies may be affected. The reduced hardening rate and slow development of the mortar's strength at low temperatures adversely affect the mortar joints (Korhonen et al. 1997). This means that the process of building masonry structures at cold temperatures is a major challenge for contractors in North America as well as other cold geographical locations. The construction industry has been forced to follow extraordinary building methods, focused primarily on protecting the freshly mixed and placed mortar from freezing for a suitable curing time. Generally, when cement and water are mixed, various chemical reactions take place, collectively known as “the hydration reaction”. Like most chemical reactions, the lowering of temperature has the effect of lowering the hydration rate and even completely stopping it when there is no water left in liquid form.

Mortar joints are considered to be vulnerable at cold temperatures due to the obvious effect of freezing temperature on the setting times and the strength gain. Therefore, the North American standards stipulate that all mortar components and concrete masonry units must be heated and/or protected from cold temperatures below a certain daily mean temperature. Canadian standard CSA A179-14 (CSA 2014) outlines specific techniques for the construction and curing of masonry assemblages when the average daily temperature drops below 4°C.

Though these heating techniques are beneficial, they may be unfavourable economically and logistically. Heat generating equipment and the protective materials necessary to

implement conventional mitigation methods normally result in considerably higher construction costs (Bigelow 2005). In addition, special care is required for heating each constituent material to produce mortar mixtures that meet the defined temperature limits imposed by the specified standard adopted, which may slow down the masonry construction process.

In 1997, Korhonen et al. estimated that the addition of antifreeze admixture systems to cement-based products can save more than 50 percent of the cost of placing normal concrete under freezing temperatures. However, it is very hard to mention the exact cost that will be saved by using the antifreeze admixture systems instead of the outlined techniques by CAN/CSA A371-14. The reason behind that is the different factors that affect the cost related to cold weather construction. After talking with different contractors, they mentioned some factors they believe to have considerable effect on the construction cost during the cold days. For example, the fuel source, the temperatures, area, etc., are factors that made it difficult to pin down a specific cost. In general terms, construction during winter months could be 20-50% of project costs. Another way to address the beneficial use of the antifreeze admixture systems is by pinning down the added days contractors would have without the need for heating and hoarding.

As outlined by CAN/CSA A371-14 (2014), heat is required during construction when temperatures are less than -4°C. Constructed masonry must be covered with insulating blankets when temperatures are less than -4°C, and heated when temperatures are less than -7°C. Applying antifreeze admixture in the mortar to be laid and cured at temperatures up to -10°C can result in decreasing the additional protection measures in Saskatoon from five months to two months (January and February), according to the average night-time temperatures. In Toronto, for example, the average night-time temperatures in January and February are about -7.5°C at the lowest, so that would mean in normal years there would have to be measures needed starting December all the way to March for some level of protection, that could all be avoided by applying antifreeze admixture system to the mortar.

Numerous investigations have been undertaken to reduce the reported negative effects of freezing curing temperature on cement-based products through the use of accelerators, antifreeze agents, or combinations of both (cold-weather admixture systems) (e.g., Barna et al. 2010; Karagöl et al. 2013; Karagöl et al. 2015). In a recent study, Saha et al. (2019) investigated the properties of mortars that included sodium nitrite, which is not known to cause damage to

either cement-based materials or steel reinforcement. The addition of sodium nitrite as an inhibiting admixture improved the concrete resistance against corrosion (Teklegiorgis et al. 2022, Maliekkal et al. 2018, Dharmaraj and Malathy 2015). The gain in strength observed under freezing conditions indicated that the sodium nitrite was indeed able to cause the hydration reactions to continue at temperatures as low as -10°C. Its effectiveness, when used for the construction of masonry assemblages, has yet to be demonstrated.

Another potential way to minimise the impact of low temperatures on the strength development of masonry mortar could be the use of novel materials (e.g., nanoparticles). Because of their ultrafine nature, nanoparticles can strongly improve the hydration of cement. Many studies (e.g., Belkowitz et al. 2015; Senff et al. 2010; Sonebi et al. 2015) have shown that by refining and densifying the porous structure of hydrated cement paste, the nanoparticles have a beneficial effect on the properties of cement materials under normal mixing and curing temperatures (22±2°C). In recent years, nanocellulose has been investigated as a prospective additive in cement materials. Nanocellulose has been found to improve the mechanical properties of cement-based products (Cao et al. 2016), enhance the degree of hydration (Cao et al. 2015), and strengthen the microstructure of cement composites (Flores et al. 2017).

Despite its importance for the development of sufficient tensile strength in masonry assemblies to resist lateral loads such as wind and earthquake forces, the bond strength levels typically present in masonry construction remain relatively low (less than 1 MPa). Just like many cement-based materials, masonry is strong in compression and relatively weak under tensile loads. Compressive strengths of masonry assemblages can be as high as 15 MPa or even higher, while their tensile strengths are typically an order of magnitude lower. This relative weakness, which may lead to cracking and similar kinds of damage, often goes unnoticed because of the relatively low tensile stresses a masonry structure is usually subjected to. However, when masonry is subjected to extreme load events, such as very high wind or an earthquake, the low tensile strengths might lead to collapse. Recognizing that tensile strength is a property of both the mortar and the masonry unit, the use of nanocellulose, which has been shown to improve many properties of cement-based materials, may have the potential ability to increase the bond strength in masonry assemblages.

1.2 Objectives

The main objective of the study was to evaluate the performance of mortars that contain nanocellulose and sodium nitrite as a cold-weather admixture in masonry assemblages under sub-freezing curing temperatures. The specific subobjectives of this project were as follows:

- To determine the effect of sodium nitrite and nanocellulose as mortar admixtures, separately and in combination, on the compressive strength of concrete brick masonry prisms cured at room temperature and -10°C; and
- To determine the effect of sodium nitrite and nanocellulose as mortar admixtures, separately and in combination, on the flexural bond strength of masonry prisms cured at room temperature and -10°C.

In addition, the following fresh and hardened properties of the mortar mixtures with and without the admixtures were determined:

- The effect of sodium nitrite and nanocellulose as mortar admixtures, separately and in combination, on the amount of water required to reach acceptable flowability of the fresh mortar;
- The effect of sodium nitrite and nanocellulose as mortar admixtures, separately and in combination, on the fresh and hardened air content of the mortar mixtures;
- The effect of sodium nitrite and nanocellulose as mortar admixtures, separately and in combination, on the initial and final setting times at room temperature and -7°C; and
- The effect of sodium nitrite and nanocellulose as mortar admixtures, separately and in combination, on the mortar compressive strength cured at room temperature and -10°C.

1.3 Scope and Methodology

An experimental program was undertaken to measure the compressive and flexural bond strengths of masonry prisms incorporating sodium nitrite and/or nanocellulose in the mortar, along with the relevant properties of companion specimens. In total, 72 standard concrete brick prisms were constructed with six masonry units stacked vertically for the compressive strength tests. Forty brick prisms, each one six units in height with five mortar joints, for a total of 200 joints, were built and tested for the flexural bond strength tests. The prisms were built at room temperature in the structural engineering lab and remained there for 4 hours. Then, half of the prisms were transported to an environmental chamber located in the Controlled Environment Facility in the Chemical Engineering Laboratory to be cured at a temperature of -10°C for 28 days, while the rest of the prisms were cured at room temperature. Mortar was proportioned by

volume in a ratio of 1:3, mortar cement type S to mortar sand. The addition of sodium nitrite was limited to 12% by mass of mixing water, as recommended by Ratinove and Rozenberg (1996), and 0.3 wt.% nanocellulose was used as it has resulted in the minimum water absorption and maximum enhancement of the flexural strength of the mortar (Akhlaghi et al. 2020).

2 LITERATURE REVIEW

2.1 Overview

The use of cement-based products for construction in cold weather is considered to be a major problem that faces masonry practitioners. The hydration reaction between cement and water depends mainly on temperature and humidity conditions. Ratinove and Rozenberg (1996) stated that theoretically the hydration reaction will stop at a temperature of -2.8°C due to freezing of mixing water, below which the mortar will suffer from durability problems and a reduction in the strength development. Furthermore, the frozen water formed due to the freezing curing temperature has a higher volume in the capillary pores compared to the liquid water present when initially mixed. According to Polat (2016), this leads to the creation of hydraulic and osmotic stresses in the cement paste, resulting in permanent damage in mortar microstructure (Karagöl et al. 2015). Consequently, different elements in masonry structures will fail to achieve their service life performance if not protected and cured at temperatures above 10ºC (Soliman 2020).

There are different techniques outlined by CAN/CSA A371-14 (2014) to deal with cold-weather problems. These include heating of the mortar ingredients, using enclosures, and providing the construction site with temperatures more than 10ºC. The idea of these techniques is to provide a curing condition that will permit the mortar to gain its intended design strength through the availability of water in liquid form, which allows the hydration reaction to proceed. However, owing to the use of large quantities of energy, masonry contractors would incur additional time and costs when implementing these measures. Therefore, to solve the difficulties of placing mortar under low temperatures, it was important to explore and discover other methods. The use of antifreeze admixtures may be another potential solution to low-temperature curing problems. Incorporation of antifreeze admixtures in the mortar can minimise the need for protection and eventually remove it completely at relatively low temperatures.

This literature review introduces the main challenge in masonry construction in cold temperatures and reviews the current regulations and practical mitigation methods practiced in

North America. The major part of this literature review focuses on antifreeze admixtures and their various effects on the fresh and hardened properties of cement-based materials at normal and cold temperatures. In addition, a brief review of the use of nanocellulose in cement-based materials is provided, including its potential to minimise the impact of low temperatures and improve the bond strength of masonry assemblages. Finally, since this study focuses on evaluating the performance of antifreeze admixture in masonry assemblages, the interaction between units and mortar, as well as other factors influencing the physical and mechanical properties of the composite are presented.

2.2 Mechanisms of Cement Hydration

In order to manufacture Portland cement, raw materials are first ground, blended, and preheated. The mixture of the raw materials is then sent to a rotary kiln at a temperature of approximately 1500°C to create a cement clinker. Then, the clinker is ground with other additives to a fine powder. The key constituents of Portland cement are formed after cooling and crystallization of cement particles, as listed in Table 2.1 (Duggal 2008).

Table 2.1 Portland cement major constituents

Major constituents	Formula	Name	Symbol	Mass percentage
Tricalcium Silicate	$3CaO{\cdot}SiO_2$	Alite	C_3S	40-70%
Dicalcium Silicate	$2CaO{\cdot}SiO_2$	Belite	C_2S	25-40%
Tricalcium Aluminate	$3CaO{\cdot}Al_2O_3$	Celite	C_3A	5-11%
Tetracalcium Aluminoferrite	$4CaO{\cdot}Al_2O_3{\cdot}Fe_2O_3$	Felite	C_4AF	8-14%

The properties of Portland cement vary substantially with the proportions of the above four compounds. Tricalcium Silicate (C_3S) hydrates quickly, resulting in the generation of high heat, and is mainly responsible for the early strength development of cement-based mixtures. Massazza (2003) indicates that Dicalcium Silicate (C_2S) does not play a major role in the early strength gain of cement-based products, since it reacts more after 28 days. Tricalcium Aluminate (C_3A) is responsible for the initial setting. It experiences greater volume changes than other constituents during hydration, which may cause cracking, and generates a high amount of heat during the early stages of the hydration process. Tetracalcium Aluminoferrite (C_4AF) is responsible for flash sets and it does not generate a high amount of heat. As water is applied to cement particles, the Tricalcium Silicate reacts to create Calcium Silicate Hydrates, lime, and heat, while the Dicalcium Silicate reacts to form Calcium Silicate Hydrates and heat, as shown in the following equations:

$$2C_3S + 6H \rightarrow C_3S_2H_3 + 3CH \quad [2\text{-}1]$$

$$C_2S + 4H \rightarrow C_3S_2H_3 + CH \quad [2\text{-}2]$$

The products of these reactions have several characteristics important to hardened cement paste formation. The Calcium Silicate Hydrate ($C_3S_2H_3$) (C-S-H), which possesses a gel structure, is also known as tobermorite gel. It makes up 50–60% of the volume of solids in a completely hydrated Portland cement paste and is responsible for the strength of the matrix. Another hydration product from the hydration of C_3S and C_2S is Calcium Hydroxide (CH), which does not greatly enhance the mechanical properties of the cement matrix. CH, also referred to as portlandite, can react with other substances (sulphates, etc.) to produce deleterious products affecting the durability of the cement material (Neville 2004). C_3A hydration creates tremendous amounts of heat and causes the rapid setting of the cementitious matrix. Calcium Sulphate Dehydrates (gypsum) is normally ground with clinker to reduce the amount of heat released and delay the setting period. Therefore, ettringite ($C_6AS_3H_{32}$) is produced, according to Eqn. [2-3], as the result of the reaction between Tricalcium Aluminate with the gypsum in the presence of water (Mindess et al. 2003).

$$C_3A + 3CSH_2 + 26H \rightarrow C_6AS_3H_{32} \quad [2\text{-}3]$$

The heat evolution resulting from the hydration process of cement Calcium Silicates (C_3S and C_2S) consists of five stages. The first stage corresponds to the significant amount of heat released due to the mechanical interaction between the particles during the mixing process. The amount of heat released drops for about four hours during the second stage, called the dormant or induction stage. The hydration continues until the concentration of calcium and hydroxyl ions have reached a critical value. At this stage, CH crystals begin to precipitate in the solution and C-S-H layers begin to form in the phases of calcium silicate. For determining the transport time of a mixture, this duration is critical as it determines the initial setting time. The rate of hydration reactions increases in the third stage and the quantity of generated heat increases due to the formation of hydration products. This stage denotes the cementitious mixture's final setting time. Hydration reactions slow down during the fourth stage, as the C-S-H barrier gets thicker and water diffusion gets harder. Under normal temperature conditions, this stage normally denotes the early strength of a mixture. Reactions begin to slow to a steady state during the last stage as the water diffusion decelerates. The later strength values are denoted by this stage (Mindess et al. 2003; Neville 1996).

2.3 Problems Associated with Masonry Construction in Cold Weather

2.3.1 Cold Weather Problems

In cold weather, masonry construction possesses two major problems. The first problem is the low strength gain due to the low hydration rate caused by the low temperatures. The second problem is of a physical nature; when the temperature drops below the water freezing point, the liquid water begins to freeze and expand, which creates a risk of damaging the cement paste microstructure (Davison 1970, Woodham and Schuller 2005). A few solutions are available for cement-based construction in cold areas. The first option is to simply suspend the construction process until a good thermal condition is present. The second option is to provide adequate thermal protection to the building materials, especially those used in the cement-based products, in order to ensure that the freshly made cementitious materials develop adequate strength before being exposed to the cold weather.

Cement-based products are commonly a mix of water, cement, and aggregates. As described earlier, upon the addition of water, these materials start to transform into the required solid-state through the hydration reaction which happens between water and cement. As with any chemical reaction, according to the Arrhenius equation, the rate of a hydration reaction depends on the temperature. As the temperature goes down, the rate of the hydration reaction slows, resulting in a lower strength gain compared to normal conditions. Liu et al. (2017) studied the degree of hydration of Portland cement at different curing temperatures. The result of this study indicated that at a temperature as low as -5°C, the degree of hydration was 63.2% after 90 days. Samples that were cured at 20°C reported 91.9% degree of hydration at 90 days. This result indicated that the hydration reaction of Portland cement is not completely stopped at -5°C, but rather delayed. If the temperature continues to decline, the hydration reaction will practically stop due to the fact that most of the liquid water in the porous structure turns into ice (Korhonen 1990). From a theoretical point of view, Korhonen and Brook (1996) state that cement continues to hydrate down to -20°C, provided that the water is prevented from freezing, but this typically does not happen in practice. Water transition from liquid to ice raises its volume by 9%. Such volume expansion can disrupt the fresh mix's weak structure by producing cracks and some permanent damage within the cement paste itself and between the cement paste and the aggregate particles.

Woodham and Schuller (2005) drew attention to two similar issues with the construction of masonry in cold weather. First, as the temperature drops, the hydration reactions become sluggish and eventually stop, which leads to lower strength gain. Second, ice development can break internal bonds and cause permanent damage to the masonry if mortar or grout is allowed to freeze. There is, however, a noticeable difference between mortar and concrete, which concerns the water content before and after placement. In order to achieve higher workability, mortar has a higher water content but is in contact with a porous material that absorbs the excess water. Thus, mortar is less vulnerable to freezing at early ages than concrete.

The rate at which the temperature drops influences the type of ice that is formed (Korhonen 1990, Suprenant 1992). The time needed for water to migrate to the colder area is not enough under rapid cooling conditions, which leads to the formation of a very uniform distribution of small ice crystals. On the other hand, water will migrate to colder regions and freeze there under slow cooling conditions. Both fast and slow freezing result in a detrimental effect on the fresh material, leading to a loss of up to 50% of the ultimate compressive strength.

Another legitimate issue that concerns designers in cold areas is durability; freezing and thawing, and exposure to de-icing salts are the major factors that affect the life span of the structure. Freezing and thawing result when the temperature fluctuates below and above the freezing temperature. The deterioration cycle results from the expansion of water as it changes from the liquid phase to the solid phase. This shift in volume creates tension within the matrix of the cement paste, leading to scaling and spalling. The consequence of freezing and thawing is especially noticeable on surfaces where saturation of the concrete or grout is more likely (Kosmatka et al. 2002).

2.3.2 Cold Weather Masonry Construction Practices

The primary and most common practice to accelerate the hydration reaction and avoid the freezing of mortar joints is to heat the mixing water or sand. Water has a great capability to pass heat to the other materials of the masonry mortar mixtures. Keeping the water temperature below 60°C is recommended, as higher temperatures will raise the risk of the flash setting of mortar (Bigelow 2005). The optimal temperature range of a mortar mixture is from 15.6°C to 26.7°C (CAN/CSA A371-14). Moreover, CAN/CSA A371-14 recommends that the masonry mortar temperature be kept below 50°C in order to avoid flash setting. An alternative way to avoid cold weather problems is to warm the units before installation or store them in an insulated space.

The other method suggested by masonry practitioners is to reduce the water content of mortar mixtures. In masonry mortar, a lower water content contributes to the development of a relatively higher compressive strength and noticeable shortening of the setting time. Decreasing the hydrated lime content, using masonry cement, and using more sand content in the mortar mixture have also been recommended (Brick Industry Association 2006). That being said, it has been observed that the colour of the finished work can change by changing the materials or using admixtures (Throop 2005), which might bring some cosmetic concerns in some applications.

Protecting constructed masonry structures from freezing is the main practice in cold weather construction. Using electric heaters, insulating blankets and insulated enclosures are common methods for warming and securing constructed masonry segments. One of the issues associated with the use of industrial heaters is that the constructed structural element typically is not heated uniformly. Therefore, due to the resulting temperature gradients, the degree of hydration of mortar joints can differ along a segment, which can lead to deformation of the constructed masonry segment (Essroc 2012b). Conventional heating methods often consume fossil fuels; however, the carbon dioxide emitted by fossil fuels can cause carbonation of the cement material under certain conditions, leading to durability concerns (Neal 2002).

Another possible response to low-temperature problems is the use of antifreeze admixtures to reduce the protection requirement and ultimately eliminate it entirely at reasonably low temperatures. Their use in masonry construction in North America is almost non-existent and is banned under the current regulations. The primary reason behind this restrictive approach is that previously used chemical compounds (calcium chloride and alcohol) have unfavourable impacts on cement-based products, including lowering the strength or promoting the corrosion of steel in reinforced structures (CSA 2004b, Woodham and Schuller 2005).

Notwithstanding the fact that concrete and masonry both contain water, cement, and aggregate, there are numerous contrasts between the two, providing justification for why research ought to be directed explicitly for antifreeze admixtures applied to masonry construction. The main contrasts between concrete and masonry binders are the initial water content, the initial rate of absorption of masonry units, aggregate size, and the possible presence of lime in the masonry cement.

2.4 Application of Chemical Admixtures in Cold Weather Construction

Usually, the use of chemical admixtures is more cost-effective compared to thermal protection of cementitious mixtures. By using chemical admixtures, significant amounts of money related to labour costs, electricity, equipment, and materials can be saved.

2.4.1 Accelerators

The use of accelerators in cold weather will help to speed up hydration of the mortar and reduce the protection requirements. However, the incorporation of accelerators in the mortar mixture does not lower the freezing point of the mixing water, and therefore thermal protection will still be needed (Throop 2005). According to Clause 5.5.4 of CSA A 179-14 (2014), using any substances for accelerating the setting time in masonry mortars is prohibited.

2.4.2 Water-Reducing Admixtures

In order to decrease the water demand without compromising the required workability, water-reducing admixtures are applied to the cement paste. By repelling and dispersing the cement particles, they effectively release the bound water molecules in the agglomerated paste (Mindess et al. 2003). The application of water-reducing admixtures decreases the required water-to-cement ratio (w/c) of the matrix. At all ages, the lower w/c ratio increases the compressive strength of the mixture, decreases the porosity, and improves the durability of the cementitious mixture (Mindess et al. 2003). The increased compressive strength at early ages could be helpful in reducing the impact of cold weather on the rate of strength gain. Therefore, the combined effect of water-reducing admixtures and accelerators on cold weather construction has been investigated by some researchers. However, high dosages of water-reducing agents have shown that they have a delaying effect on the cement hydration reaction (Mindess et al. 2003).

2.4.3 Antifreeze Admixtures

Antifreeze admixtures are chemical compounds mixed with the cementitious mixtures mainly to depress the freezing point of the mixing water and accelerate the hydration rate of cement paste at the same time (ACI 2010). Antifreeze admixture systems should also meet other requirements, such as maintaining workability, achieving an acceptable setting time, not lowering strength at normal temperatures, not fostering corrosion reactions, and being cost-effective (Korhonen et al. 1997). This family of admixtures has many names: low temperature, cold weather, freezing protection, and antifreeze.

The incorporation of antifreeze admixtures in concrete or mortar results in depressing the freezing point of the mixing water and speeds up the cement hydration process (Kozikowski et al. 2014b), which allows various cement-based products to be placed and cured at freezing temperatures without weakening them, thereby offering a new approach to casting concrete and mortar in cold weather without any need for enclosures or artificial heating. Antifreeze admixture systems have the ability to save more than 50 percent of the cost of placing normal concrete under freezing temperatures (Korhonen et al. 1997), making them an effective and energy-efficient solution.

Since 1990, extensive work on the development of antifreeze admixtures for the concrete industry has been carried out by the Cold Region Research and Engineering Laboratory (CRREL). They examined 40 mortar mixtures with different water-cement ratios and different dosages of admixtures ranging from 1% to 24% by weight of cement. They found the freezing point is one of the most important parameters in determining the effectiveness of antifreeze admixtures (Korhonen 1999, 2006).

Korhonen et al. (1997) stated that the use of antifreeze admixtures does not require specific skills; however, they developed guidelines regarding the proper addition time for the admixtures. Regarding the mixing method, three different approaches were examined: introducing the admixtures at the mixing plant, adding some at the mixing plant and some at the construction site, and adding all at the construction site. They found that the mixing method did not result in significant differences; however, each method had its own advantages and drawbacks (Korhonen et al. 2004a). It is also advisable to use cement with good quality and at a convenient dose which is achieved by increasing the dosage of cement by 60 kg/m^3. ACI 306R-10 (ACI COMMITTEE 306 2010a) favors the application of type HE cements or increasing the cement dosage in combination with antifreeze admixtures.

Korhonen and Orchino (2001) examined the combined effect of commercial accelerators and water-reducing agents on mortar mixtures that were cured at -5°C. The results showed that the freezing point of the mixing water decreased to about -5°C when the two admixtures worked together. However, a delaying effect was imparted by the water reducing agent, so that the initial and final setting times were around two hours longer than those of the control mixture. Therefore, the use of a combination of chemical admixtures will depress the water's freezing point but may not speed up the hydration reaction (Arslan et al. 2011).

According to Clause 5.5.4 of CSA A179-14 (2014), the use of accelerators or antifreeze admixtures to develop cold weather admixture systems is currently prohibited in masonry construction due to the risk of flash setting associated with heating the constituent materials and discoloration. In addition, there is still a need for more research on the impact of cold weather chemical admixtures on cement-based materials. Therefore, many studies have been conducted recently to investigate the performance of different cement-based products that incorporate different antifreeze admixtures in order to improve the strength gain of the mortar or concrete at cold temperature (Barna et al. 2011, Karagöl et al. 2013, Karagöl et al. 2015, Kazempour et al. 2017, Saha et al. 2019).

It was reported that the addition of antifreeze admixtures had a positive effect on the mechanical properties of cement-based products (Korhonen et al. 2004b). It was clear that after a 28-day curing period, concrete with antifreeze admixtures gained more strength at the low temperature (-5°C) than the cured control sample at a higher temperature (5°C).

The freeze-thaw resistance of concrete is enhanced by most antifreeze admixtures, although the mechanisms differ among admixtures. Due to leaching, a partial washout of the admixture-related products tends to render the freeze-thaw resistance of antifreeze-added concrete close to normal concrete after a long time under saturated conditions (Ratinov and Rozenberg 1996). The influence of urea and calcium nitrate on the freeze-thaw durability after 28 cycles was studied by Polat (2016). Their use resulted in reductions in compressive strength of 53 percent and 28 percent, respectively, compared to 72 percent for the control sample. It has also been found that the addition of sodium nitrite decreases the pore size in the cement paste, which results in decreasing the foaming strength of the air-entraining agents (Li et al. 2016). Korhonen (2002b, 2006) researched the impact of high-dose admixtures on the freeze-thaw durability and found that the freeze-thaw deterioration mechanism was not stopped by air-entraining agents; they only slowed it down.

Several admixtures can accelerate the cement hydration reaction by different chemical mechanisms (Nmai 1998). Liu et al. (2020) examined the performance of cement mortar at low temperatures using chemical accelerators, such as calcium chloride, sodium nitrite, potassium carbonate, and sodium sulphate. Based on the calorimetry measurement, the chemical admixtures accelerated the hydration reactions. Calcium chloride showed the best acceleration of compressive strength development, followed by sodium nitrite. According to Korhonen (1990), sodium nitrite is relatively effective in accelerating the hydration of cement at

temperatures down to 0°C. Results show that chemical accelerators have lowered both the flexural strength and the compressive strength of mortars (Oey et al. 2015).

Reducing the setting time of the cement mixture decreases the protection time required and reduces the risk of the mixing water freezing. Mortar mixtures set at a slower rate at freezing temperatures, which adversely affects the construction schedule and increases the time and manpower required to complete the job. In cold weather concreting, it is suggested to use additional cement, rapid setting cement or accelerating admixtures to reduce the setting time of the concrete to shorten the protection time (ACI COMMITTEE 306 2016).

Antifreeze admixtures based on calcium chloride, potash, and others, greatly decrease concrete setting time (Ratinove and Rozenberg, 1996). Therefore, these admixtures are used with organic or inorganic retarders when concrete has to be transported over a long distance. According to Ratinove and Rozenberg (1996), the setting time is not greatly affected by sodium nitrite, while carbamide retards setting times. Table 2.2 gives the setting time of cement containing different dosages of sodium nitrite as an antifreeze admixture reported by Ratinove and Rozenberg (1996). It is important to point out that all the performed studies used samples cured at room temperatures, without taking into account the actual effect of the freezing temperatures on the setting times.

Table 2.2 Setting time of mortar containing SN at +20°C (Ratinove and Rozenberg 1996)

Admixture		Portland Cement Setting Time (hr:min)		
Composition	Amount by Mass of Water (%)	Initial	Final	Setting Period Δt
No additive	–	2:50	6:10	3:20
Sodium Nitrite	8	2:35	4:35	2:00
	12	2:56	6:16	3:20
	16	3:18	6:18	3:00
	20	4:00	6:30	2:30

In a recent study, Liu et al. (2020) measured the setting times of cements mixed with 1.5% calcium chloride ($CaCl_2$), 1.0% potassium carbonate (K_2CO_3), 1.0% sodium nitrite ($NaNO_2$), and 1.5% sodium sulphate (Na_2SO_4). The study implies that the setting times were decreased as intended for all the treated samples with 400 min of pre-curing. Calcium chloride, followed by sodium nitrite and sodium sulphate, showed the best acceleration of compressive strength development. The compressive strength of cement mortars cured at 5°C was not affected by the addition of sodium nitrite. The compressive strength of the sample containing calcium chloride was comparable to that of the plain sample, and their time intervals between initial

and final setting were roughly the same. In addition, samples containing sodium sulphate and potassium carbonate had the same setting time and had very similar compressive strength values. A relationship between cracking and strength was suggested by further microstructure studies. In the setting time, shorter setting period (Δt) induced more cracks and decreased the mechanical strength, which was also true for the pre-curing treatment. As a conclusion, the best solution at low temperatures was said to be a chemical able to accelerate the cement hydration reaction while not shortening its Δt during the setting time (Liu et al. 2020).

Saha et al (2019) examined the effect of different sodium nitrite dosages in masonry mortar. The acquired compressive strength of masonry mortars cured at -10°C confirmed the effectiveness of sodium nitrite in depressing the freezing point of the mixing water which made the hydration reaction proceed at the freezing temperature. After noticing the effectiveness provided by the sodium nitrite on the gain of strength, different dosages of sodium nitrite between 2% and 6% were examined, resulting in 5% sodium nitrite by weight of cement to be recommended as the optimal dosage.

Since antifreeze admixtures perform their function by lowering the freezing point of water, determining their dosage by mass of mixing water is a reasonable approach. At the same dosage of admixture by weight of cement, the higher the ratio of water to cement, the less concentrated the solution will be and this will affect the rate of hardening at temperatures below 0°C; such a problem will not take place when the dosage of admixture is specified with respect to the mass of mixing water (Ratinove and Rozenberg 1996). The recommended dosage of sodium nitrite stated by Ratinove and Rozenberg (1996) is 12% by mass of mixing water when the mixture is exposed to a curing temperature of -6°C to -10°C. In the case of a w/c of 0.4, the equivalent dosage of sodium nitrite is 5% by mass of cement, which was the value reported by Saha et al (2019) as the optimal dosage.

The effect of sodium nitrite as an antifreeze admixture on cement paste hydration when cured at -10°C was investigated by Saha et al. (2020), using time domain reflectometry (TDR). TDR was used as a non-destructive technique to monitor the volumetric evolution of water content of the control and antifreeze-added cement pastes. Compared to the control cement paste, mortar with sodium nitrite still had water in liquid form at a -10°C curing temperature. The decreasing amount of water over time implied that the hydration reaction was still proceeding at this temperature.

2.5 Earlier Studies on Bond Strength of Brick Masonry

If a masonry structure is to perform well, the achievement of an effective bond between mortar and masonry units is essential. Bond is affected by different factors including pore water suction within the masonry unit, mortar water retention, mortar components, additive use, and laying methods. If appropriate bonding is not obtained, the mortar joints will act as weak planes, and cracking will take place due to wind, soil movement or minor earthquake shaking. Long-term degradation and unacceptable water ingress through the wall are also probable (Hendry and Khalaf 2001; De Vekey et al. 1989; De Groot 1987).

There have been a large number of investigations into the bond strength of masonry assemblies. Lawrence and Cao (1987) sought to understand the mechanisms for developing the bond between brick and mortar. Such studies showed that the bond was due to the network of concrete hydration products on the surface of the brick and also in the pores of the brick. The initial moisture content in the brick plays a part in absorbing hydration products into the pores of the brick. They claim that the brick-mortar bond is mostly of a mechanical type. Including lime in the cement tends to enhance the hydration product network, but there is insufficient evidence of a change in bond strength.

Scrivener et al. (1992), in Australia, researched the in-situ bond strength of clay brickwork. For such a purpose, they used the bond wrench test at building sites. The mean bond strength was found to vary from 0.21 to 0.85 MPa, with a coefficient of variation from 0.16 to 0.49, respectively. It was revealed that the variation in flexural bond strength could be quite high under field conditions with minimal supervision although the strength values tended to be reasonably high.

The impact of Sri Lanka's high absorption rate, low strength bricks on the brick-mortar bond was investigated by Samarasinghe and Lawrence (1992) through masonry triplets shear test. They observed that partly wet bricks showed greater bond strength than both dry and saturated bricks. The maximum intensity of the shear bond was shown to vary from 0.10 to 0.30 MPa over a wide range. Generally, the intensity of the shear bond decreased as the mortar's compressive strength improved.

Groot (1993) conducted a comprehensive study of the various factors affecting brick-mortar bonding. This study highlighted the importance of moisture transport between mortar and brick in influencing the hydration of cementing materials. The rate of absorption in the brick and the moisture retention in the mortar appeared to play an important role. He also found that the bond

issues in burnt clay brick masonry were mainly caused by the unfavourable ratio of cement to the interfacial zone's fine inert content.

The findings from three experimental studies examining the bond strength of masonry cement (MC) and Portland cement/lime (PCL) mortars were analysed with many types of clay brick and concrete units by Ghosh (1991). The results indicated that PCL mortars showed relatively better bonding strength compared to the MC mortars. It is worth mentioning that there were large variations of bonding strength for different studies even with the use of the same mortar type; this was attributed to the fact that the bonding strength is not just a property of the mortar, but rather a combined property between units and mortar. The unit absorption rate and roughness of the surface, as well as curing conditions, were significant factors in determining the bond strength (Drysdale et al. 1999, Borchelt et al. 1999, and Drysdale and Hamid 2005).

Rao et al. (1996) used a bond wrench test setup to conduct extensive investigations on the flexural bond strength of masonry. In general, the strength of the flexural bond improved with an improvement in mortar strength for cement mortar, regardless of the type of masonry structure. Composite mortars such as a combination of cement mortar and cement lime mortar exhibited better bond strength than cement mortars alone. Brick strength did not significantly affect the strength of the flexural bond. The brick's moisture content (at the time of laying) also significantly influenced the strength of the flexural bond. There was an optimum content of moisture which led to maximum bond strength. Partially saturated bricks with values of moisture content near to moisture content of saturation (80–85 percent) produced the maximum bond strength.

Sarangapani et al. (2005) conducted bond wrench and shear bond tests on prisms made using three different types of bricks and four different grades of mortar. Different bond strengthening approaches were also implemented, leading to an increase in the masonry bond and compressive strengths without altering the content of the mortar. These approaches included coating of the brick surface using cement slurry or Epoxy resin; increasing the frog area; or the addition of lime or soil to cement mortar. The compressive strength of the prism is affected in a noticeable way with the variation in the bond strength. For constant mortar strength, the prism compressive strength increases with the increase in the bond strength.

Reddy and Gupta (2006) examined the bond between cement-soil blocks and cement/soil/sand mortar masonry and observed that the strength of the masonry tensile bond

improved as the compressive strength of the block structure improved. Furthermore, Reddy and Vyas (2008) researched three variations of cement-soil block/mortar combining five different techniques of bond enhancement. If combinations of soft block-stiff mortar were used, the strength of the masonry flexural bond improved in line with the compressive strength of the masonry prisms.

According to Gumaste et al. (2007), improving the bond strength while retaining a constant mortar content and strength resulted in an increase in compressive strength for prisms made of masonry. A four-fold increase in the strength of the flexural bond led to a doubling of the compressive strength of the masonry prisms. It should be noted here that the compressive failure of a masonry prism is often followed by bond splitting of one or more joints when the bond strength is weak. However, prisms will exhibit a diagonal failure through web with the mortar joint intact when the bond strength is quite high. An increase in the compressive strength of the masonry prism was observed with both an improvement in the strength of the flexural bond and an improvement in the strength of the shear bond. This study indicates that the compressive strength of a masonry prism is more sensitive to the strength of the brick-mortar bond than to the compressive strength of the mortar.

Previous studies clearly illustrate that (1) the brick mortar bond is mechanical in nature and forms as a consequence of the interaction of hydration products at the mortar and brick interface; and (2) the brick's moisture content at the time of building has a considerable influence on the brick-mortar bond strength.

2.6 Reinforcing Mortar with Cellulose Nano-fibres

The advancement of nanotechnology in construction materials engineering has made cellulose nanofibres among the most advanced green reinforcing materials due to their high mechanical properties, relatively low cost, and availability. Cellulose nano-fibres (CNFs) are classified as natural fibres that are derived from wood and other plants. The fibrils are separated from any source of cellulose via high pressure, high temperature and high-velocity homogenization, grinding or micro-fluidization (Kafy et al. 2017). In contrast to other nanofibres such as carbon nanotubes, cellulose nano-fibres have more sustainable benefits (Moon et al. 2016). Cellulose fibres have a higher elastic modulus and larger length-to-diameter ratios compared to traditional fibres, making them effective in stabilizing cracks in cementitious materials.

The inclusion of fibres has been shown to enhance the properties of cement-based materials across its characteristics by controlling crack initiation and propagation in response to externally applied stress or environmental deformation caused by thermal or shrinkage strains. The incorporation of fibres in concrete enhances the material's fracture, fatigue and impact properties and can change its response from brittle to ductile. It is also possible to greatly reduce the movement of liquids and gases in concrete and thus significantly enhance the resistance of fibre-reinforced concrete to carbonation and corrosion attacks, resulting in increased resilience and longer service life of concrete structures (Banthia 2009).

Cellulose fibres are expected to increase a cementitious material's toughness and fracture-energy performance, especially when used at the nano size (Bhalerao 2015). Based on previous research (Thomson et al. 2012, Weerawarna et al. 2014, Weerawarna et al. 2015, Youngblood et al. 2016), adding CNFs can provide exceptional increases in flexural and compressive strength, along with improving the microstructure and degree of hydration of the cement paste. The flexural and compressive strengths of cement paste with 0.15 percent CNFs were found to be 15% and 20% higher than the control paste, respectively (Jiao et al. 2016). Including only 0.2% CNFs by weight of cement can also improve the performance of cement paste by enhancing the flexural strength by roughly 30% (Bhalerao et al. 2015).

The effect of using cellulose nanofibres produced from plant-derived cellulose as reinforcement in ultra-high-performance (UHP) mortar was investigated in a recent research study (Supit and Nishiwaki 2019). The effect of using different doses of CNFs, including 0.05 percent, 0.1 percent, and 0.15 percent by weight of binders (premixed low-heat cement and silica fume) with a fixed water-to-binding ratio of 0.15, was measured on the basis of compressive and flexural strengths on the seventh day after steam curing. The use of 0.05 percent CNFs relative to plain UHP mortar resulted in an increase in the compressive strength. The compressive strength was 184 MPa, approximately 8 percent higher than the control mortar and about 4-8 percent higher than 0.1% and 0.15% CNF mortars, respectively. Nevertheless, raising the volume fraction of CNFs tended to decrease the compressive strength. This was attributed to reactions in cellulose molecules between the hydroxyl and carboxyl groups with Ca^{2+}, which can delay the initiation period of hydration and setting time, as well as to an increase in the porosity and agglomeration of CNFs, which diminishes the bonding interfaces and encourages stress concentration.

De Pellegrin et al. (2019) measured the impact of including cellulose nano-fibres on the mechanical properties of fibre-reinforced mortar composites. Only the volume of fibre was found to produce statistically significant changes to compressive strength, having a negative impact; that is, lower fibre content resulted in greater compressive strength. Among the variables tested for flexural strength, the fibre length and volume fraction together were found to have a significant effect.

The cement paste pore size decreases with increasing CNF content. The swelling of CNFs due high-water adsorption properties allows the release of water to promote hydration of un-hydrated cement particles, which can form more cement hydrates and reduce the macro-pores or micro-pores. This results in smaller pores, and the porosity of cement pastes has been observed to decrease with a modest addition of CNFs (Jiao et al. 2016). The addition of cellulose nanofibres to concrete equivalent mortar (CEM) tend to improve workability and reduce agglomeration during mixing (Nilsson and Sargenius 2011).

Reinforcement of cement mortar with cellulose nano-fibres was observed to decrease the water absorption significantly. The addition of a low volume fraction (0.1%) of CNF is effective in decreasing the water absorption while the use of 0.3% CNF showed the minimum water absorption. Thus, the durability of cement mortar structures can be enhanced by the proper use of cellulose nano-fibres (Akhlaghi et al. 2020).

Multiple researchers have proven the effect of nanocellulose on cement hydration. Shuzhen et al. (2011) were among the first to report that the inclusion of nanocellulose accelerated CSH production during cement hardening. Hoyos et al. (2013) examined the hydration reaction of cement through thermogravimetric analysis and demonstrated that the use of nanocellulose increased the hydration rate during cement paste curing. Onuaguluchi et al. (2014) clarified this effect in terms of internal curing as nanocellulose tends to retain water at early ages and release it later. In 2016, Osong et al. stated that the higher surface area of CNF and CNC acts as nuclei to foster the nucleation of hydration product crystals at the early stages of cement hardening. The addition of nanocellulose to cement mixtures is believed to accelerate the cement hydration process, and increase flexural strength (Fu et al. 2017). With cellulose nanomaterials, the concrete's mechanical properties and fracture characteristics can be improved by arresting micro-cracks produced during hydration and preventing their further growth.

2.7 Masonry Assemblage Strengths and Properties

2.7.1 Overview

Masonry structures are estimated to have been in use for more than 6000 years; therefore, masonry is claimed to be the oldest building material known to human history. Masonry consists of two distinct materials: the masonry units and the mortar phase. Masonry units can be solid or hollow and can be manufactured using a wide variety of materials. A weak interface connects the two material phases in masonry; therefore, masonry is normally weak in resisting tensile load. The conventional design practice emphasizes that masonry structures are subjected to compressive stresses alone and therefore it is important to accurately assess the compressive strength. Empirical values for the strength of a masonry assembly are proposed in different standards based on the unit strength and properties of mortar. Alternatively, masonry specimens can be constructed and tested in order to provide a more reliable value for the compressive strength.

The compressive strength of masonry assemblies is evaluated in the laboratory by testing prisms, wallettes, or wall panels. Prisms and wallettes are built as small assemblages of masonry units with a thickness of one to three units for prisms and having a width of three or more units for wallettes, as illustrated in Figure 2.2. Masonry wall samples are close to real walls and have greater heights than prisms and wallettes. Using masonry wall specimens in testing is very costly and it is, therefore, preferable to test prisms to determine the strength of masonry. Prisms are a good reflection of the real construction of masonry as it involves the effects of the properties of the masonry constituents and the nature of workmanship.

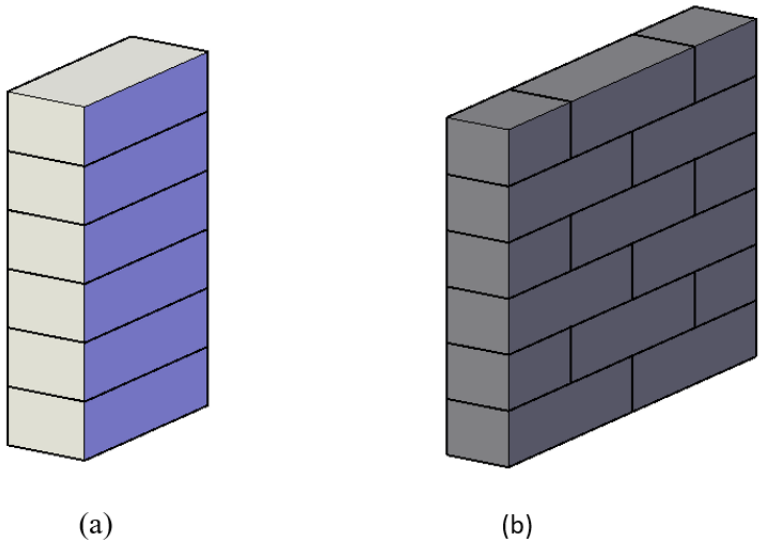

Figure 2.1 Masonry assemblies: (a) Prisms, and (b) Wallettes

Masonry assemblies consist of masonry units, mortar, and grout if the assemblage is grouted. To understand the fundamental behaviour of masonry, knowledge of the interaction between these materials and other factors influencing the physical and mechanical properties of the composite are required.

2.7.2 Construction of Prisms

Prisms are constructed from the same components that will be used to build the wall and are used to estimate the properties of the wall. In other words, in prism construction, the brick or hollow units, sand and cement, mortar mix, and grout (if necessary) should be the same as the materials to be used in the structure. In addition, the bedding of the mortar, the thickness, the grouting, and the quality of the units should be the same as those used in the wall construction, but there should be no reinforcement (ASTM International 2016).

Prisms are to be built on a level base and in a moisture-tightened open plastic bag, big enough to completely cover the completed prism. The prisms must be built at a place where they will stay undisturbed until they are relocated or moved for testing. Where the cross-sections of the units differ due to architectural surfaces or cell taper, the same placement must be used as stated in the construction of a project. The prisms should be kept undisturbed in the plastic bags for at least 48 hours after construction and grouting (ASTM International 2016).

2.7.3 Factors Affecting Masonry Compressive Strength of Ungrouted Masonry

Compressive strength is the most important mechanical property of masonry, similar to reinforced concrete, because it is the property most closely linked to load resistance, serviceability, and durability. Compressive strength of masonry, stress-strain behaviour, and modulus of elasticity are obtained through direct compression testing of prisms to failure. The compressive strength of the assembly, f'_m, differs from that of individual units due to the presence of mortar (Drysdale and Hamid 2005). The analysis of the existing database shows that the compressive behaviour of ungrouted masonry prisms is influenced by different parameters, at both material and specimen levels. Among these, the strength of the unit, the strength of the mortar, the kind of bedding, and the ratio of height to thickness are the most important factors.

2.7.3.1 Effect of Unit Compressive Strength (f_{bl})

Research evidence (Chahine and Drysdale 1989, Khalaf et al. 1994, Gayed et al. 2012) has shown that the compressive strength of masonry prisms increases as the compressive strength

of the unit (f_{bl}) increases. The relation between prism strength and block strength is roughly linear within the range of typical block strengths (10–30 MPa).

Researchers around the world have proposed various models with different parameters to predict the compressive strength of masonry. In 1982, Mann (1982) performed tests on specimens with a slenderness ratio equal to five using solid and hollow brick masonry units made of different materials. A model was proposed based on the results to predict the compressive strength of the masonry assemblage using the strength of the masonry unit and the mortar. Dayaratnam (1987) proposed a model that gives equal importance to the compressive strengths of brick and mortar. A series of experiments on structural clay tile prisms were performed by Bennett et al. (1997) and an equation was proposed for estimating prism strength using masonry unit strength. After conducting a regression analysis, Dymiotis and Gutlederer (2002) developed a set of second-order polynomial equations and proposed a model accounting for the compression strengths of the mortar (f_{mr}) and brick (f_{bl}). In total, 84 masonry prisms were tested using four types of bricks and three types of mortar by Kaushik et al. (2007). A linear regression model was proposed taking into account the compressive strengths of bricks and mortar. Tests on 45 masonry prisms made with vintage clay bricks removed from existing buildings in New Zealand were performed by Lumantarna et al. (2014) to study the compressive behaviour of existing masonry buildings. A regression model that included brick and mortar compressive strengths was proposed to predict the masonry compressive strength. Table 2.3 presents the various mentioned prediction models and the parameters considered in each model. The brick compressive strength and mortar compressive strength in these models are in MPa. Based on the different prediction models, it can be stated that the unit compressive strength (f_{bl}) plays a major role in estimating masonry compressive strength.

Table 2.3 Prediction models for masonry compressive strength

Reference	Model
Mann 1982	$f'_m\,(MPa) = 0.83\ {f_{bl}}^{0.66} \times {f_{mr}}^{0.18}$
Dayaratnam 1987	$f'_m\,(MPa) = 0.275\ {f_{bl}}^{0.5} \times {f_{mr}}^{0.5}$
Bennett et al. 1997	$f'_m\,(MPa) = 0.3\ f_{bl}$
Dymiotis and Gutlederer 2002	$f'_m\,(MPa) = 0.3266\ f_{bl} \times (1 - 0.0027\ f_{bl} + 0.0147\ f_{mr})$
Kaushik et al. 2007	$f'_m\,(MPa) = 0.317\ {f_{bl}}^{0.866} \times {f_{mr}}^{0.134}$
Lumantarna et al. 2014	$f'_m\,(MPa) = 0.75\ {f_{bl}}^{0.75} \times {f_{mr}}^{0.31}$

2.7.3.2 Effect of Mortar Strength (f_{mr})

In the construction of masonry, mortar acts as a key component for bonding individual units into a composite assembly and providing uniform bearing between units. Mortar is commonly classified in North America as types M, S, N, O, and K. Masonry construction in Canada recognizes only the type S and N mortars. Extensive testing (Mohamad et al. 2007, Barbosa et al. 2010, Gayed et al. 2012) has shown that the strength of the mortar (f_{mr}) and its type determines f'_m. Higher mortar strength results in a lower level of induced lateral tensile stress, which is the main cause of prism failure in masonry (Khalaf and Hendry 1994). Khalaf (1996) studied the effect of different mortar strengths on hollow and grouted prisms. Khalaf reported a noticeable increase in the prism compressive strength with an increase in the mortar compressive strength for the hollow prisms, whereas in the grouted prisms there was no significant difference with different mortar strengths.

2.7.3.3 Mortar Joint Thickness

Many studies have reported the significant impact of joint thickness on the compressive strength of masonry assemblages. Khalaf (1996) performed experiments on prisms with various joint thicknesses, and he noted a reduction in the compressive strength of the hollow and the grouted prisms when the mortar thickness was increased from 5 cm to 20 cm. Hollow prisms showed a larger reduction in the compressive strength compared to the grouted prisms. The effect of joint thickness was also studied by Drysdale and Hamid (1979) through prism tests, and their findings were in conformance with those of Khalaf (1996). The reduction of the compressive strength was reported to be 3% for grouted prisms, and 16% for hollow prisms (Khalaf 1996). These studies revealed that the thickness of the mortar joint has some effect on hollow prisms while it has almost no effect on grouted prisms.

2.7.3.4 Effect of h/t

The ratio of the height of a prism to its thickness (h/t) is well known to influence its compressive capacity. Many researchers (e.g., Maurenbrecher 1978, Wong and Drysdale 1985) have observed that the compressive strength diminishes as h/t increases, although the effect of h/t becomes marginal above a certain height. This reduction in strength can be attributed to the decreasing impact of platen restraint (Das et al. 2013), while Maurenbrecher (1978) and Page and Shrive (1988) report that the effect of h/t on block prisms depends on whether full or face shell bedding is used in prism construction. Other researchers (Das et al. 2013), on the other hand, reported that the compressive strength of ungrouted masonry prisms decreases by increasing the h/t ratio regardless of the type of bedding when using high-resistance capping.

The effect of h/t is expressed in various masonry codes by the use of correction factors to convert the measured *f'm* to a standard h/t value. Correction factors for the compressive strength of masonry prisms (Canadian Standards Association 2014) are presented in Table 2.4.

Table 2.4 Correction Factors for the Compressive Strength of Masonry Prisms (CSA S304-14)

h/t	2.0	3.0	4.0	5.0
Correction Factor CSA S304-14	0.85	0.90	0.95	1.00

2.7.3.6 Failure Modes

Many researchers have discussed the failure modes for concrete masonry prisms (Wong and Drysdale 1985; Drysdale and Hamid 1979; and Mohamad et al. 2007). For hollow block prisms, conical shear failure due to the end-restraint effect is the standard failure mode for two-course high prisms. When the number of courses is three or more, the top and bottom blocks will still experience shear failure, as is the case for two-course high prisms. However, the prism's main body failure mode (mid-height) changes. Initial splitting of cross webs has been observed during loading caused by bending stresses due to deep beam action. This may be preceded by a splitting of the face shell under a higher compressive load.

The failure mode of solid masonry during compression is well identified and known from previous studies. The incompatible elastic characteristics of unit and mortar cause cracking parallel to the direction of compression force in the masonry units or mortar (Thaickavil and Thomas 2018, Thamboo and Dhanasekar 2019).

2.7.3.7 Testing Procedure

In CSA S304-14, Annex D sets out normative criteria for evaluating the compressive strength and modulus of elasticity of masonry prisms; testing equipment, test specimens, test procedures, and reporting for prism tests are defined. A typical prism is usually one masonry unit wide, one unit thick, and can be built up to different heights (typically between two and five times the thickness). Different types of units and mortar joints may be used for prism construction. A key characteristic of prism testing is the mechanism of load transfer at the top and bottom of the prism. This involves capping to provide flat bearing surfaces and thick loading plates to evenly disperse the load to the specimen.

This method allows f'_m to be calculated from experiments on masonry assemblages. The research protocol is illustrated in S304-14, Annex D. The compressive strength of each

specimen is determined by dividing the failure load at an age of 28-days by the effective cross-sectional area. At least five specimens must be tested. The test prisms must have a height-to-thickness ratio (h/t) greater than two to produce the vertical splitting failure mode experienced for full-size masonry walls under compression (Canadian Standards Association 2014).

2.7.4 Flexural Tensile Strength

Masonry is constructed primarily to withstand compressive gravitational loads. Due to its low tensile strength, which is essentially determined by the bond between the units and the mortar, masonry is never designed primarily to resist pure tension. In reality, due to eccentricity, gravitational force rarely acts through a centroidal axis on the wall and therefore creates some flexural stresses. There are also situations where masonry is required to withstand flexural stresses under wind pressure acting on exterior walls. Therefore, it is essential to address flexural resistance.

The flexural tensile strength, f_t, also referred to as the modulus of rupture, is the most influential parameter which directly affects the resistance to flexural load. As shown in Table 2.5, the flexural tensile strength depends on the orientation of the flexural tensile stresses with respect to the bed and head joints. Together with other physical properties such as the initial rate of absorption, the strengths of the mortar and masonry units determines the mode of failure and affects the value of f_t. Table 2.5 lists the specified f_t values for different types of hollow and solid or grouted units built using mortar types S and N, as given in S304-14 (Drysdale and Hamid 2005).

Table 2.5 Specified flexural tensile strength, f_t (CSA S304-14)

	Normal to bed joints (MPa)		**Parallel to bed joints (MPa)**	
Unit type	**Mortar Type**		**Mortar Type**	
	S	**N**	**S**	**N**
Concrete brick and block	**0.40**	**0.30**	**0.80**	**0.55**

Rao et al. (1996) used a bond wrench test setup (CAN/CSA A3004-C9) to perform thorough studies of the flexural bond strength of masonry. The principal findings of this study are: 1) In general, the strength of the flexural bond increases with an increase in mortar strength for cement mortar, irrespective of the form of masonry unit; 2) Composite mortars such as combinations of cement mortar and cement lime mortar demonstrate stronger bond strengths

than cement mortars alone; and 3) The brick's moisture content at laying time, had a significant influence on the strength of the flexural bond.

2.7.4.1 Test methods

The bond strength between masonry units and mortar has been of great interest to researchers. In particular, the flexural bond strength of masonry is necessary for the design of masonry walls subjected to horizontal forces such as wind. To evaluate the flexural bond strength, researchers and standards have proposed various types of specimens and test procedures. These include tests on small walls, the beam test, and the bond wrench test.

Small wall tests

The testing of small brick/block wall specimens (wallettes) under four-point loading is defined by BS 5628 (British 1992) as a standard test for the determination of the flexural bond strength of masonry bed joints, as shown in Figure 2.2. The tested specimens do not give the direct tensile bond strength, but many engineers consider it to be of practical value. An index of wall strength derived from its flexural performance is given by the test. The problem with the BS 5628 test is the large specimen necessary for the test and the design of the test, which makes it difficult to perform.

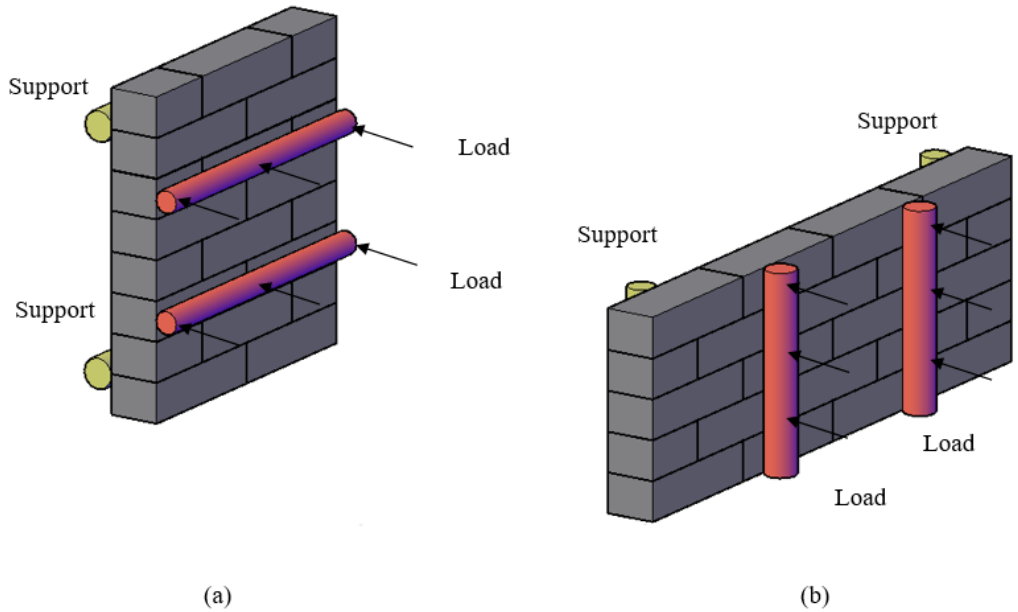

Figure 2.2 Testing arrangement of four-point loading on wallettes: (a) plain of failure parallel to bed joints, and (b) plain of failure normal to bed joints

Beam test

ASTM E518 describes beam tests of stack-bonded prisms with a height of at least 450 mm and either third-point loading or uniformly distributed loading. The beam test is used to determine flexural bond strength. For the third-point loading application, two steel supporting bars are used to stabilize the prism (hinge support and roller support), as shown in Figure 2.3. On the upper surface, the load is applied through two bars. At a constant rate, the load is applied evenly between the two bars until failure.

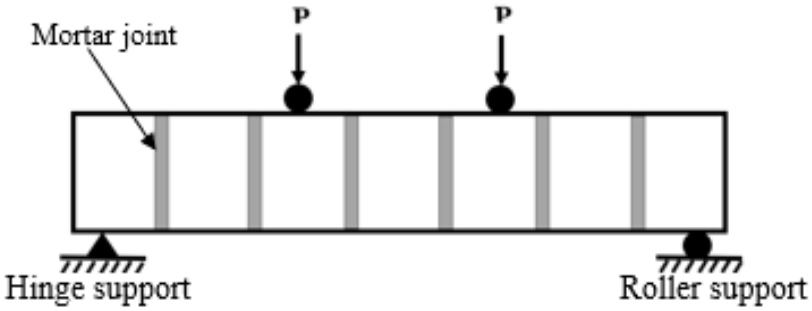

Figure 2.3 Third-point loading

Bond wrench test

For many years, a bond wrench test developed in Australia has been in use for laboratory bond strength testing, as a quality control method for newly constructed masonry, and for in situ measurement on existing structures. The test is defined in the Australian Code of Practice AS 3700 (Australian 1998). The use of the bond wrench test in the laboratory is now covered in the United States by ASTM Standards C1072 (ASTM 2000). In Canada, the bond wrench method is described in CSA S304-14 (Annex E). The bond wrench test, a schematic of which is shown in Figure 2.4, was developed to provide a larger set of data in which each joint of a prism is tested. Testing all the joints eliminates the beam test bias of recording the weakest joint as the bond strength of masonry.

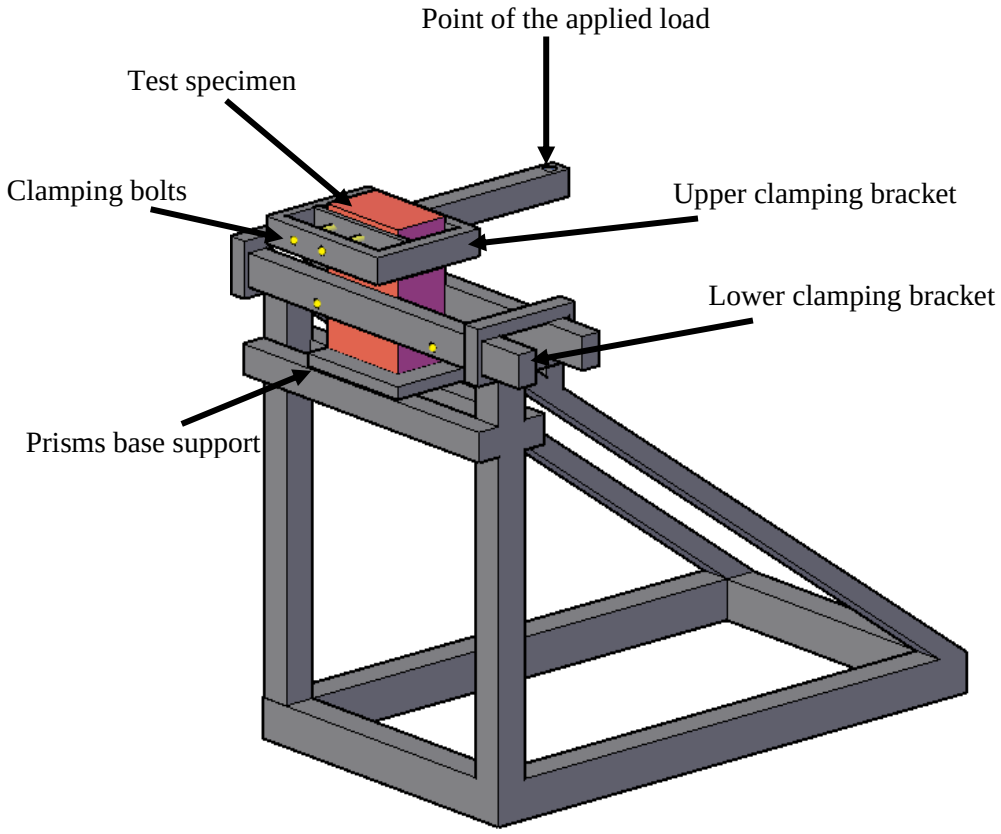

Figure 2.4 Bond wrench testing apparatus (CAN/CSA A3005-13)

There has been a considerable amount of research on the flexural tensile strength of ungrouted masonry (Radcliffe et al. 2004, Khalaf 2005, McGinley and Greenwald 2005). For bond wrench tests, more data are available than for full-scale or smaller-scale wall panels. Instead of larger units, most of the studies have been performed with bricks (concrete or clay). Moreover, it was indicated in some of the literature (Harris 2010) that only full-scale wall or smaller-scale wall panel testing should be used in determining the flexural bond strength, suggesting that bond wrench tests be used for comparative purposes only.

According to ASTM C1072 (ASTM 2013), the bond wrench test is intended to provide an easy and cost-effective means of evaluating the comparative values of flexural bond strength. The bond strengths evaluated from this test can be used as a means of evaluating the compatibility of mortars and masonry units. It is not acceptable to interpret the flexural bond strength calculated by this test method as the flexural bond strength of a wall built of the same material. This can be explained by the fact that there is no universally accepted configuration for the test setup, and by the relatively high variability in bond strengths results from this test. However, results can be used to predict the flexural strength of a wall. It is generally considered more acceptable to determine the flexural strength using full-scale wall panels (Harris 2010).

2.7.4.2 Failure Modes

Masonry bond strength research was carried out using different mortars and flexural tests using a modified ASTM C1072 bond wrench test by Sarangapani et al. (2005). Three categories of flexural prism failures were observed in the study, based on the results obtained. Type 1 is a bond failure that is characterized by brick-mortar interface failure. Type 2 is a failure within the brick material. Type 3 is a combination of type 1 and type 2 failures.

2.8 Summary

When exposed to cold conditions during construction and curing in autumn, winter, and spring, the performance of masonry assemblies may be affected. This means that the process of building masonry structures at cold temperatures is a major challenge for contractors in North America as well as other cold geographical locations.

In this chapter, many investigations were presented which have been undertaken to reduce the reported negative effects of freezing curing temperature on cement-based products through the use of accelerators, antifreeze agents, or combinations of both (cold-weather admixture systems). Based on the findings of Saha et al. (2019), the primary focus of the current study was on the effect of sodium nitrite in the Type S mortar joints on the mechanical properties of masonry assemblages cured at -10°C after being pre-cured at room temperature for 4 hours. The incorporation of nanocellulose in this study was motivated by its potential ability to increase the bond strength in masonry assemblages, since the literature review indicated that antifreeze admixtures such as sodium nitrite may lower the bond strength.

For the purpose of this study, two types of experiments were performed on masonry prisms. The first test was the compressive test to assess the compressive strength and failure behaviour of the assemblies. The second test was the flexural bond strength test using the bond wrench method described in CSA A3004-C9.

3 EXPERIMENTAL PROGRAM

3.1 Overview

For the purpose of this study, two experiments were performed on masonry prisms constructed with four different kinds of mortars and cured under both sub-freezing and room temperatures. The first test was the compressive test to assess the compressive strength and failure behaviour of the assemblies. The compressive strength depends on the mortar properties, the mortar bedded area, and whether or not the blocks are grouted, in the case of block prisms. Because the purpose of the study was to determine the effectiveness of anti-freeze admixtures in the mortar, only the type of mortar varied among specimens, with full bedding joints in six unit high brick prisms used for all tests. The second test was the flexural bond strength test using the bond wrench method described in CSA A3004-C9. The tensile bond strength between the masonry units and the mortar depends mainly on the type of mortar and the constituent materials. In addition, a number of companion tests and fresh mortar property tests were performed.

3.2 Mortar Materials and Properties

3.2.1 Materials and Preparation

A ready mixed Type S mortar cement provided by Spec mix company (with lime content) with fine aggregate was used, due to its regular use in cold areas. The admixtures included sodium nitrite, as used by Saha et al. (2019), and nanocellulose fibres, neither of which have been documented to damage cement-based materials. The dosage of sodium nitrite was 12% by mass of mixing water, as recommended by Ratinove and Rozenberg (1996). The dosage of CNF was 0.3% by mass of cement, selected because it has resulted in the minimum water absorption and maximum enhancement of flexural strength of mortar (Akhlaghi et al., 2020). The sodium nitrite powder was obtained from the chemistry store at the University of Saskatchewan. The nanocellulose used in this study was provided by Blue Goose Biorefineries, located in Saskatoon, Saskatchewan.

The mortar was prepared in a 20 L Hobart cement mixer following the mixing method specified in the Text Book of Canadian Masonry (CMCA 2010). As specified by this process, first, three-quarters of the water was poured into the mixing bowl, and the mixer was started at low speed. Half of the mortar cement ready-mix was added and then the remainder of the mortar cement mix quantity was added gradually as mixing continued. After mixing for another two minutes, the mixer was stopped and the sides of the bowl were scraped. When the mixer was restarted, half of the remaining water was added before, and half after, the remaining mortar cement ready-mix was added. Mixing continued at medium speed for three further minutes, resulting in a total mixing time of about 12 minutes. When sodium nitrite was used, it was added to the mixing water and mixed completely in it before the water was poured into the mixing bowl. When nanocellulose was used, it was added to the dry mortar cement ready mix and dispersed into the mix using another 10 L Hobart mixer, then by a trowel, and then again in the mixer in order to make sure a uniform distribution of the nanocellulose was achieved.

Table 3.1 lists the four types of mortars tested in this study, defining batch labels for later reference, mix proportions, and curing conditions.

Table 3.1 Mortar ingredients, mix proportions and curing conditions

Batch Label	Ingredients	Proportions	Curing Temperature (°C)	Curing Period (Days)
Ctr	Ready mix Mortar cement and sand	cement-to-sand volumetric ratio 1:3	-10°C and +23°C	28
	Water	60%		
SN	Ctr + $NaNO_2$	12% $NaNO_2$ by mass of water	-10°C and +23°C	28
NC	Ctr +CNFs	0.3% CNF by mass of cement	-10°C and +23°C	28
NN	SN+CNFs	12%+0.3%	-10°C and +23°C	28

3.2.2 Flowability of Fresh Mortar

The flowability of the fresh mortars was determined using a standard flow table and following the procedure specified in CSA A3004-C1-13 (CSA 2013c). Water was added to get the flowability to fall within the specified limits (110±5%). The cone mould was placed at the centre of the flow table and loaded with the mortar mixture. Afterward, the mould was removed

and the mortar table was dropped. Then, the diameter increase was measured in four directions as shown in Figure 3.1. The measured lengths were averaged and reported. The precision of the flowability measurements was $\pm$0.1mm.

Figure 3.1 Flow of masonry mortar mixture

3.2.3 Air Content of Fresh Mortar

The air content of fresh mortar mixtures was determined according to CSA A3004-C4-13 (CSA 2013d) using three replicate tests for each mixture. Following the standard, the mass and density of the different ingredients including the admixture mass (which is not included in the standard equation) were taken into account according to the following equation for measurement of the air content:

$$D=\frac{Cement\ mass+Sand\ mass+Water\ mass+Admixture\ mass}{\frac{Cement\ mass}{CD}+\frac{Sand\ mass}{SD}+\frac{Water\ mass}{WD}+\frac{Admixture\ mass}{AD}} \quad [3\text{-}1]$$

where:

D = density of the air-free mortar

CD = cement density = 3.15 g/cm^3 according to CSA A3004-A2-13

SD = sand density = 2.65 g/cm^3 as stated in CSA A3004-C4-13

WD = water density = 1.00 g/cm^3

AD = admixture density for Sodium Nitrite = 2.18 g/cm^3 according to the data sheet provided by the chemistry store, or Nanocellulose = 1.60 g/cm^3 according to data sheet provided by Blue Goose Biorefineries.

The mortar was placed gently in the 400 mL container in three equal layers as described in CSA A3004-C4-13 (CSA 2013d). Each layer was tamped 20 times with the tamper. After the container had been filled and tamped, the sides of the container were tamped lightly five times with the tamping stick. The excess mortar was struck off with a steel straightedge. The entire operation was accomplished within 1.5 minutes. All mortar and water that had adhered to the outer surface of the container were wiped off before weighing the container. The mass of the container was subtracted from the total and the mass of the mortar was reported in grams. The air content was then calculated according to the following equation:

$$A = 100 - \frac{M}{4D} \qquad [3\text{-}2]$$

where:

A = percentage of air content

M = mass of mortar, g

D = density of the air-free mortar

3.2.4 Air Content of Hardened Mortar

Since the compressive strength of masonry mortar is highly affected by the air content in its hardened state, an air content analysis was performed for the hardened mortar to assess the effect of incorporating sodium nitrite and/or nanocellulose. The method used in this study is known as the Flatbed Scanner Method (Figure 3.2). This method is not new; it was introduced by Peterson et al. (2001). This method has the advantage of replacing the microscope and mechanical stage required by the traditional approach with a high-definition flatbed scanner; a personal computer can take the place of the microscopist and tally counter.

Figure 3.2 Air content for hardened concrete test set up

Six mortar cylinders for each mortar group were prepared and cut horizontally in half using a water-cooled diamond saw, as seen in Figure 3.3. After cutting, a series of polishing steps were carried out on the cut surface using nominal grit sizes of 35, 17.5, and 12.5 μm. Polishing was performed using hand pressure on a vibrating-polishing table, as shown in Figure 3.4.

Figure 3.3 Water-cooled diamond saw

Figure 3.4 Vibrating-polishing table

The polished surface of a sample was painted black using a wide tipped black permanent marker, and the air voids were filled with lime. This process is known as contrast enhancement. It is important since it allows for easy distinguishing of the air content present in the mortar. Figure 3.5 shows a scanned surface of the sample after the contrast enhancement process and prior to any image analysis.

Figure 3.5 Scanned image of the sample after the contrast enhancement

After the contrast enhancement process, the surface of the mortar cylinder was scanned using a high-definition scanner (Epson V750 PRO). The flatbed scanner used in this test was the same one used by Song (2017); therefore, the threshold value was calibrated with the use of the concrete slabs that were used in his study. Moreover, as another check for the threshold value, the values attained by the flatbed scanner method were compared to the fresh mortar air content results according to CSA A3004-C4-13. Image analysis of the scanned images was performed using the freely available software known as Bubble Counter, coded at Michigan Technological University. The area fraction of white pixels was calculated as well as the total area in order to calculate the air content for each sample. Finally, the output of the image analysis was opened in Microsoft Excel for further processing.

3.2.5 Setting Time Test

The setting time test was performed according to CSA A3004-B2-13 (CSA 2013) using the Vicat apparatus shown in Figure 3.6. Three different samples of mortar for every mortar group were placed in stainless steel test containers and tested by determining the penetration depth caused by a 1 mm needle every 15 minutes. The initial setting time corresponded to a penetration depth of 25 mm or less. After obtaining the initial setting time, subsequent penetrations were performed at 15 minutes time intervals until the 1 mm needle did not sink visibly in the mixture, which was defined as the final setting time. During the test, the Vicat apparatus was free of vibration, and the needle was clean and straight for every penetration to ensure the accuracy of the setting time curves produced from this test. These tests were performed for each mortar group when cured at room temperature, and also when cured at -7°C. The relative humidity for both curing conditions was measured using OMEGAETTE

HH311 humidity temperature meter. The relative humidity at room temperature was 29%. The precision of the relative humidity measurement was ±2%. For the freezing curing condition, specimens were placed in a Maytag freezer with a digital thermal calibration sat at -7°C, with a relative humidity of 90%. The freezer temperature was also checked using RS7 Digital Thermometer Infrared. Each specimen was removed from the freezer for testing for a 1 minute duration, then returned immediately to the freezer.

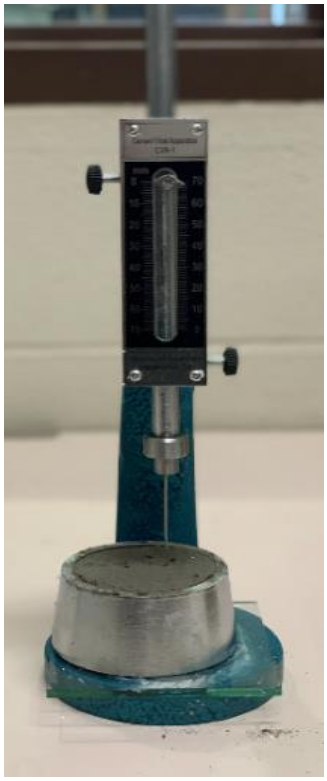

Figure 3.6 Vicat apparatus

3.2.6 Compressive Strength of Mortar Cubes

The compressive strength of twelve mortar cubes per batch was determined at 28 days according to the approach specified in CSA A3004-C2-13 (CSA 2013) using an Instron 600 DX universal testing machine. Mortar was poured into brass cube moulds made with a side length of 50 mm, conforming to CSA A 179-14 (CSA-Masonry-Standard, 2014), in two equal layers that were tamped uniformly 32 times in four rounds. Prior to casting the mortar cubes, the flow test was carried out to decide the amount of water to ensure the mortar flow reached 110±5%, as specified by CSA A3004-C2-13. The required quantity of water for 21 kg of Type S dry mortar ranged from 3.2 to 3.7 L. The mortar cubes were prepared at room temperature in the structural lab. Mortar cubes were removed from moulds after 24 hours of casting them. Twelve mortar cubes were made for each mortar mix batch; six of them were tested after

28 days of curing at room temperature covered by plastic sheet immediately after moulding to provide a moist environment, and the other six were cured for four hours at room temperature then they were transported to the environmental chamber located in the Chemical Engineering Department to be cured at -10°C and then tested on the prism-test day (28 days). The testing speed was set at 8 MPa/min for most of the samples, except that the speed was reduced to 1 MPa/min for the control and nanocellulose mortar samples cured at -10°C for 28 days of curing due to the expected low compressive strengths in these samples. Mortar cubes were centred and any loose sand grains or incrustations were removed from the faces that were in contact with the bearing plate to ensure a uniform load distribution on the mortar surface due to surface irregularities, as shown in Figure 3.7. The specimen was placed such that the load was applied to a surface that had been cast against the side surface of the mould. The precision of the measurements was $\pm$0.1 MPa.

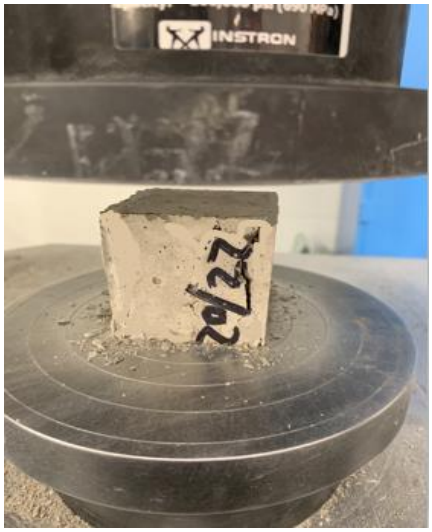

Figure 3.7 Mortar cube for compression testing

3.3 Brick Properties

3.3.1 Material and Dimensions

The brick masonry units used in this investigation were made from concrete with standard dimensions of 190 x 90 x 57 mm (L x W x T) provided by Expocrete in Saskatchewan, Saskatoon. The bricks were hollow concrete bricks with 18.8% voids.

3.3.2 Water absorption

The water absorption value of bricks is highly dependent on the raw material that was used to produce them. Higher water absorption is an indication of a higher number of pores in the brick, which will be easily filled with water. The distribution of pore sizes and their spacing is an important factor in determining the resistance of bricks to freeze-thaw cycles.

Five brick specimens from each pallet were chosen randomly to perform the water absorption test. The received mass of each specimen was recorded in kg as W_r by weighing the brick with its delivered condition. The precision of the reported measurements was $\pm$0.001 kg. Then, the test specimens were immersed in water at room temperature of 25$\pm$2°C for 24 hours. As illustrated in Figure 3.8, specimens were separated from each other and from the bottom of the tank as required by ASTM C140 by using metal wires. The green colour shown in Figure 3.8 is due to light reflection. The water used was regular Saskatoon tap water without any added chemical substance. After 24 hours of immersion, the specimens were weighed while suspended by the metal wire while they were completely submerged in water and the immersed mass was recorded in kg as W_i. Subsequently, bricks were removed from the water and drained for 60$\pm$5 s, then they were weighed and their mass recorded as W_s. After that, all specimens were dried in the ventilated dry oven located in the Geotechnical Engineering Lab at 105°C for 24 hours, after which they were weighed and mass recorded as W_d.The water absorption was calculated using the following equation:

$$Absorption,\ \% = \frac{(W_s - W_d)}{W_d} \times 100 \qquad [3\text{-}3]$$

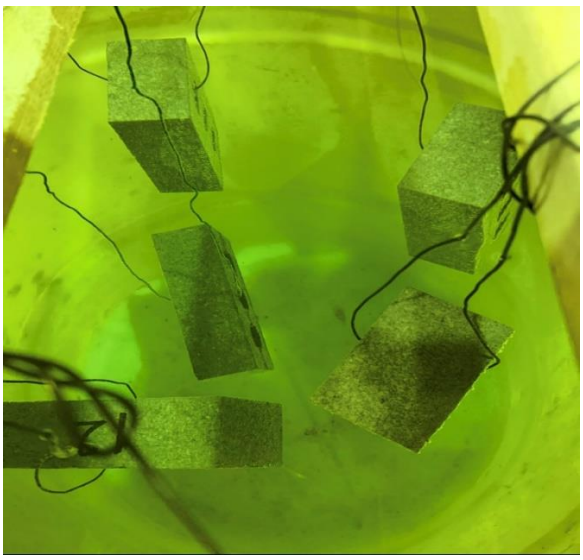

Figure 3.8 Bricks immersed in water, suspended by wires

3.3.2 Initial Rate of Absorption

The initial rate of absorption (IRA) represents the amount of water absorbed over a period of one minute by the bed area of the brick. The initial rate of absorption is one of the brick's critical properties since it affects its bond with the mortar and grout. As a result, the IRA has a direct effect on the durability of the final materials. The IRA for the bricks was measured using bricks that had been oven-dried for 24 hours at 105°C using the ventilated dry oven located in the Geotechnical Engineering Lab. Five full-size specimens were tested per pallet as required by ASTM C67. The results were reported in grams of water gained per cm^2 when the brick was soaked in 3 mm of water for 1 min, as illustrated in Figure 3.9.

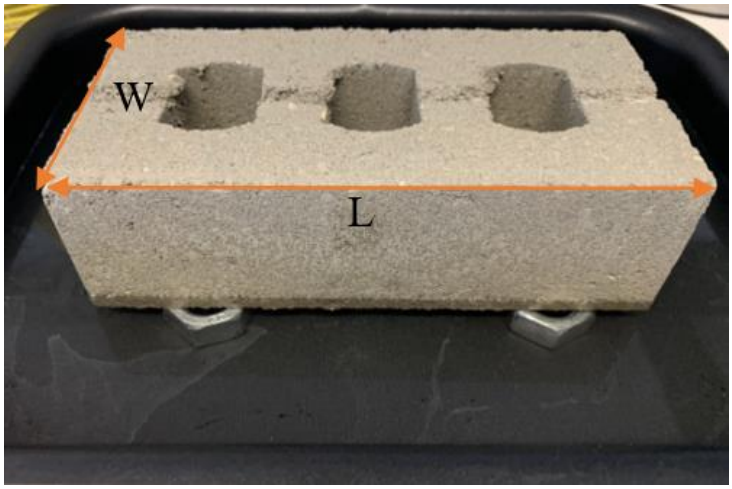

Figure 3.9 Brick being soaked in 3 mm of water

The calculation of IRA was performed according to the following formula with a precision of ± 0.0001 g/cm^2/min:

$$IRA = \frac{W_W - D_W}{L \times W \times (1 - void\%)} \quad [3\text{-}3]$$

where:

W_W = is the mass of the specimen in grams after one minute of soaking,

D_W = is the mass of the specimen in grams after being oven-dried for 24 hours,

L = length of specimen in cm, and

W = width of specimen, in cm.

3.3.3 Brick Compressive Strength

To ascertain the compressive strength of the bricks, 14 bricks were selected randomly, then capped using sulphur capping compound on the top and bottom of the brick according to ASTM C140 (ASTM 2021) and tested under axial compression. The manufacturer reported a specified compressive strength of 55 MPa. Testing of the bricks was performed using a 200-tonne capacity Amsler Beam Bender machine. The loading rate was controlled manually by applying half of the expected load in the first 1 minute then the remaining half in the range of 1 to 2 minutes. However, the reported compressive strength by the manufacturer was not accurate; which resulted in an inaccurate loading rate. The machine was equipped with an upper spherical head and a lower bearing steel beam, as shown in Figure 3.10. The precision of the strength measurement was $\pm$0.1 MPa.

Figure 3.10 Capped brick for the compression testing using Amsler Beam Bender machine

3.4 Number of Specimens

A one-tailed t-test was performed to determine the minimum number of prism specimens required to establish whether statistically significant differences between different groups of prisms existed. A one-tailed test was used since negative temperatures were expected to harm the physical properties of the prisms.

When applying the t-test, the null hypothesis assumes that there is no significant difference between the mean values of the two groups being compared (H_0: $\overline{x_1} - \overline{x_2} = 0$), whereas the

alternative hypothesis assumes that there is a significant difference between the mean values (H_1: $\overline{x_1} - \overline{x_2} > 0$).

The t parameter is calculated as follows:

$$t = \frac{(\overline{x_1} - \overline{x_2})}{Sp * \sqrt{\frac{1}{n_1} + \frac{1}{n_2}}} \quad [3\text{-}4]$$

where

$$S_p^2 = \frac{S_1^2(n_1 - 1) + S_2^2(n_2 - 1)}{n_1 + n_2 - 2} \quad [3\text{-}5]$$

In these equations:

S_p is the pooled standard deviation

$\overline{x_1}$ is the mean of the data of sample 1

$\overline{x_2}$ is the mean of the data of sample 2

n_1 is the size of sample 1

n_2 is the size of sample 2

S_1 is the standard deviation of sample 1

S_2 is the standard deviation of sample 2

By referring to Saha et al. (2019), and Bolhassani et al. (2015), values for compressive strength and flexural bond strength were assumed to be 12.5 MPa and 0.24 MPa, respectively, to make an estimation of the number of specimens required for each group. The assumed difference between mean values was taken to be 10% for both the compressive and flexural bond strengths. In addition, the coefficient of variation was taken to be 10% for the compressive strength and 15% for the flexural bond strength. These values were chosen as they were reported in the study by Saha et al. (2019) for the compressive strength, and Akhlaghi et al. (2020) for the flexural bond strength. The confidence level was set to 95% to determine the critical t-value, which is considered relatively high when applied to civil engineering problems.

After running the t-test, a sample size of seven specimens was found to be the minimum number required to identify a significant difference between the compressive strength values, while twenty joints were required to be tested to identify a significant difference between the flexural bond strength values of two different prism groups.

Although the t-test indicated that seven prisms were needed for compression tests and four prisms for flexural bond tests, it was considered prudent to build extra prisms for each set to account for possible damage that might occur during the transportation process. The sample sizes were therefore increased to nine specimens for compression tests, and 25 joints for flexural bond tests.

3.5 Prism Construction Process

3.5.1 Prism Size

The prisms used for this project were one brick long, one 90 mm unit thick, and six bricks high, as shown in Figure 3.11. They were constructed of hollow concrete bricks stacked vertically with full bedding mortar joints. The prisms were constructed at room temperature in the structural engineering laboratory following the standard procedure stated in ASTM C1072 (ASTM 2013). The relative humidity of the structural engineering lab was 29%, as it was measured using OMEGAETTE HH311 humidity temperature meter with a precision of $\pm$2%.

Figure 3.11 The six-brick prisms used for compression tests

Each prism was built in an opened moisture-tight bag that was large enough to enclose and seal the completed prism. The first brick of each prism was placed on a plywood block in an alignment jig, as shown in Figure 3.12. The jig had an L-shaped base that allowed it to sit next to the prism rather than under it so that immediately after completion, the jig could be moved away from the prism. The mortar template was placed on the first brick, maintaining a 12 mm mortar bed depth prior to compaction. Then the mortar was placed in the template, and excess mortar was struck off with a straight edge. After removing the template, the next brick was placed immediately on the mortar bed. Then, a drop hammer was placed on top of the brick,

and from a height of 38 mm, the 1.8-kg steel rod was dropped. These steps were repeated until the six-brick-high concrete prism was completed. Specimens cured at -10°C remained in the Structural Engineering Lab for four hours after construction and before being moved to the environmental chamber located in the Chemical Engineering Department, while the rest of the specimens remained in the Structural Engineering Lab to be cured at room temperature for 28 days. Inside the environmental chamber, specimens were not placed in plastic bags because the relative humidity in the freezing chamber was relatively high (86% $\pm$ 2%). After 28 days, prisms were removed from the environmental chamber to the Structural Engineering Lab and stored for 90 minutes before being tested.

Figure 3.12 A partially constructed prism showing the use of alignment jig and mortar template to build the prisms

3.5.2 Transporting Prisms

Given that mishandling of the prisms could have had a significant detrimental effect on the properties of the prisms during transportation between the construction, curing, and test locations, extreme care was taken to protect them from being damaged during transport. In total, 112 prisms were built in the structural engineering lab. Out of these prisms, 72 were constructed for the compressive strength tests, and 40 brick prisms were used for the flexural bond strength tests. After four hours of curing at room temperature, 56 prisms were transported to the environmental chamber located in the Chemical Engineering Department to be cured at -10°C. The pre-curing time can be justified by taking into account that when laying the bricks

or blocks at below-freezing temperatures, the masons would need a temporary heated shelter that provides the pre-curing environment for a certain duration.

Prior to transporting the 56 prisms to the environmental chamber, they were clamped and supported from both sides using plywood, as shown in Figure 3.13, to prevent any damage during the transportation. Tightly clamping plywood to the side of the prism was able to prevent the mortar joint from being subjected to tensile stresses during handling. All prisms were carried individually by hand when being transported. A pilot test was performed prior to constructing the prisms that would be tested for compressive and flexural bond strengths, during which no bouncing during the transportation process was noticed. In order to give more control of the prisms, a handle was made to hold the plywood together, and to be used in carrying the prisms.

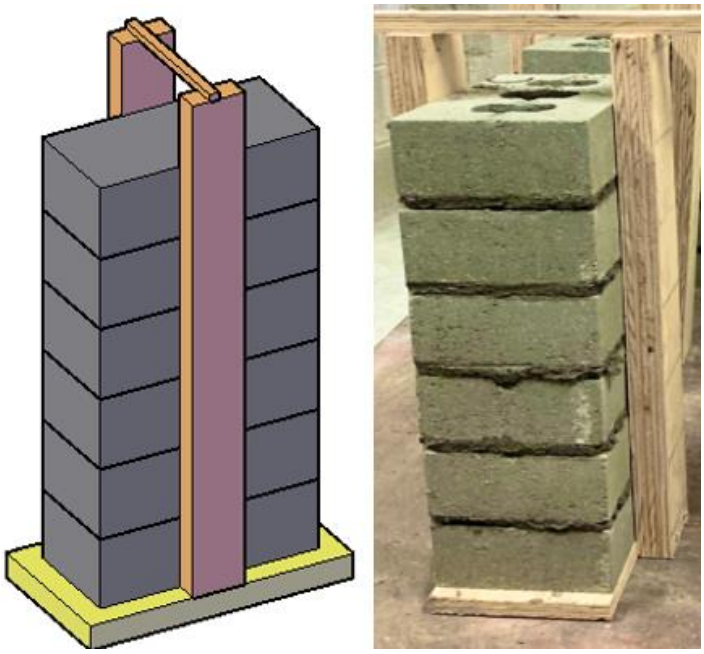

Figure 3.13 Clamped prism for transportation

Before conducting any tests on the mortar cubes or the constructed prisms, the frozen samples were transferred from the environmental chamber to the structural engineering lab and allowed to rest until the centre of the mortar bed joint had reached a temperature of at least 10°C. This step was important to make sure that no ice was present at the time of testing. The thawing time was measured on a dummy sample, as seen in Figure 3.14, through the use of an embedded thermocouple in the mortar joint. The temperature values were recorded and are plotted in the graph shown in Figure 3.15. From these data, the time required for thawing was

determined to be approximately 90 minutes. A longer post-freezing duration would be unjustifiable because strength recovery would start even during this short period.

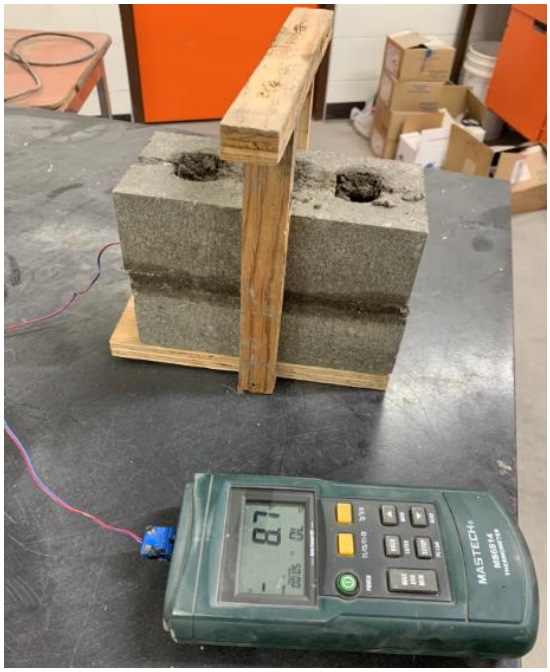

Figure 3.14 Embedded thermocouple in the mortar joint

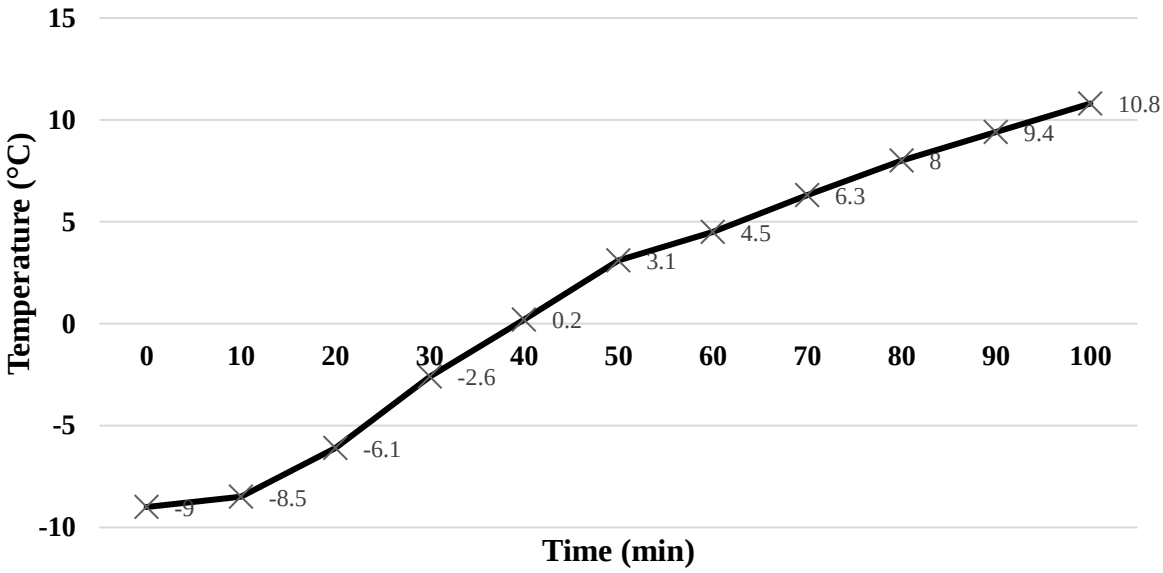

Figure 3.15 Evolution of mortar temperature after removal from freezing chamber

3.6 Compressive Strength Test

3.6.1 Specimen Groups

The main objective of this set of tests was to obtain the compressive strength of the prisms and compare the strength of prisms constructed with mortar containing different admixtures and cured at different temperatures. A total of 72 prisms were built, consisting of four groups of 18 identical prisms, corresponding to the four different mortar groups identified in Section 3.2. Nine specimens from each group were cured at -10°C and the remaining nine specimens were cured at +23°C. Due to limitations to the number of prisms that could be constructed and transported in a single day, each group was prepared in two separate batches. Twelve prisms were constructed from the first batch, and six prisms were constructed from the second batch. As shown in Table 3.2, each prism was given a unique name to indicate its most important attributes: the first term denoted the mortar type (Ct, SN, NC, or NN); the second term represented the curing temperature (+23°C or -10°C); and the last number indicated the specimen number within the group (1 to 9).

Table 3.2 Prism labelling system

Prism label	Mortar type	Curing temperature	Number of specimens
Ct+23/1to9	Control	+23°C	9
Ct-10/1to9	Control	-10°C	9
SN+23/1to9	Sodium Nitrite (SN)	+23°C	9
SN-10/1to9	Sodium Nitrite (SN)	-10°C	9
NC+23/1to9	Nano cellulose (NC)	+23°C	9
NC-10/1to9	Nano cellulose (NC)	-10°C	9
NN+23/1to9	Sodium Nitrite + Nano cellulose (NN)	+23°C	9
NN-10/1to9	Sodium Nitrite + Nano cellulose (NN)	-10°C	9

3.6.2 Experimental Setup and Procedure

The compressive strength tests on the masonry brick prisms were conducted using the Instron 600 DX universal testing machine shown in Figure 3.16. Prisms were placed on the steel platform of the machine with fibreboard above and below, and load was applied by hydraulic actuator through a spherical head and upper platen.

As stated in Appendix D of CSA S304-14 (Canadian Standards Association 2014), a quasi-static monotonically increasing load was applied with testing speed set at 12 MPa/min until the prism failed. Since the upper platen of the Instron machine was not large enough to fully cover the prism, a 10 mm thick steel bearing plate was placed between the specimen and platform to cover the full surface area of the prisms.

Figure 3.16 Compressive strength test setup for brick prisms

The manufacturing process for masonry units (blocks or bricks) creates rough and uneven surfaces that produce stress concentrations when tested and decrease the measured compressive strength. Thus, prism capping becomes necessary, since it mitigates the effect of these imperfections and distributes the load evenly (Ozyildirim and Carino 2006).

Prism capping was confirmed to be in accordance with CSA S304-14 provisions. In order to comply with the standard, new fibreboard was used for each prism, and the thickness of the fibreboard did not exceed 10 mm.

The specified compressive strength (*f'm*) of prisms was determined according to CSA S304-14 using the following equations:

$$\text{Compressive strength: } f = \frac{P}{A} \qquad [3\text{-}6]$$

$$\text{Average compressive strength: } f_{av} = \frac{\sum f}{n} \qquad [3\text{-}7]$$

Standard deviation: $S = \sqrt{\frac{\sum(f-f_{av})^2}{n-1}}$ [3-8]

Specified masonry strength: $f'_m = f_{av} - 1.64S$ [3-9]

where P is the maximum compressive load, kN

A is the net effective area = 13950 mm^2

n is the number of tested specimens

3.7 Flexural Bond Strength Test

3.7.1 Specimen Groups

The test program for measuring the flexural bond strength included constructing 40 prisms identical to those used for compression tests. Each prism was six units in height with five mortar joints for a total of 200 joints. The 40 prisms consisted of four groups of 10 identical prisms, with half the prisms in each group cured at each of the two curing temperatures. The construction procedure was identical to that described in Section 3.5. After finishing the second batch used for compressive tests, a new first batch was made for the flexural bond strength test. Six prisms were constructed from the first batch, and four prisms were constructed from the second batch. The reason for using separate batches from the compressive strength test was to have time between shifting between the two tests during the testing days which will reduce the time difference factor between the samples.

The bond wrench test described in CSA A3004-C9 (CSA 2013) was used to determine the flexural bond strength of the masonry prisms. This test method is designed for testing standard concrete masonry units with dimensions of 92 mm wide by 57 mm high (within a tolerance of $\pm$3 mm). The units must have a length of not less than 178 mm nor more than 194 mm (within a tolerance of $\pm$3 mm) (CSA 2013). The masonry brick units that were used in this study had measurements of 190 mm x 90 mm x 57 mm (L x W x T). Since moisture content affects the bond strength, concrete bricks were tested for the initial rate of absorption, as described in Section 3.3, in order to decide if they needed to be stored at high humidity prior to construction.

Each prism was given a unique name, as shown in Table 3.3, to indicate its most important attributes: the first term denotes the mortar type (Ct, SN, NC, or NN); the second term represents the curing temperature (+23°C or -10°C); and the last number indicates the specimen number within the group (1 to 5).

Table 3.3 Prism labelling system used for flexural bond strength tests

Prism label	Mortar type	Curing temperature	Number of specimens
Ct+23/1to5	Control	+23°C	5
Ct-10/1to5	Control	-10°C	5
SN+23/1to5	Sodium Nitrite (SN)	+23°C	5
SN-10/1to5	Sodium Nitrite (SN)	-10°C	5
NC+23/1to5	Nano cellulose (NC)	+23°C	5
NC-10/1to5	Nano cellulose (NC)	-10°C	5
NN+23/1to5	Sodium Nitrite + Nano cellulose (NN)	+23°C	5
NN-10/1to5	Sodium Nitrite + Nano cellulose (NN)	-10°C	5

3.7.2 Experimental Setup and Procedure

The flexural bond strength was measured using the bond wrench test, which allowed more than one mortar joint to be tested for each prism. Figure 3.17 shows a photograph of the test set up with various components labelled. The brick under the tested mortar joint was clamped to the testing frame, and the upper brick was subjected to an eccentric load that wrenched the brick. Load was applied through a cantilevered arm, which induces a combination of axial and flexural stresses on a mortar joint. The lower part of the frame has a mechanism to clamp the prism to the base, and the upper part clamps and applies a moment to the uppermost brick. A hydraulic pump with a calibrated pressure gauge was used to apply pressure to a hydraulic actuator that pressed down on a load-cell attached to the loading arm of the bond wrench apparatus. The load-cell was connected to a programmed laptop to record the failure load. The addition of the hydraulic actuator was a modification to the test method that was able to provide careful control of the loading. This resulted in a lower range of variation in the acquired data.

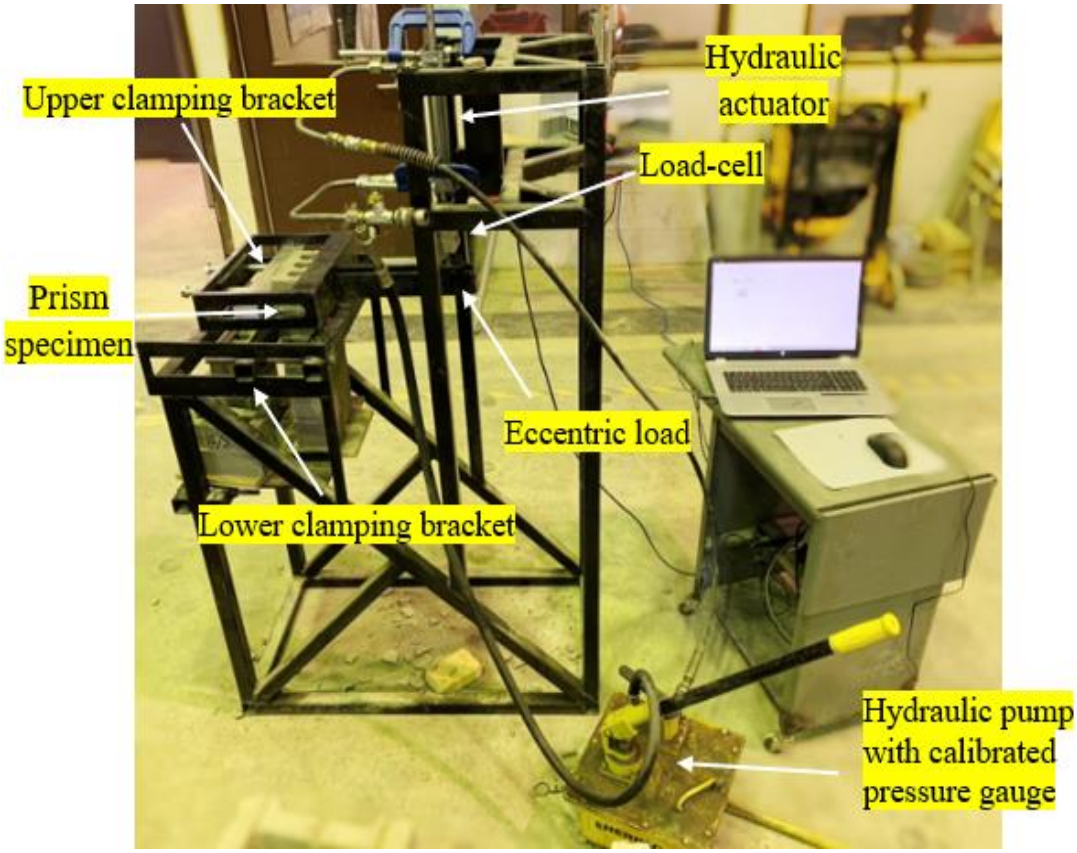

Figure 3.17 Bond wrench test set up with various components labelled

3.7.3 Analysis

Figure 3.18 shows a schematic diagram of the upper portion of a prism specimen within the test frame, along with the variables used in the analysis.

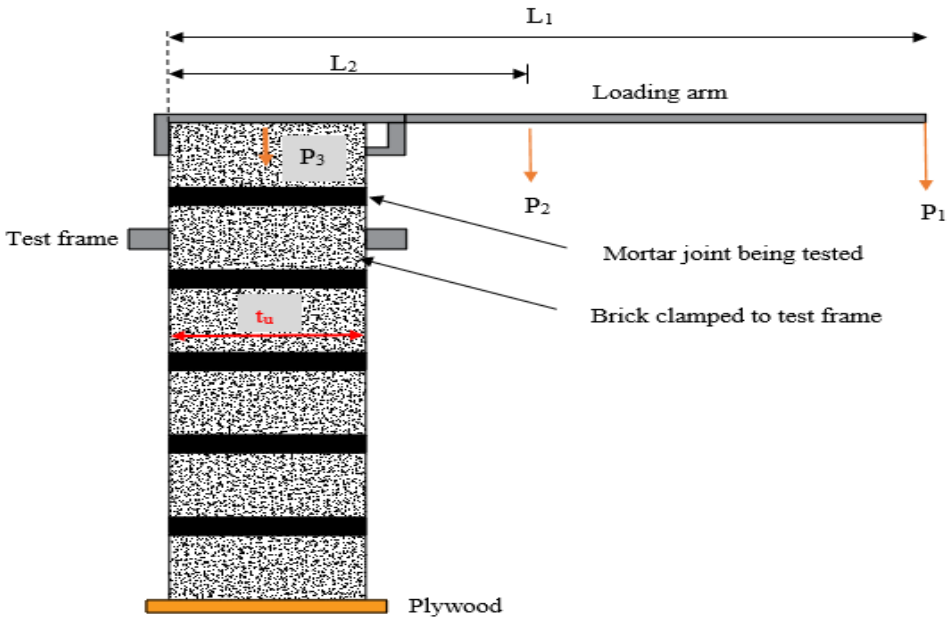

Figure 3.18 Schematic diagram of bond wrench apparatus, showing the variables used to calculate the flexural strength

To calculate the flexural bond strength, the following variables are required: the self-weight of the loading arm (P_2), self-weight of the brick (P_3), the applied load at failure (P_1), the distance from the outside edge of the prism to the centre of gravity of the loading arm (L_2) in mm, the distance from the edge of the prism to the location of applied load in mm (L_1), and the width of the masonry unit (t_u).

For prisms that are symmetrical about their centroid, the flexural bond strength of a mortar joint is determined using the following equation:

$$f_t = \frac{M}{S} - \frac{P}{A_e} \qquad [3\text{-}10]$$

where

f_t = flexural tensile bond strength, MPa

M = moment about the centroid of the mortar bedded area of the test joint, in N.mm

$= P_1 (L_1 - t_u/2) + P_2 (L_2 - t_u/2)$

S = section modulus of the cross-section of the joint, mm^3

$= \frac{I_e}{(t_u/2)}$ for prisms with solid masonry units with full mortar bedding, where I_e is the effective moment of inertia, $mm^3 = \frac{1}{12} \times (length) \times (width)^3$

P = the total vertical compressive load applied to the test mortar joint, N

$= P_1 + P_2 + P_3$

A_e = effective cross-sectional area, mm^2

$= bt_u$ for prisms of solid masonry units with full mortar bedding

According to CSA S304-14, the minimum bond strength required is 0.20 MPa at 28 days.

4 RESULTS AND DISCUSSION

In this chapter, the experimental and analytical results from the different tests described in Chapter 3 are provided. The experimental test results are first provided for the fresh and hardened mortar properties, followed by the brick properties, and finally the mechanical properties of masonry assemblages. Statistical analyses were carried out to determine whether the addition of sodium nitrite and/or nanocellulose had a significant effect on the compressive strengths and flexural bond strengths of the prisms.

4.1 Mortar Properties

Results for the fresh and hardened mortar properties are presented in this section. Results for flowability, air content, and setting times are followed by results for compressive tests of mortar cubes. These tests were included to meet the requirements of CSA A3000 (2013), CSA S304 (2014) and CSA A179 (2014).

4.1.1 Flow Test Results

According to CSA A3004-C2-13, the desired flowability of the mortar ranges between 105% and 115%. In order to determine the amount of water required to meet the specifications, trial batches with different batch sizes were prepared and tested. The control samples of mortar indicated that a water/cement ratio of 0.5 was sufficient to achieve the required flowability. However, and as is illustrated in Figure 4.1, the addition of 12% sodium nitrite by mass of mixing water increased the flowability, such that a reduced water/cement ratio of 0.42 was required for mortar samples with sodium nitrite as an antifreeze admixture to reach the specified flowability. This can be attributed to the ability of sodium nitrite to release the bound water molecules in the agglomerated paste through repelling and dispersing the cement particles. Since sodium nitrite decreases the water-to-cement ratio (w/c) as discussed in Chapter 2, its addition should result in an increase in the compressive strength at early ages, which will be helpful in reducing the impact of cold weather on the rate of strength gain.

The addition of a small amount of CNF (0.3% by mass of cement) was also effective in increasing the flowability of the mortar mixture, as depicted in Figure 4.1. Mortar samples with nanocellulose reached the specified flowability with a water-to-cement ratio of 0.44. The incorporation of the nanocellulose improved the workability and reduced agglomeration during mixing.

Similarly, the combined addition of sodium nitrite and nanocellulose led to an increase in the flowability values compared to the control samples, as demonstrated in Figure 4.1. In this case, the specified flowability was achieved with a w/c ratio of 0.43.

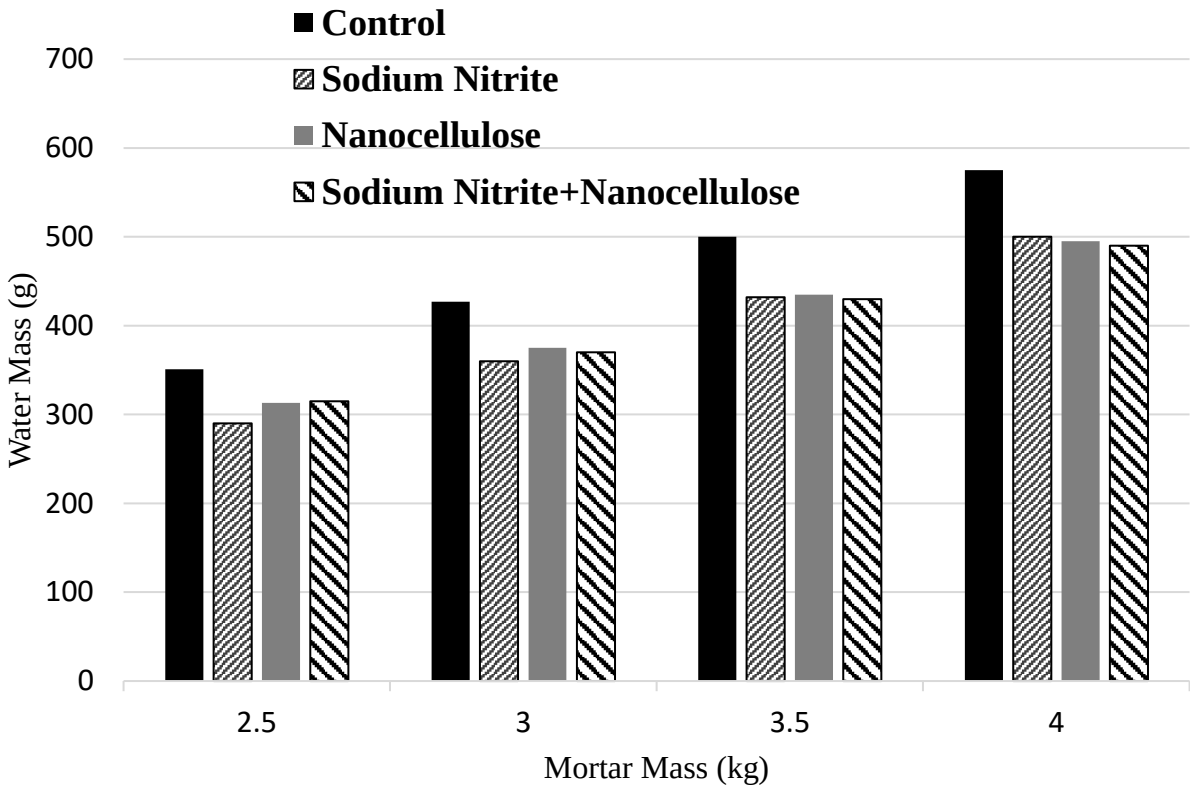

Figure 4.1 Mass of water required to achieve the specified flowability of mortar mixtures for samples of different batch sizes

In order to compare the effects of the three admixture combinations on the flowability of fresh mortar, samples were prepared using a fixed mass of Type S dry mortar (1500 g) mixed with 230 g of water and each of the admixtures. This produced a w/c ratio of 0.51. The resulting flowability for various mortar types is shown in Figure 4.2. The control sample showed the lowest flowability (105%), which is the lowest acceptable value according to CSA A3004-C2-13. The sodium nitrite sample, which contained 27.6 g of sodium nitrite, showed much higher flowability compared with the control sample, with a value of 130%; this means that to meet

the specification, less water is needed, which will result in a higher compressive strength at all ages. Incorporating 1.3 g of nanocellulose resulted in a flowability of 115%, which was higher than the control sample and matched the maximum specified flowability value as per CSA A3004-C2-13. The addition of both 27.6 g of sodium nitrite and 1.3 g of nanocellulose resulted in the highest flowability of 140%. Thus, all the admixtures reduced the required w/c ratio, so that the compressive strength of mortar containing these admixtures should be higher than that of the control sample.

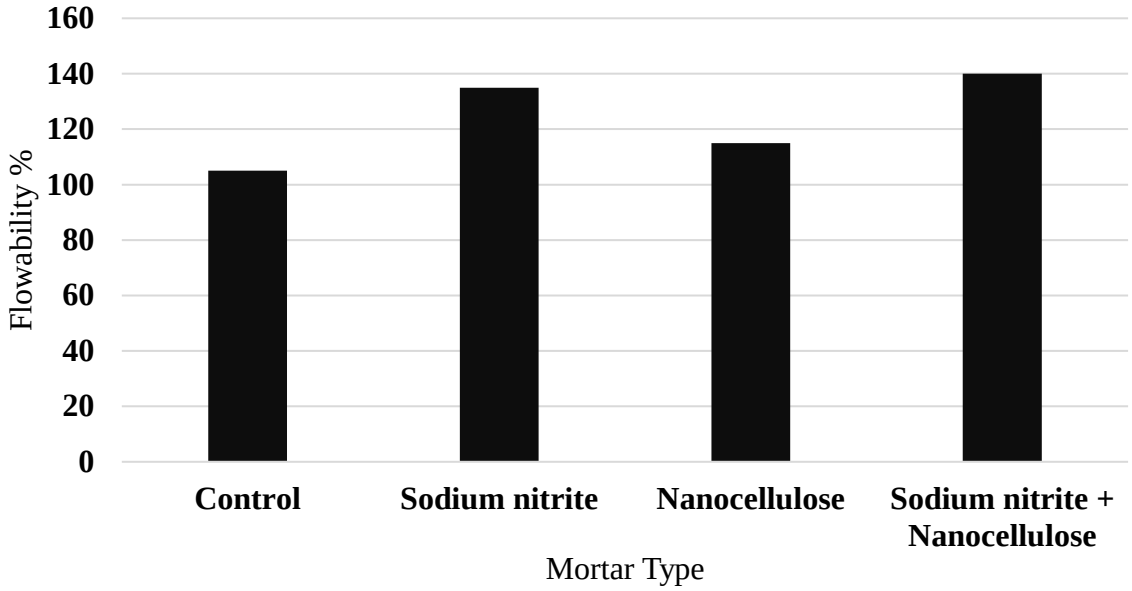

Figure 4.2 Flowability of mortar mixtures with the same w/c ratio of 0.51

The results shown in Figure 4.1 and 4.2 illustrate that the differences of the three admixture combinations on the flowability of fresh mortar are large. However, due to the few numbers of the tested samples, it was not possible to comment on statistical significance.

4.1.2 Air Content

Table 4.1 presents the air contents as measured in fresh and hardened mortar samples following the procedures described in Section 3.2. The values reported in this table represent the results of three replicate tests for the fresh mortar mixtures and six replicate tests for hardened specimen measurements.

Table 4.1 Air content of fresh and hardened mortar mixtures

Mixture	Fresh Properties			Hardened Air Content		
	Density (g/cm^3)	Average Air Content (%)	Standard Deviation	Average Air Content (%)	Standard Deviation	Coefficient of Variation (%)
Control	1.94 1.96 1.93	14	0.60	13	0.47	3.7
Sodium Nitrite	1.94 1.95 1.94	11	0.40	9	0.30	3.6
Nanocellulose	1.98 1.97 1.99	12	0.32	11	0.84	7.8
Sodium Nitrite and Nanocellulose	2.10 2.06 1.99	10	0.41	8	0.48	6.4

The introduction of sodium nitrite resulted in a drop in the air content in both the fresh and hardened mortar samples by 21% and 31%, respectively. This reduction may be attributed to the ability of the sodium nitrite to decrease the pore size of air voids in cement-based products (Li et al. 2016).

The addition of nanocellulose also reduced the air content, although not by as much as the sodium nitrite. This reduction was 14% for the fresh mortar samples, and 15% for the hardened mortar samples compared to the control samples. For this study, the amount of nanocellulose was limited to 0.3% by weight of cement; however, increasing the dosage of nanocellulose is expected to result in a greater reduction in the air content. The addition of both sodium nitrite and nanocellulose led to the lowest air contents (10% for the fresh mortar, and 8% for the hardened mortar) compared to the other mortar samples.

The effect of sodium nitrite and nanocellulose on the air content of mortar at the hardened state followed the same trend as was observed with the fresh mortar measurements. The highest air content was observed in the control mortar, with a value of 13%, while the lowest air content was 8%, which was observed in the mortar samples that contained sodium nitrite and nanocellulose.

For the investigated mixtures, the air content measured in fresh mortar was slightly higher than that observed in the hardened mortar (ranging between 7% to 25%). On average, the

measured air contents in the fresh mortar was 8 to 25% greater than that determined using the Flatbed Scanner Method on the hardened mortar. This corresponds to approximately 1 to 2% additional air content found in the fresh mortar. This finding is consistent with results reported in the literature (Khayat and Nasser 1991). One of the purposes of measuring the air content of the fresh and hardened mortar was to determine whether some of the differences in compressive strength among the mortars could be attributed to differences in air content.

4.1.3 Setting Time

As described in Chapter 3 (Section 3.2), three samples were prepared and tested every 15 minutes for every mortar mixture to determine the setting time as described in ASTM C403-13 (ASTM 2013). According to ASTM C403-13, the initial setting time is reached when the 1 mm needle penetrates the paste 25 mm, while the final setting time corresponds to when the needle does not visibly penetrate the paste. The change in penetration depth over time for representative samples of each mortar mixture at room temperature is shown in Figure 4.3, and Table 4.2 lists the resulting initial and final setting times for every mortar mixture which were very consistent among the three replicates.

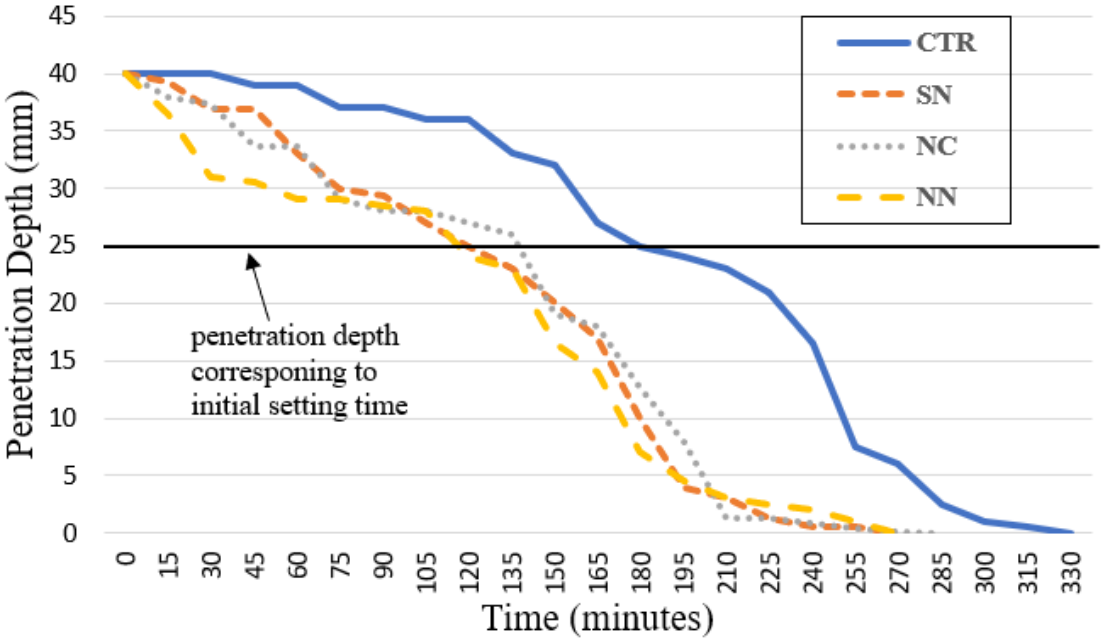

Figure 4.3 Setting time results for representative samples of mortar mixtures at room temperature

Table 4.2 Average setting time results for samples cured at room temperature

	Mortar Setting Time (hr-min)		
Composition	**Initial**	**Final**	**setting period Δt**
Control	3-00	5-30	2-30
Sodium Nitrite	2-00	4-30	2-30
Nanocellulose	2-21	4-45	2-24
Sodium Nitrite + Nanocellulose	1-55	4-30	2-35

These results show that the initial and final setting times for mortar samples with 12% sodium nitrite by mass of mixing water were shorter than those of the control sample. This result may be explained in part by the lower w/c ratio of the sodium nitrite since a lower w/c ratio has been shown to decrease setting times (Dodson 1994). Since the addition of sodium nitrite decreases the w/c ratio of the matrix and shortens the setting time, it is expected that the compressive strength of the mortar will be higher than the control sample at early ages, which will help to reduce the negative impact of cold weather on strength development.

Figure 4.3 and Table 4.2 show that the addition of a low mass fraction (0.3%) of CNF by mass of cement as well as a combination of sodium nitrite and CNF are also effective in accelerating the setting time of the mortar mixture. These results are also related to the lower w/c ratios required for these mixtures.

The average setting times listed in Table 4.2 demonstrate that the acceleration in the initial and final setting times for the sodium nitrite mixture was 60 minutes compared to the control mixtures. This finding differs from that of Ratinove and Rozenberg (1996), who reported that using 12% sodium nitrite by mass of mixing water resulted in slowing the setting time by 6 minutes. This difference is explained by the w/c ratio that was used by Ratinove and Rozenberg, which was similar for control and sodium nitrite mixes. Mixtures with nanocellulose shortened the initial and final setting time by 39 minutes and 45 minutes, respectively. Combining sodium nitrite and nanocellulose shortened the initial and final setting time by 65 minutes and 60 minutes respectively. Despite the accelerating effect of the admixtures, the setting period (i.e. the time between initial and final setting) did not vary substantially among all four mixtures.

The penetration depth over time for representative samples of each mortar mixture when cured at -7°C is shown in Figure 4.4, and Table 4.3 shows the corresponding initial and final setting times. The different tested samples reported identical initial and final setting time; therefore, the standard deviation and the covariance were not mentioned in the table.

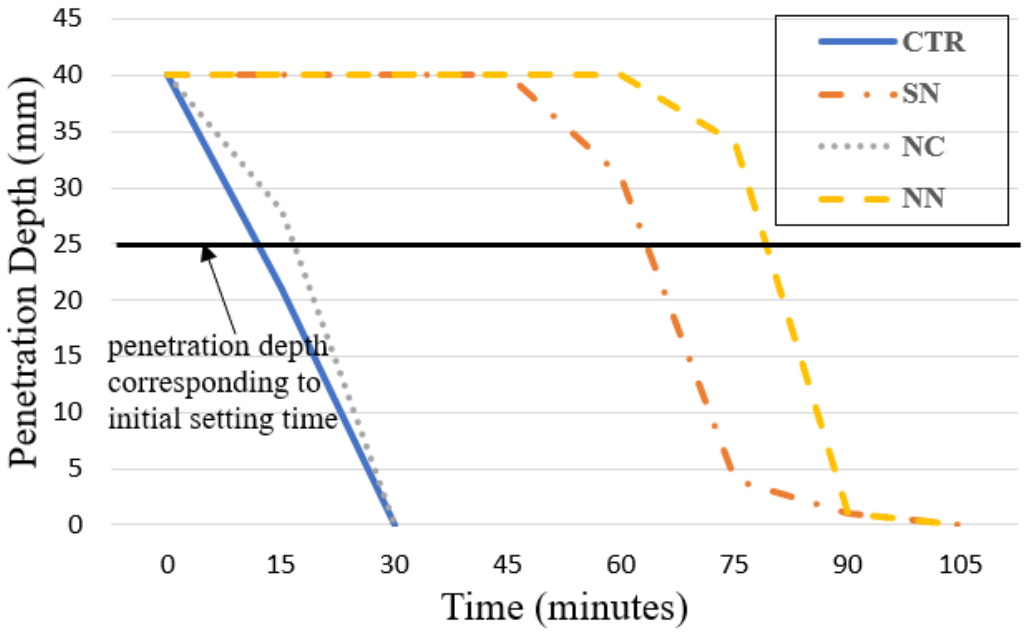

Figure 4.4 Setting time results for representative samples of mortar mixtures at -7°C

Table 4.3 Average setting time results for samples cured at -7°C

	Mortar Setting Time (hr-min)		
Composition	**Initial**	**Final**	**setting period Δt**
Control	0-12	0-30	0-18
Sodium Nitrite	1-04	1-45	0-41
Nanocellulose	0-17	0-30	0-13
Sodium Nitrite + Nanocellulose	1-19	1-45	0-26

As shown in Figure 4.4, the control sample and the nanocellulose sample began to freeze immediately, and after 30 minutes, the needle stopped penetrating the paste due to the ice formation in the mixture. On the other hand, the samples that contained sodium nitrite were evidently prevented from freezing and continued to cure until final setting after 105 minutes.

The final setting times reported in Table 4.3 corresponded to the time at which the needle did not penetrate the paste by any visible level. For the control sample and the nanocellulose sample this happened after 30 minutes. However, it was obvious that this did not actually represent the real setting time for these mixtures because once they were removed from the freezer, the water in the samples started to melt and the paste became more flowable with time, which demonstrated that the samples had not yet set. The case with the sodium nitrite samples was quite different. When these samples were removed from the freezer, they remained in their hardened state, providing evidence that the sodium nitrite had lowered the freezing point of the water, which allowed the cement hydration process to proceed at -7°C and reach final setting after 105 minutes. The use of sodium nitrite evidently lowered the freezing point of the water and accelerated the cement hydration process.

Generally, the setting times of mortar mixtures cured at freezing temperatures are much longer than that for mixtures prepared and cured at room temperatures, which adversely affects the construction schedule. This is due to the fact that the mixing water in the mortar mixture will start freezing and eliminating the liquid water required for the hydration reaction to proceed. One of the most important criteria to measure the efficacy of the antifreeze admixtures is their ability to lower the freezing point of the mixing water, thus allowing cement hydration to continue, resulting in ongoing hardening of cement mixtures.

4.1.4 Mortar Compressive Strength

The compressive strength test results of the mortar cubes are summarized in Table 4.4. The mean 28-day compressive strengths of all the mortar cubes cured at room temperature exceeded the minimum specified value 12.5 MPa for Type S mortar at 28 days (CSA 2014). The incorporation of sodium nitrite and nanocellulose resulted in an increase in the compressive strength relative to the control mortar of about 10% and 6.7%, respectively. This may be attributed to the ability of sodium nitrite and nanocellulose to lower the w/c ratio while maintaining the required flowability, as well as to the reduction in air content in these samples (See Table 4.1).

Table 4.4 28-day compressive strengths of mortar cubes cured at room temperature

Sample	Avg (MPa)	Std. Deviation	Coefficient of Variation (%)
First batch CTR+23	17.5	0.37	2.1
Second batch CTR+23	17.0	0.59	3.5
First batch SN+23	19.0	1.2	6.3
Second batch SN+23	19.0	0.35	1.8
First batch NC+23	18.5	0.86	4.6
Second batch NC+23	18.3	0.37	2.0
First batch NN+23	20.8	0.48	2.3
Second batch NN+23	21.0	0.86	4.0

The 28-day compressive strengths obtained for different mortar mixtures at a curing temperature of -10°C are presented in Table 4.5. The samples were transferred to the freezing chamber after 4 hours of pre-curing with $\pm$3 minutes tolerance, and after 28 days samples were removed from the freezing chamber 90 minutes before being tested with $\pm$5 minutes tolerance. The compressive strengths of both the control and nanocellulose mortar cubes were very low, barely reaching 1 MPa at 28 days. On the other hand, samples that contained sodium nitrite had much higher compressive strength after 28 days of curing at -10°C compared to the other mortar samples. They obtained compressive strengths of 8.8 to 9.0 MPa. This represents a reduction in the compressive strength of about 48% compared to the control mortar cubes cured at room temperature. It is worth mentioning that the strength requirement for Type S mortar according to CSA A179-14 (CSA 2014) differs depending on the preparation of the mortar. If mortar is prepared for lab purposes, it should have a flow value of 110$\pm$5% and a minimum compressive strength of 12.5 MPa. However, this flowability level is not considered sufficient to produce a mortar with a workable consistency suitable for laying masonry bricks. Therefore, as per CSA A179, the minimum specified compressive strength for Type S mortar prepared with a flowability suitable for laying masonry brick is 8.5 MPa. Hence, the compressive strength obtained for mortar samples that contained sodium nitrite and cured at -10°C complies with the Canadian standard. In addition, these samples are expected to continue to gain strength over time after removal from freezing conditions. The incorporation of nanocellulose with

sodium nitrite did not result in any considerable change in the compressive strength after 28 days of curing at -10°C. Overall, the coefficients of variation were below 7% for all test groups, suggesting that strengths for all batches were consistent.

Table 4.5 28-day compressive strengths of mortar cubes cured at -10°C

Sample	Average compressive strength (MPa)	Std. Deviation	Coefficient of Variation (%)
First batch CTR-10	1.0	0.06	6.0
Second batch CTR-10	0.9	0.05	5.6
First batch SN-10	8.9	0.17	1.9
Second batch SN-10	8.8	0.35	3.9
First batch NC-10	1.0	0.03	3.1
Second batch NC-10	0.9	0.04	4.4
First batch NN-10	9.0	0.22	2.5
Second batch NN-10	9.0	0.40	4.4

The control and the nanocellulose mortar specimens cured at -10°C failed in a non-cohesive mode, in which they were reduced to powder form, as seen in Figure 4.5. The failed samples had wet internal surfaces, which means that there was an abundance of water inside that had not reacted with the cement. All the other mortar specimens, including those with sodium nitrite that were cured at -10°C, failed normally, initially cracking vertically from the top then propagating to the bottom with increase in load, followed by crushing of the mortar cubes, as seen in Figure 4.6.

Figure 4.5 Failure of the control sample cured at -10°C

Figure 4.6 Representative failure of mortar cubes of different mixtures cured at room temperature and those containing sodium nitrite cured at -10°C

With a pre-curing time of 4 hours, followed by curing at -10°C for 28 days, the control and nanocellulose mortar specimens did not show significant gain in compressive strength. On the other hand, the sodium nitrite mortar specimens were able to gain acceptable compressive strengths of at least 8.8 MPa when cured at -10°C. These results are acceptable because the minimum specified compressive strength for Type S mortar prepared with a flowability suitable for laying masonry brick, which was the case for these samples, is 8.5 MPa according to CSA A179. The results obtained for samples containing the sodium nitrite as an antifreeze admixture and cured at -10°C compare very well with the findings reported by Saha et al. (2019). The observed gain in the compressive strength at a curing temperature of -10°C is

attributed to the ability of sodium nitrite to lower the freezing temperature of the mixing water, making it available for the hydration reaction to proceed.

Although it was not the focus of this study, the incorporation of a 4 hour pre-curing period in combination with the use of 12% sodium nitrite by mass of mixing water is thought to be important for strength development. Increasing the pre-curing time to 6 or 8 hours is expected to result in higher compressive strength (Saha et al. 2019). This finding indicates that the addition of sodium nitrite as an antifreeze admixture combined with heated protection for 4 to 8 hours should significantly enhance the compressive strength of the mortar. As a result, the 24 to 48 hour freezing protection time required by the Canadian CSA A371 standard when building at temperatures below 4°C could be reduced to a much shorter duration, which is more favourable economically.

4.2 Brick Properties

Results for the brick properties from different companion tests are presented in this section. Results for water absorption, initial rate of absorption, and compressive strengths of standard concrete masonry bricks are discussed. These tests were performed due to their direct effect on the compressive and flexural bond strengths of masonry assemblages, and to meet the requirements of CSA A179 (2014) and CSA S304 (2014).

4.2.1 Water Absorption

Water absorption is an essential parameter to be considered when assessing the bricks' quality and durability. Higher water absorption values are undesirable since they can result in cracks in the ceramic body and, as a result, lower durability. Very low values should also be discouraged, as rainwater may run rapidly into the mortar joints and find its way into the building instead of being partially absorbed by the bricks, which will reduce the durability of the mortar joints (Kayali 2005; Eliche-Quesada et al. 2012). The acceptable range of water absorption has been found to be between 5% and 20% (Kayali 2005). The average water absorption values for the two sets of samples tested for the current study were 5.9% and 5.3%, with standard deviations of 0.2 and 0.1, respectively. These values were low, but still within the acceptable range of 5% to 20%. Detailed water absorption test results are provided in Appendix D.

In addition to compressive strength, water absorption is an important property for masonry units, especially during cold weather construction. This property has a direct effect on the

brick's strength as well as the strength of the bond between the brick and mortar in masonry structures. In cold weather construction, the bricks should not have higher water absorption values, since this may result in changes in the volume of bricks, which will cause cracks that may damage the masonry assemblage.

4.2.2 Initial Rate of Absorption

As defined by ASTM C67, the water absorbed in a duration of one minute by a brick bed area is known as the initial rate of absorption (IRA). The bond achieved between bricks and mortar paste is greatly influenced by the bricks' IRA as well as the water holding capacity of the mortar paste. If the bricks absorb water rapidly from the mortar paste, the mortar hydration process will be negatively affected. Accordingly, the bond will be disrupted, which will result in a weak interaction between brick courses. On the other hand, if bricks do not absorb a sufficient amount of water, the next brick course appears to float over the mortar paste, resulting in weak bonding (Christy and Tensing 2011). Therefore, to ensure an adequate bond between bricks and mortar paste, the IRA parameter should be taken into account. For bricks, ASTM C62 states that the acceptable IRA range is 0.025–0.150 g/cm^2/min (Henry et al. 2007; Kadir and Mohajerani 2015).

Detailed initial rate of absorption test results are provided in Appendix E. The average IRA for all measured brick specimens for the first and second pallets was 0.0328 g/cm^2/min, and 0.0289 g/cm^2/min, respectively, with standard deviations of 0.004 and 0.0001, respectively (C.O.V.=12% and 0.3%). The average IRA for both pallets lies within the acceptable range specified by ASTM C67. Since this IRA value is relatively low, which indicates a slow rate of water absorption by the bricks, the bricks were not moistened before laying in order to achieve a proper bond between bricks and mortar paste.

4.2.3 Compressive Strength of Masonry Bricks

Seven standard concrete bricks were randomly selected from each pallet and tested in compression as described in Chapter 3. The average compressive strength of the bricks was 39.3 MPa for the first pallet, and 39.5 MPa for the second pallet, with corresponding standard deviations of 3.6 MPa and 3.3 MPa, respectively. The coefficient of variation for both pallets was less than 15% (9.1 and 8.3%, respectively), which is considered to be acceptable. Detailed results for each individual test are provided in Appendix F. The compressive strength of masonry bricks was lower than the reported compressive strength by the manufacturer (55 MPa). This difference can be explained by the difference in testing procedure; the

manufacturer tested the mix using paving units, which is not the same as the brick units. Pavers are not manufactured with cores and would typically have a fairly high strength as a result of the mix design needed because they are an exposed element. In order to meet salt scaling and freeze-thaw durability requirements, pavers are expected to be manufactured with a less porous, denser, and therefore stronger mix. Also, the testing setup used in this test did not meet the ASTM requirements, since it did not have a well-controlled rate of loading. However, it was used since it was the only setup that could provide the calculated failure load.

4.3Mechanical Properties of Masonry Assemblages

Since a masonry structure consists of at least two distinct materials, the masonry units and the mortar joints, it is important to assess the performance of mortar with antifreeze admixtures in assemblages. Therefore, the main objective of this project was to evaluate the performance of mortars that contained sodium nitrite and nanocellulose as a cold-weather admixture in masonry assemblages under sub-freezing curing temperatures. This section presents the compressive and the flexural bond strength test results for masonry assemblages in order to perform this evaluation.

4.3.1 Compressive Strength of Masonry Prisms

4.3.1.1 Compressive Strengths

The purpose of the prism compressive strength tests was to determine the specified compressive strength (*f'm*) for prism groups with different mortar types when cured at room and sub-freezing temperatures (+23°C and -10°C, respectively), in order to determine whether sodium nitrite and/or nanocellulose influence this property. Determination of *f'm* plays a major role in the process of designing masonry structures.

The average compressive strength values at 28 days of all prisms that were tested are shown in Table 4.6, along with their corresponding standard deviations and coefficients of variation. Results are presented graphically in Figure 4.7, in which error bars correspond to one standard deviation on either side of the mean. Detailed results for individual prism tests may be found in Appendix A, along with details of the statistical comparisons.

Table 4.6 Average compressive strength of prisms cured at room temperature and at -10°C

Sample	Average compressive strength (MPa)	Std. Deviation	COV (%)	*f'm* (MPa)
CTR+23	24.1	1.1	4.6	22.3
CTR-10	12.4	0.9	7.0	10.9
SN+23	26.7	1.4	5.4	24.3
SN-10	21.2	1.5	7.0	18.8
NC+23	27.9	1.3	4.7	25.7
NC-10	12.9	0.9	6.7	11.5
NN+23	28.1	1.4	4.8	25.9
NN-10	21.8	1.0	4.6	20.2

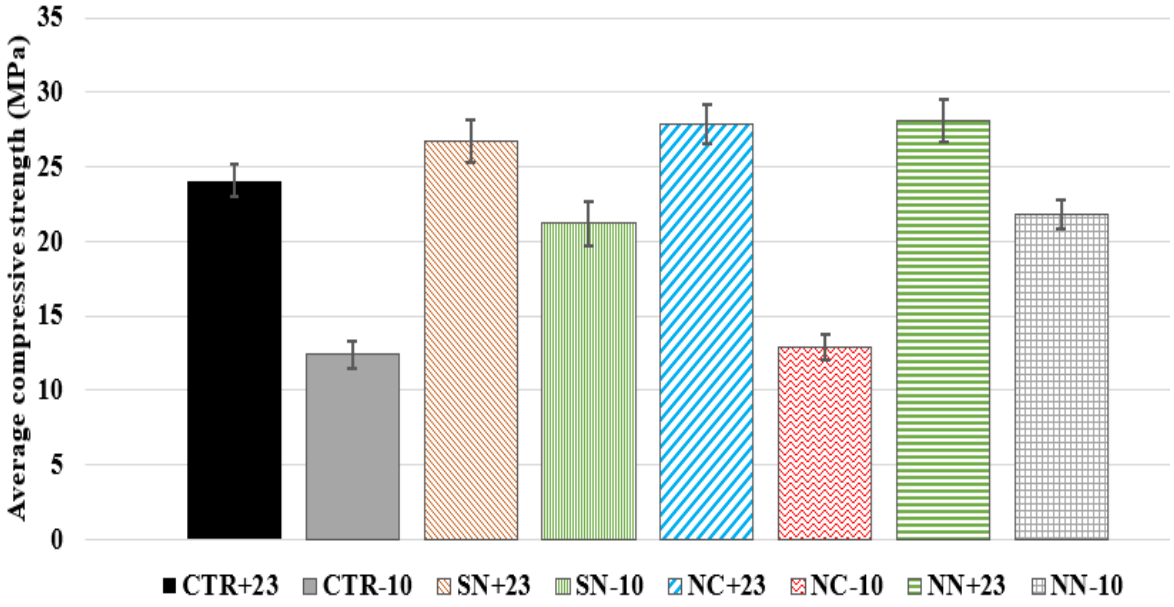

Figure 4.7 Average compressive strengths of different prism groups cured at room temperature and at -10°C

Comparing the compressive strengths of the control prisms cured at 23°C and -10°C, those cured under freezing curing conditions were 49% weaker than those cured at room temperature. This difference is statistically significant at the 95% level of confidence, which supports the hypothesis that curing at freezing temperatures has a significant impact on the compressive strength of masonry prisms. This result is consistent with the results of the mortar cube compressive strength tests, which showed that the mortar cubes cured at -10°C lost almost 95% of their strength compared to those cured at room temperature.

The addition of 12% sodium nitrite by mass of mixing water to the mortar in the prisms improved the compressive strength at both curing temperatures. The increases relative to the control samples were 11% and 71% when cured at 23°C and -10°C, respectively, in which only the samples cured at -10°C showed a statistically significant difference at the 95% level of confidence. The strength development observed in the group cured at -10°C strongly indicates an ongoing hydration reaction in the mortar joints, suggesting that the use of sodium nitrite managed to lower the freezing point of mixing water. These findings are consistent with the mortar cube strength tests, which showed that mortar specimens with sodium nitrite gained substantial strength when cured at -10°C. Although the addition of sodium nitrite promoted strength gain when cured at -10°C, the freezing curing temperature also had a significant negative impact on the compressive strength of these prisms. The average compressive strength of the prisms with sodium nitrite cured at -10°C was 21% lower than those cured at room temperature. This reduction was statistically significant at the 95% level of confidence. This result is also consistent with the mortar cube strength tests, since the compressive strength of mortar cubes cured at -10°C was 53% lower than that of those cured at room temperature.

The incorporation of nanocellulose did not have any effect on improving the compressive strength of masonry prisms cured at -10°C. The average compressive strength of 12.9 MPa did not differ significantly from that of the control samples cured at this temperature. This finding is in conformance with the results of the setting time test conducted at -7°C, where the cement hydration process of the mixture with nanocellulose stopped after 30 minutes as indicated by the fact that the needle did not penetrate the paste at any visible level due to the sample being frozen. Nanocellulose was effective at reducing the required w/c ratio and air content of the mixture, resulting in a potential accelerating effect, but it had no effect on lowering the freezing point of the water in the samples. The average compressive strength for brick prisms cured at -10°C was 54% lower than that of prisms cured at room temperature.

The combined effect of sodium nitrite and nanocellulose in the mortar joints of the prisms was similar to the effect of the sodium nitrite alone. This combination produced the highest compressive strengths among all groups at both curing temperatures. The compressive strength of the specimens cured at -10°C reached 21.8 MPa, which was 22% lower than the combined sodium nitrite and nanocellulose specimens cured at room temperature. It is clear that the combination of additives allowed the hydration reaction to proceed at -10°C, resulting in substantial strength gain by 76% compared to the control samples cured at -10°C.

An important comparison to make is between the sodium nitrite samples that were cured at -10°C and the control sample that was cured at room temperature, since it addresses one of the main motivations of this study. As shown in Table 4.6 and Figure 4.7, the average compressive strength of the sodium nitrite samples cured at -10°C was 21.2 MPa, which is 12% lower than that of the control samples cured at room temperature (24.1 MPa). The difference is statistically significant at the 95% level of confidence. It is worth mentioning that the reduction in compressive strength due to the exposure to freezing conditions is relatively small compared to the 49% reduction compressive strength observed for the control samples that were cured at room temperature and -10°C. When a combination of sodium nitrite and nanocellulose was used, the observed reduction in the compressive strength due to the freezing condition was approximately 9% compared to the control group cured at room temperature. This difference was still statistically significant at the 95% confidence level.

The effect of the subfreezing curing temperature on the various mortar mixtures was not the same. Whereas the control sample cured at -10°C showed the lowest average compressive strength, as illustrated in Figure 4.7, samples with 12% sodium nitrite by mass of mixing water cured at the same temperature were 71% stronger. In a similar trend to the control sample, the prisms with nanocellulose cured at the subfreezing temperature achieved a compressive strength that was not different than that of the control prisms at the 95% level of confidence. Combining the sodium nitrite with nanocellulose resulted in an increase in the average compressive strength compared to the control sample by 76%, which was the best performance among all groups cured at -10°C. These results are explained by the ability of both additives to reduce the water content, reduce the air content, accelerate the cement hydration reaction, and the special ability of sodium nitrite to lower the freezing point of the mixing water.

Figure 4.7 also illustrates the effect of incorporating sodium nitrite and nanocellulose in the mortar of the prisms on the compressive strength development of the brick prisms when cured at room temperature. The prisms constructed with mortar containing both sodium nitrite and nanocellulose achieved the highest compressive strength (28.1 MPa), while the control prisms attained the lowest compressive strength (24.1 MPa). The incorporation of nanocellulose in the mortar resulted in an increase in the compressive strength of the brick prisms by 15% compared to the control sample, while the use of sodium nitrite in the mortar resulted in an 11% increase in the compressive strength compared to the control prisms. The outcomes are in good agreement with the trends observed with the companion tests already discussed, where the addition of sodium nitrite and nanocellulose resulted in reduction in the amount of mixing

water needed to attain sufficient flowability and a reduction in the air content in the fresh and hardened mortar. They are also consistent with the trends in the compressive strength of mortar cubes that were discussed in Section 4.1.

As stated in Clause 5.1.1 in CSA S304-14 (Canadian Standards Association 2014), the specified compressive strength at 28 days of the masonry assemblage shall be determined by testing the compression strength of prisms or selected from Table 3 or Table 4 of the standard, depending on the type of masonry unit used. As illustrated in Table 4.7, the selection of the masonry prism compressive strength is based on the brick compressive strength and type of the masonry mortar.

Table 4.7 Solid brick masonry specified compressive strength normal to bed joint (reproduced from CSA S304-14 (CSA 2014))

Brick compressive strength (MPa)	*f'm* (MPa)	
	Type S mortar	Type N mortar
90	25	21
80	23	19
70	20	17
55	16	14
40	13	11

The specified compressive strength (*f'm*) according to standard CSA S304-14 is 13 MPa, as shown in Table 4.7 for 40 MPa brick compressive strength. As shown in Table 4.6, all samples exceeded this value, except the control and nanocellulose samples cured at -10°C. This demonstrates that the sodium nitrite is effective as an antifreeze admixture.

4.3.1.2 Failure Mode

Masonry brick prisms are constructed with two nonhomogeneous materials with different elastic properties. Usually, the bricks are stronger and stiffer than the mortar. Because of its lower elastic modulus and higher Poisson's ratio, lateral strain in the mortar increases more rapidly than in the bricks when compressive loads are applied to masonry prisms. However, the rough surface of the stiffer bricks induces friction and bond at the brick-mortar interface, which prevents lateral deformation in the mortar. As a result, both the bricks and the mortar are subjected to triaxial stress conditions, with uniaxial compression and biaxial tension for the bricks and triaxial compression for the mortar.

Failure in masonry prisms with a strong mortar, including all the prisms cured at room temperature, initiated with the formation of vertical splitting cracks, followed by the crushing of bricks, as shown in Figure 4.8. The most common failure mode in prisms with sodium nitrite cured at the subfreezing temperature was also the same, as illustrated in Figure 4.9. Despite the fact that bond strength increases with mortar strength, bond failure was not observed during the experiments, and all the brick-mortar joints remained in place until the end of the test, including prisms with the weak mortar joints. However, as seen in Figure 4.10, joint crushing was observed for the weak mortar prisms, which was the case for the control and nanocellulose prisms that were cured at -10°C. Figure 4.11 shows one of the failure modes that happened randomly in prisms with strong or intermediate mortar strengths, which was crushing of some bricks followed by the splitting failure; this mode can be explained by the fact that some bricks were relatively stronger than others, as supported by the large coefficient of variation of the brick compressive strength that was mentioned earlier (see Section 4.2).

The incorporation of nanocellulose mitigate against micro-cracking, and therefore, reduce lateral expansion under compression. This was identified in the failure mode and cracking patterns observed in the prisms with nanocellulose cured at room temperature. The addition of nanocellulose delayed the lateral expansion of the mortar, resulting in seeing more crushing in the brick itself.

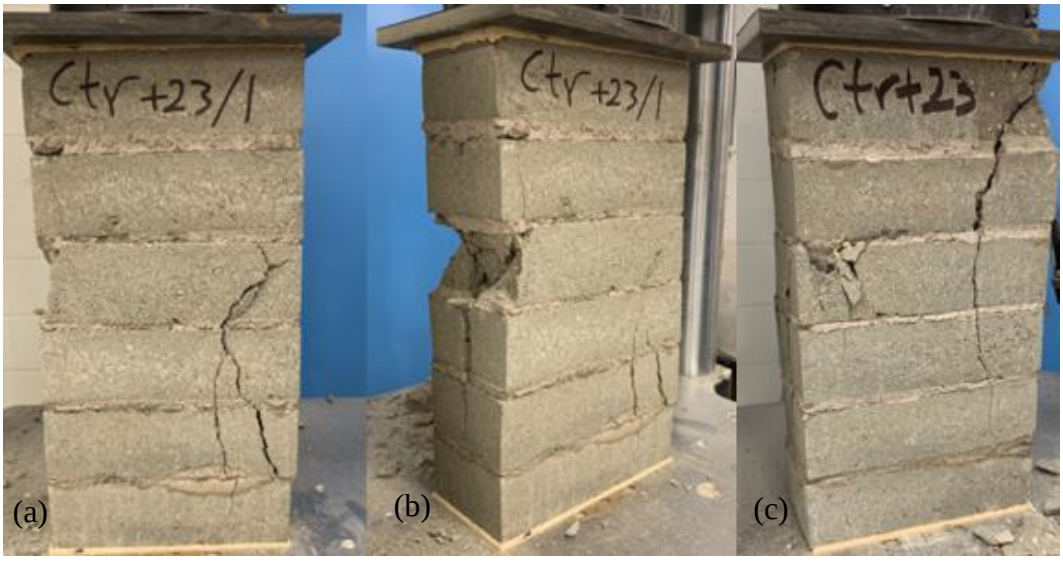

Figure 4.8 Progressive failure of a prism with the control mortar cured at room temperature: (a) vertical splitting cracks, (b) followed by crushing of the bricks, and (c) another prism followed the same progressive failure

Figure 4.9 Failure of a prism with sodium nitrite cured at the subfreezing temperature, showing vertical splitting cracks

Figure 4.10 Failure due to mortar joint crushing in a control specimen cured at -10°C

Figure 4.11 Failure mode associated with crushing of bricks followed by splitting failure

4.3.1.3 Proposed Model for Compressive Strength of Brick Prisms

The results reported earlier in this section demonstrate that the compressive strength of masonry prisms is directly related to the mortar compressive strength. This observation is in conformance with the findings reported by Ravula and Subramaniam (2017). The average compressive strength values of all prisms that were tested, along with the corresponding average mortar compressive strength values, are shown in Table 4.8. Results are also presented graphically in Figure 4.12. The compressive strength of the masonry prism was found to increase by approximately 67% when the mortar strength increased from 1.0 MPa to 9.0 MPa. The increase in prism compressive strength was found to be approximately 11% when the mortar compressive strength increased from 9.0 MPa to 17.0 MPa.

Table 4.8 Average compressive strengths of different prism groups with their corresponding mortar compressive strength

Sample	Batch	Cube Strength (MPa)	Prism Strength (MPa)
CTR+23	First	17.5	23.9
	Second	17.0	24.4
CTR-10	First	1.0	12.4
	Second	0.9	12.2
SN+23	First	18.8	26.4
	Second	19.0	27.3
SN-10	First	8.9	20.6
	Second	8.8	22.5
NC+23	First	18.5	27.8
	Second	18.0	28.0
NC-10	First	1.0	12.6
	Second	0.9	13.5
NN+23	First	20.8	27.8
	Second	21.1	28.6
NN-10	First	9.0	21.8
	Second	9.0	21.9

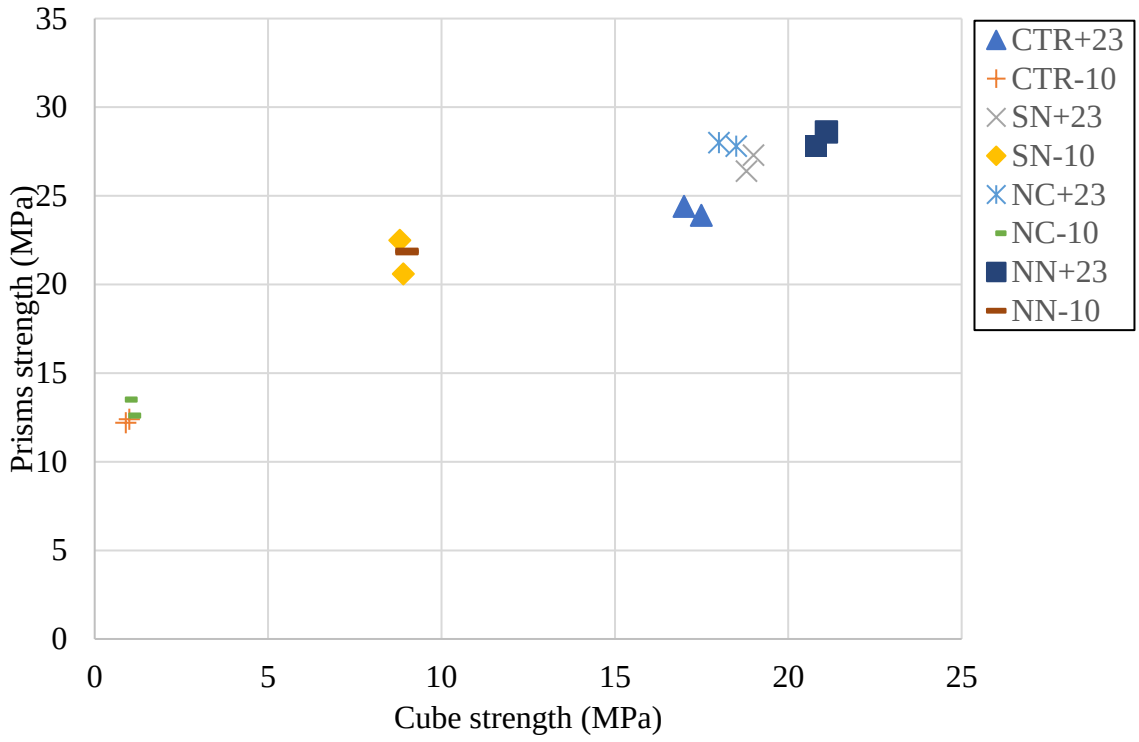

Figure 4.12 Graphical representation of the variation of the average compressive strength of different prism groups with their average mortar compressive strength

The strengths of both the masonry units and the mortar are believed to have a direct effect on the strength of the masonry prisms. In this study, only the mortar strength varied, while the other parameters were fixed in order to examine the effectiveness of the antifreeze admixtures. In general, it is important to account for the other parameters, including the compressive strength of the masonry units, h/t ratio, etc., in order to have higher accuracy in the prediction model of masonry strength. Statistical regression analysis was carried out using 72 data points from the present study. Detailed results may be found in Appendix B. A model was developed to estimate the compressive strength of a prism as a function of brick strength and mortar strength, resulting in the following equation:

$$f_{prism} = 0.33(f_{brick}) + 0.75(f_{mortar}) - 0.085 \qquad [4\text{-}1]$$

Here f_{brick} and f_{mortar} are the compressive strengths of the bricks and mortar in MPa, respectively.

The coefficient of determination (R^2) value corresponding to the equation is 0.93, which means that the proposed formula is able to account for 93% of the variation in the masonry prism compressive strength. The developed model is also presented graphically in Figure 4.13.

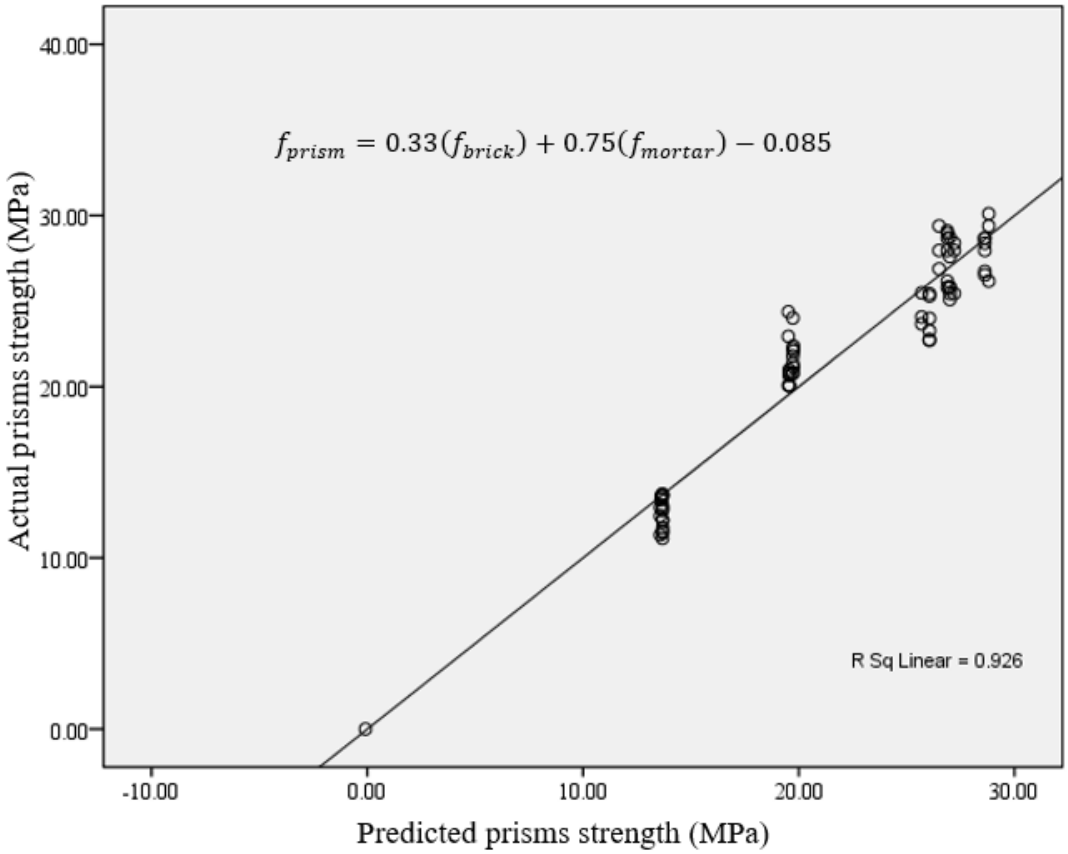

Figure 4.13 Graphical representation of the developed model

The purpose of the proposed regression analysis is to provide an empirical model for the observed correlation between the average compressive strength of masonry prisms as a function of the average mortar compressive strength. This model was generated by depending mainly on the variation in the compressive strength of the mortar strength. In order to have a more reliable model, a noticeable variation in the compressive strength of the bricks should be included, along with other parameters. However, the limited strength variation of the mortar in this study served to examine the effectiveness of the antifreeze admixtures, and the generated prediction model evidently illustrates the significant effect of the mortar strength on the compressive strength of masonry assemblages. Most of the prediction model examined the compressive strength of prisms with a mortar strengths range between 12 MPa and 21 MPa, which was shown in this study to have 11% increase in the compressive strength. On the other hand, the compressive strength of the masonry prism was found to increase by approximately 67% when the mortar strength increased from 1.0 MPa to 9.0 MPa. Unlike the proposed prediction model by Bennett et al. (1997), this study demonstrates that the compressive strength of masonry prisms is directly related to the mortar compressive strength.

4.3.2 Flexural Bond Test Results

The average flexural bond strengths measured for all prism groups are listed in Table 4.9, along with the associated standard deviations and coefficients of variation. Figure 4.14 plots the results. Detailed individual test results are provided in Appendix C. There were no physical or significant outliers identified in the test results.

Table 4.9 Flexural bond strength test results for all prisms cured at room temperature and at -10°C

Sample	Average flexural bond strength (MPa)	Std. Deviation	Coefficient of Variation (%)
CTR+23	0.471	0.070	14.9
CTR-10	0.148	0.020	13.5
SN+23	0.406	0.061	15.0
SN-10	0.404	0.063	15.6
NC+23	0.534	0.060	11.2
NC-10	0.149	0.022	14.8
NN+23	0.538	0.057	10.6
NN-10	0.512	0.066	12.9

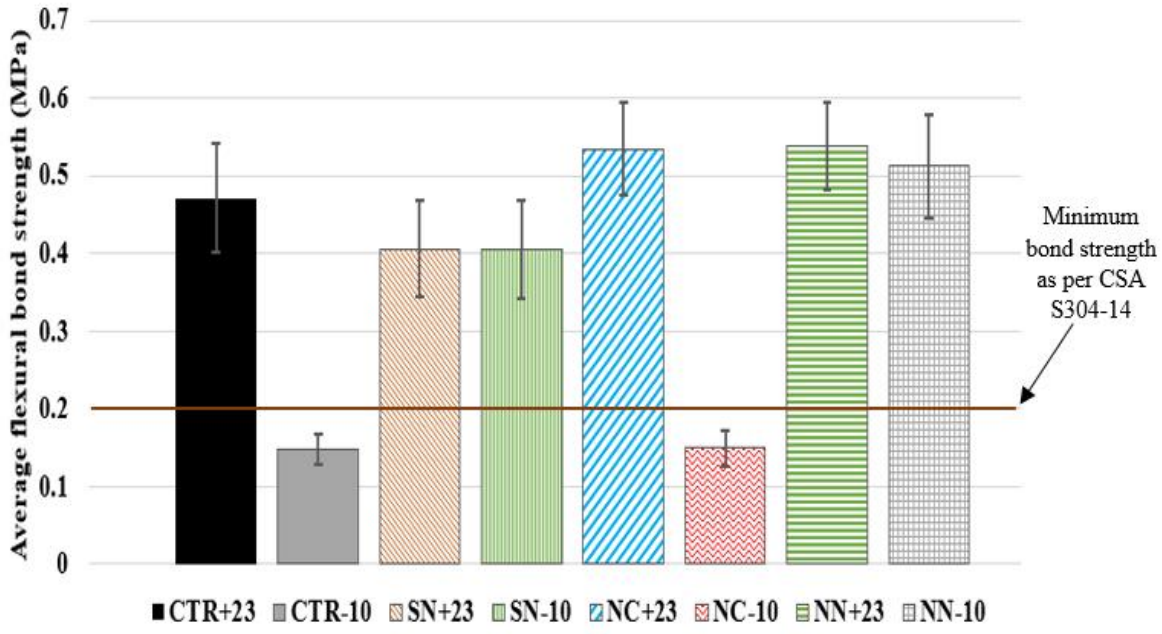

Figure 4.14 Average flexural bond strengths of different prism groups cured at room temperature and at -10°C

At 28 days of curing at room temperature, the average results indicate that the addition of sodium nitrite lowered the flexural bond strength by 14%, while incorporating nanocellulose improved the flexural bond strength by 13%. These differences were statistically significant at

the 95% level of confidence. The prisms that contain both sodium nitrite and nanocellulose showed an improvement in the flexural bond strength of approximately 14% compared to the control prisms, which indicates that the nanocellulose successfully counteracted the negative impact of sodium nitrite alone on the bond strength. The findings are generally in agreement with the mortar cube compressive strength test results, in the sense that the flexural bond strengths of the prisms were affected by the strength of mortar.

The subfreezing curing temperature severely affected the flexural bond strength of both the control sample and the nanocellulose brick prisms reducing their strengths by 69% and 72%, respectively, relative to their respective bond strengths when cured at room temperature. On the other hand, the flexural bond strength of the sodium nitrite prisms was not affected by the subfreezing curing temperature, achieving a value that was virtually identical to that when cured at room temperature. This result is explained by the ability of sodium nitrite to lower the freezing point of the water, such that the cement hydration reaction proceeded at a temperature of -10°C. In order to decide whether a statistically significant difference existed due to the different curing temperatures for the same mortar ingredients, the paired sample t-test with a 95% confidence level was performed. The results are reported in Appendix C.

The 14% decrease in the flexural bond strength of the prisms that contained sodium nitrite and were cured at room temperature as compared to the control prisms was found to be significant according to the paired sample t-test. However, samples that contained sodium nitrite and nanocellulose and were cured at -10°C showed a statistically significant increase in the flexural bond strength of about 9%.

The targeted flexural bond strength in this study was 0.20 MPa, which is the minimum acceptable bond strength specified in standard CSA S304-14. All samples exceeded this value, except the control and nanocellulose samples cured at -10°C. This demonstrates that the sodium nitrite is effective as an antifreeze admixture.

The observed flexural failure mode of prisms that were cured at room temperature and those that contained sodium nitrite and were cured at -10°C was a failure at the brick-mortar interface (Figure 4.15), which is a direct sign of a bond failure. For these prism groups, the flexural strength of the mortar was stronger than the flexural strength of the brick-mortar interface. If the flexural strength of the brick-mortar interface had been higher than that of the mortar and or the brick, this would have resulted in either failure of the brick, or in a failure that combines brick and bond. On the other hand, control prisms and prisms that included nanocellulose and

were cured at -10°C experienced a different kind of failure. The bed joints in these prisms failed in flexure (Figure 4.16), which indicated that the mortar joints did not attain good flexural strength due to the subfreezing curing temperature. The flexural strength of the mortar in these cases was evidently lower than the flexural strength of the brick-mortar interface. The green colour of the bricks in Figure 4.15 and Figure 4.16 is due to the light in the structural engineering lab.

Figure 4.15 Failure at the brick-mortar interface, as demonstrated in prisms cured at room temperature

(a) (b) (c)

Figure 4.16 Flexural failure in the bed joint, illustrated for control and nanocellulose prisms cured at -10°C: (a) and (b) are control joints, and (c) nanocellulose joint

Based on the observed results, it is evident that adding nanocellulose improved the flexural bond strength when liquid water was available for the hydration to proceed. This was the case for prisms cured at room temperature. When used alone at -10°C, the nanocellulose was ineffective because the water was not prevented from freezing. When used in combination with sodium nitrite at -10°C, the liquid water again became available, allowing the nanocellulose to improve the flexural bond strength.

The mechanism by which nanocellulose improves the mechanical properties, and flexural bond strength in particular, is believed to be "enhanced hydration". It is hypothesized that the addition of nanocellulose led to an increase in the degree of hydration, as has been observed in previous studies mentioned in Chapter 2 (Section 2.6) (e.g., Weerawarna et al. 2015, Youngblood et al. 2016). The mortar with cellulose nanocrystals appears to provide a channel for water to transport through the hydration products to the unhydrated cement particles, thereby improving hydration. It is well also known that a higher level of hydration products, such as C-S-H, leads to higher strength. Another explanation that has been proposed is that hydroxyl groups in nanocellulose are able to form a nano-network within the intermolecular atomic structure and lead to enhanced material strength and stiffness (Abraham et al. 2012; Shak et al. 2018).

5 CONCLUSIONS AND RECOMMENDATIONS

5.1 Summary

The observed gain in strength in masonry mortar examined by Saha et al. (2019) under freezing conditions indicated that the addition of sodium nitrite to the fresh mortar was able to cause the hydration reactions to continue at temperatures as low as -10°C. However, its effectiveness when used for the construction of masonry assemblages had yet to be demonstrated. Since a masonry structure consists of at least two distinct materials, the masonry units and the mortar joints, it is important to assess the performance of mortar with antifreeze admixtures in assemblages. Therefore, the main objective of this project was to evaluate the performance of mortars that contained sodium nitrite and nanocellulose as a cold-weather admixture in masonry assemblages under sub-freezing curing temperatures.

The experimental program consisted of testing six-brick concrete prisms prepared with four different mortar mixes (control, with sodium nitrite, with nanocellulose, with both sodium nitrite and nanocellulose) and cured at room temperature and -10°C to measure compressive strength and flexural bond strength. In addition, fresh mortar properties were measured and companion tests were conducted to measure flowability, air content, and setting time. The addition of sodium nitrite was limited to 12% by the mass of mixing water, and the amount of nanocellulose was limited to 0.3% by the mass of cement.

Based on the findings of Saha et al. (2019), the primary focus of this study was on the effect of sodium nitrite in the Type S mortar joints on the mechanical properties of masonry assemblages cured at -10°C after being pre-cured at room temperature for 4 hours. The incorporation of nanocellulose in this study was motivated by its potential ability to increase the bond strength in masonry assemblages, which according to the literature review, could be compromised by including antifreeze admixtures such as sodium nitrite.

5.2 Conclusions

Based on the results of this study, the following conclusions are made to address the specific objectives defined in Chapter 1:

- Brick prisms constructed with mortar that contained 12% sodium nitrite by mass of mixing water reached an average compressive strength of 21.2 MPa when cured at -10°C for 28 days. This was 72% higher than the control prisms cured at the same temperature and 12% less than the strength attained by the control prisms cured at room temperature. When cured at -10°C, control samples showed the lowest average compressive strength (12.4 MPa), while those with both sodium nitrite and nanocellulose in combination had the highest compressive strength (21.8 MPa). The addition of nanocellulose alone did not significantly affect the compressive strength relative to the control prisms. For the prisms cured at room temperature, the incorporation of nanocellulose in the mortar resulted in an increase in the compressive strength of the brick prisms by 15% compared to the control sample, while the addition of sodium nitrite resulted in an 11% increase in the compressive strength compared to the control prisms. Adding both admixtures in combination resulted in the highest compressive strength, 17% higher than the control prisms. The outcomes are consistent with other observations, including the ability of the sodium nitrite and nanocellulose to reduce the amount of mixing water needed to attain sufficient flowability, to reduce the air content of the fresh and hardened mortar, and to increase the strength of the mortar cubes. Most of the prisms with acceptable mortar strength failed after vertical splitting cracks were initiated in the bricks. For prisms with weak mortar strength, the failure started in the mortar joints. These failure behaviours are generally in agreement with the literature.

- When cured at -10°C, only prisms constructed with mortar that contained sodium nitrite attained flexural bond strengths that exceeded 0.2 MPa, which is the minimum bond strength required according to CSA S304-14. When cured at room temperature, the flexural bond strength of the prisms that contained sodium nitrite was found to be 14% lower than that of the control prisms, while the addition of nanocellulose increased the flexural bond strength by 13%. On the other hand, samples that contained sodium nitrite and nanocellulose in combination and were cured at -10°C showed an increase in the flexural bond strength of approximately 9% compared to the control sample cured at

room temperature. When cured at room temperature, the flexural bond strength of all prism groups exceeded the minimum specified strength of 0.2 MPa by a substantial margin.

- The fresh and hardened properties of Type S masonry mortar varied considerably with curing temperature and admixture. Masonry mortar with 12% sodium nitrite by mass of mixing water reached compressive strengths of 19.0 MPa and 8.9 MPa when cured at room temperature and -10°C, respectively, as compared to 17.5 MPa and 1.0 MPa, respectively, for control batches.

- The addition of the sodium nitrite and nanocellulose to masonry mortar mixtures, both together and separately, resulted in increased flowability at a constant water-to-cement ratio. Therefore, less water was required to achieve the required flowability for constructing masonry prisms. Since the addition of sodium nitrite and nanocellulose decreases the water-to-cement ratio of the mortar, the compressive strength of the hardened mortar is expected to be higher than mortar without the additives.

- The air content tests indicated that the introduction of sodium nitrite and/or nanocellulose resulted in a decrease in the air content of the fresh and hardened mortar. The reduction in air content may be attributed to the ability of sodium nitrite and nanocellulose to decrease the pore size of air voids in cement-based products. The highest air content (14%) was found in the control mortar, while the lowest air content (10%) was found in the mortar samples that contained a combination of sodium nitrite and nanocellulose.

- The average setting time results for mixtures cured at room temperature and containing sodium nitrite and/or nanocellulose indicated an acceleration in both the initial and final setting times compared to the control mixtures. In comparison to the control mixtures, the sodium nitrite mixture's initial and final setting times were 60 minutes shorter. Nanocellulose also reduced the initial and final setting times by 39 and 45 minutes, respectively. The initial and final setting times were reduced by 65 and 60 minutes, respectively, when sodium nitrite and nanocellulose were combined.

- At -7°C, the hydration process for the control and nanocellulose samples essentially stopped after 30 minutes, as evidenced by the fact that the Vicat needle did not penetrate the paste by any visible level due to the formation of ice in the mixture and the samples became soft after removal from the freezing environment. When sodium nitrite was added to the mortar, the hydration process continued and a final setting time of 105 minutes was observed. This was confirmed by the observation that sodium nitrite samples remained in their hardened state after being removed from the freezing environment, providing evidence that sodium nitrite was able to lower the freezing point of the water, which allowed the cement hydration process to proceed at -7°C.

- Sodium nitrite and nanocellulose affected the compressive strength of the mortar cubes differently depending on the curing temperature. When cured at room temperature, mortar cubes with sodium nitrite and/or nanocellulose had higher compressive strengths than the control mortar. Those with nanocellulose had the highest compressive strengths, approximately 21% higher than the control mix. The strength gained by the addition of these admixtures at room temperature can be attributed to their lower water-to-cement ratio, lower air content, and the acceleration effect they produced. Only groups with sodium nitrite showed an acceptable gain of strength when cured at -10°C, reaching average compressive strengths of 8.8 to 9.0 MPa at 28 days. The strength gain in these mixtures at is attributed to the ability of sodium nitrite to lower the freezing point of the water, as demonstrated by the Vicat needle tests performed at -7°C.

- The use of sodium nitrite as an antifreeze admixture in mortar was found to shorten the setting time and increase the compressive strength development of masonry mortar mixtures at a curing temperature of -10°C, allowing brick prisms to reach acceptable compressive and flexural bond strengths. Thus, the addition of sodium nitrite in masonry mortar mixtures can extend the construction season into colder periods and speed up masonry construction during winter, requiring only a 4-8 hour pre-curing period, which is much relaxed compared to the 48 hours stated by the Canadian CSA A371 standard. In addition, the use of a low amount of nanocellulose under normal curing conditions showed promising results in terms of increasing the compressive and flexural bond strengths of masonry assemblages. The use of nanocellulose by itself in subfreezing temperatures did not result in any improved properties relative to control mortars. However, incorporating nanocellulose with sodium nitrite produced the

highest compressive and flexural bond strengths when cured at both room temperature and -10°C. As a result, their combined effect counteracted the reduction in bond strength associated with the use of sodium nitrite alone. The combination also allowed the hydration reaction to continue at -10°C, which was mainly due to the ability of sodium nitrite to lower the freezing point of the water.

5.3 Recommendations

The following recommendations are made based on the outcomes of this study:

1. It is highly recommended that more tests be conducted on masonry mortar including sodium nitrite and nanocellulose to measure flexural strength, and efflorescence.
2. It is recommended that the effect of sodium nitrite and nanocellulose be determined on other mortar cement types, prisms with bricks having a higher initial rate of absorption, and concrete block prisms.
3. It is also recommended that the effect of sodium nitrite and nanocellulose on the properties of grout be studied, as it contains higher initial water content.
4. The observed behaviour of the mortar and prisms tested at -10°C led to an inference that there would be no need for a pre-curing period for temperatures around -5°C. Therefore, it is recommended that the same tests be performed at -5°C and other temperature patterns that might be encountered in field conditions.
5. Investigating the durability performance (freeze and thaw, porosity, alkali-aggregate reactions, etc.) of mortar joints containing the combination of sodium nitrite and nanocellulose at -10°C is recommended.
6. It is highly recommended that further studies be performed using different types of nanocellulose and at different concentrations since the performance varies according to these factors.
7. In order to capture the microstructural development and characterize the hydration products in the cementitious matrix, it is highly recommended that scanning electron microscope analysis be performed with energy dispersive X-ray and thermogravimetric analyses.

REFERENCES

Abraham, E., Elbi, P. A., Deepa, B., Jyotishkumar, P., Pothen, L. A., Narine, S. S., and Thomas, S. (2012). X-ray diffraction and biodegradation analysis of green composites of natural rubber/nanocellulose. Polymer Degradation and Stability, 97(11), 2378-2387.

Akhlaghi, M. A., Bagherpour, R., and Kalhori, H. (2020). Application of bacterial nanocellulose fibres as reinforcement in cement composites. Construction and Building Materials, 241, 118061.

American Concrete Institute. (2016). ACI 306R-16 Guide to cold weather concreting. Farmington Hills, Michigan, United States.

Arslan, M., Cullu, M., And Durmus, G. (2011). The effect of antifreeze admixtures on compressive strength of concretes subjected to frost action. Gazi University Journal of Science, 24(2), 299-307.

ASTM International. (2016). ASTM C1314-16: Standard Test Method for Compressive Strength of Masonry Prisms. West Conshohocken, PA, USA. https://doi.org/10.1520/C1314-16.2.

ASTM. (2015). Standard Test Method for Resistance of Concrete to Rapid Freezing and Thawing. ASTM C666/C666M-15. American Society for Testing and Materials, West Conshohocken, PA, USA.

ASTM. (2021). Standard Test Methods for Sampling and Testing Concrete Masonry Units and Related Units. ASTM C140/C140M-20a. American Society for Testing and Materials, West Conshohocken, PA, USA.

Banthia, N. (2009, October). Fibre reinforced concrete for sustainable and intelligent infrastructure. In First International Conference on Sustainable Built Environment Infrastructures in Developing Countries, Algeria (pp. 337-350).

Barbosa, C. S., Lourenço, P. B., and Hanai, J. B. (2010). On the compressive strength prediction for concrete masonry prisms. Materials and Structures, 43(3), 331-344.

Barna, L. A., Seman, P. M., and Korhonen, C. J. (2010). Cold weather admixture systems demonstration at Fort Wainwright, Alaska. Engineer Research and Development Center Hanover Nh Cold Regions Research and Engineering Lab.

Barna, L. A., Seman, P. M., and Korhonen, C. J. (2011). Energy-efficient approach to cold-weather concreting. Journal of materials in civil engineering, 23(11), 1544-1551.

Belkowitz, J. S., Belkowitz, W. B., Moser, R. D., Fisher, F. T., and Weiss, C. A. (2015). The influence of nano silica size and surface area on phase development, chemical shrinkage and compressive strength of cement composites. In Nanotechnology in Construction (pp. 207-212). Springer, Cham.

Bennett, R. M., Boyd, K. A., and Flanagan, R. D. (1997). Compressive properties of structural clay tile prisms. Journal of Structural Engineering, 123(7), 920-926.

Bhalerao, N., Wayal, A.S., Patil, P.G., and Bharimalla, A.K. (2015). A review on the effect of nano-cellulose on concrete. International Journal of Civil and Structural Engineering Research, vol.3, (p. 251-254).

Bigelow, O. (2005). Ensuring quality in cold-weather masonry construction. Construction Specifier, 58(11), 58.

Bolhassani, M., Hamid, A. A., Lau, A. C., and Moon, F. (2015). Simplified micro modeling of partially grouted masonry assemblages. Construction and Building Materials, 83, 159-173.

Borchelt, J. G., Melander, J. M., and Nelson, R. L. (1999). Bond Strength and water penetration of high IRA brick and mortar. PCA RandD Serial, (2222).

Brick Industry Association. (2006). Technical Notes on Brick Construction: Cold and Hot Weather Construction. Reston, VA, USA, 1–9.

Canadian Standards Association. (2014). CSA S304-14: Design of masonry structures. Mississauga, Ontario, Canada.

Cao, Y., Zavaterri, P., Youngblood, J., Moon, R., and Weiss, J. (2015). The influence of cellulose nanocrystal additions on the performance of cement paste. Cement and Concrete Composites, 56, 73-83.

Cao, Y., Zavattieri, P., Youngblood, J., Moon, R., and Weiss, J. (2016). The relationship between cellulose nanocrystal dispersion and strength. Construction and Building Materials, 119, 71-79.

Chahine, G. N., and Drysdale, R. G. (1989). Influence of test conditions on the compressive strength and behaviour of faceshell mortar bedded concrete block prisms. In 5th Canadian Masonry Symposium (pp. 651-660).

Christy, C. F., and Tensing, D. (2011). Greener building material with fly ash. Asian Journal of Civil Engineering, 12(1), 87-105.

CMCA. 2010. Text Book of Canadian Masonry. Canadian Masonry Contractors Association, Mississauga, ON, Canada.

CSA. 2004. Masonry construction for building. Standard CAN/CSA A371-04. Canadian Standards Association, Mississauga, ON, Canada.

CSA. 2014. Mortar and grout for unit masonry. Standard CAN/CSA A179-14. Canadian Standards Association, Mississauga, ON, Canada.

Dharmaraj, R., and Malathy, R. (2015). Performance evaluation of sodium nitrite corrosion inhibitor in self compacting concrete. Indian Journal of Science and Technology, 8(36), 1-6.

Das, S., Liu, J., El-Sayed, M., and Sturgeon, G. (2013, June). Effect of height-to-thickness ratio on compressive Strength of hollow concrete masonry. In 12th Canadian masonry symposium (CMS 2013).

Davison, J. I. (1970). Cold weather masonry construction. In Canadian building digests 101-150 (pp.4-4).

Dayaratnam, P. (1987). Brick and reinforced brick structures. South Asia Books.

De Groot, C. J. W. P. (1987). Bond in masonry. Proc., 5th International Conference on Structural Engineering Analysis and Modeling, University of Science and Technology, Kumasi, Ghana.

De Pellegrin, M. Z., Acordi, J., and Montedo, O. R. K. (2019). Influence of the length and the content of cellulose fibres obtained from sugarcane bagasse on the mechanical properties of fibre-reinforced mortar composites. Journal of Natural Fibres.

De Vekey, R. C., Edgell, G. J., and Dukes, R. (1989, October). Effect of sand grading on the performance and properties of masonry. In Masonry (4). Proc. 2nd Int. Masonry Conf. London (Vol. 23, No. 25).

Dodson, V. H. (1994). Time of setting. In Significance of Tests and Properties of Concrete and Concrete-Making Materials. ASTM International.

Drysdale, R. G., and Hamid, A. A. (1979, June). Behaviour of concrete block masonry under axial compression. In Journal Proceedings (Vol. 76, No. 6, pp. 707-722).

Drysdale, R. G., and Hamid, A. A. (2005). Masonry Structures: Behaviour and Design. Mississauga, Ontario, Canada.

Drysdale, R.G., A.A. Hamid, and L.R. Baker (1999). Masonry structures behaviour and design. The Masonry Society, 2nd Edition, Boulder, CO.

Duggal, S. (2008). Building materials (3rd ed.). New Delhi: New Age International.

Dymiotis, C., and Gutlederer, B. M. (2002). Allowing for uncertainties in the modelling of masonry compressive strength. Construction and building materials, 16(8), 443-452.

Eliche-Quesada, D., Corpas-Iglesias, F. A., Pérez-Villarejo, L., and Iglesias-Godino, F. J. (2012). Recycling of sawdust, spent earth from oil filtration, compost and marble residues for brick manufacturing. Construction and Building Materials, 34, 275-284.

Essroc. (2012a). Essroc Technical Notes: Cold Weather Masonry. Nazareth, PA, USA, 1–2.

Essroc. (2012b). Essroc Technical Notes: Masonry Construction in Cold Weather. Nazareth, PA, USA, 1–2.

Flores, J., Kamali, M., and Ghahremaninezhad, A. (2017). An investigation into the properties and microstructure of cement mixtures modified with cellulose nanocrystal. Materials, 10(5), 498.

Fu, T., Montes, F., Suraneni, P., Youngblood, J., and Weiss, J. (2017). The influence of cellulose nanocrystals on the hydration and flexural strength of Portland cement pastes. Polymers, 9(9), 424.

Gayed, M., Korany, Y., and Sturgeon, G. (2012). Examination of the prescribed concrete block masonry compressive strength in the Canadian masonry design standard, CSA S304. 1-04. In 15th International brick and block masonry conference, Florianopolis, Brazil.

Ghosh, S. K. (1991). Flexural bond strength of masonry: experimental review. Masonry Soc. J., 9(2), 64-72.

Groot, C. (1993). Effects of water on mortar-brick bond PhD thesis. University of Delft, Delft, The Netherlands.

Gumaste, K. S., Rao, K. N., Reddy, B. V., and Jagadish, K. S. (2007). Strength and elasticity of brick masonry prisms and wallettes under compression. Materials and structures, 40(2), 241-253.

Hamid, A. A., and Chukwunenye, A. O. (1986). Compression behaviour of concrete masonry prisms. Journal of Structural Engineering, 112(3), 605-613.

Harris, B. H. (2010). Investigation of the lower bound compressive and flexural strengths of conventional concrete and clay masonry (Doctoral dissertation, The University of Texas at Arlington).

Hendry, A. W., and Khalaf, F. M. (2001). Masonry wall construction. E and FN Spon, London.

Henry, L., Shankha, B., William, J., and Melissa, S. (2007). Test on mercury vapour emission from fly ash bricks. World of Coal Ash, Covington, Kentucky, USA.

Hoyos, C. G., Cristia, E., and Vázquez, A. (2013). Effect of cellulose microcrystalline particles on properties of cement-based composites. Materials and Design, 51, 810-818.

Jiao, L., Su, M., Chen, L., Wang, Y., Zhu, H., Dai, H. (2016). Natural Cellulose Nanofibres as Sustainable Enhancers in Construction Cement. PLOS ONE, 11, e0168422.

Kadir, A. A., and Mohajerani, A. (2015). Effect of heating rate on gas emissions and properties of fired clay bricks and fired clay bricks incorporated with cigarette butts. Applied Clay Science, 104, 269-276.

Kafy, A., Kim, H. C., Zhai, L., Kim, J. W., and Kang, T. J. (2017). Cellulose long fibres fabricated from cellulose nanofibres and its strong and tough characteristics. Scientific reports, 7(1), 1-8.

Karagöl, F., Demirboga, R., and Khushefati, W. H. (2015). Behaviour of fresh and hardened concretes with antifreeze admixtures in deep-freeze low temperatures and exterior winter conditions. Construction and Building Materials, 76, 388-395.

Karagöl, F., Demirboğa, R., Kaygusuz, M. A., Yadollahi, M. M., and Polat, R. (2013). The influence of calcium nitrate as antifreeze admixture on the compressive strength of concrete exposed to low temperatures. Cold Regions Science and Technology, 89, 30-35.

Kaushik, H. B., Rai, D. C., and Jain, S. K. (2007). Stress-strain characteristics of clay brick masonry under uniaxial compression. Journal of materials in Civil Engineering, 19(9), 728-739.

Kazempour, H., Bassuoni, M. T., and Hashemian, F. (2017). Masonry mortar with nanoparticles at a low temperature. Proceedings of the Institution of Civil Engineers-Construction Materials, 170(6), 297-308.

Kayali, O. (2005, April). High performance bricks from fly ash. In Proceedings of the World of Coal Ash Conference, Lexinton, Kentucky (Vol. 11).

Khalaf, F. M. (1996). Factors influencing compressive strength of concrete masonry prisms. Magazine of Concrete Research, 48(175), 95-101.

Khalaf, F. M., Hendry, A. W., and Fairbairn, D. R. (1994). Study of the compressive strength of blockwork masonry. Structural Journal, 91(4), 367-375.

Khayat, K. H., and Nasser, K. W. (1991). Comparison of air contents in fresh and hardened concretes using different air meters. Cement, concrete and aggregates, 13(1), 18-24.

Korhonen, C.J. (1990). Antifreeze admixtures for cold regions concreting: A literature review. U.S. Army Cold Regions Research and Engineering Laboratory, Hanover, NH, USA.

Korhonen, C. J. (1999). Expedient low-temperature concrete admixtures for the Army.

Korhonen, C. J. (2002). Effect of high doses of chemical admixtures on the freeze-thaw durability of Portland cement concrete.

Korhonen, C. J. (2006). Extending the season for concrete construction and repair. Phase II, Defining engineering parameters.

Korhonen, C. J., and Brook, J. W. (1996). Freezing temperature protection admixture for Portland cement concrete.

Korhonen, C. J., and Orchino, S. A. (2001). Off-the-shelf antifreeze admixture for concrete: initial laboratory investigation.

Korhonen, C. J., Semen, P. M., and Barna, L. A. (2004). Extending the season for concrete construction and repair. Phase I, establishing the technology.

Korhonen, C.J., Semen, P.M., and Barna, L.A. (2004). An off-the-shelf approach to winter concreting. In Proceedings of the 12th International Specialty Conference on Cold Regions Engineering.

Korhonen, C. J., Thomas, R. D., and Cortez, E. R. (1997). Increasing cold weather masonry construction productivity. COLD REGIONS RESEARCH AND ENGINEERING LAB HANOVER NH.

Kosmatka, S. H., Kerkhoff, B., and Panarese, W. C. (2002). Design and control of concrete mixtures (Vol. 5420, pp. 60077-1083). Skokie, IL: Portland Cement Association.

Kozikowski, R. L., McCall, W. C., and Suprenant, B. A. (2014). Cold weather concreting strategies. Concrete international, 36(5), 45-49.

Lawrence, S. J., and Cao, H. T. (1987, August). An experimental study of the interface between brick and mortar. In Proceedings of the Fourth North American Masonry Conference (Los Angeles) (p. 48).

Li, Q., Ge, Y., and Yang, W. (2016). Effect of sodium sulphate and sodium nitrite on air-void system in air-entrained concrete. Magazine of Concrete Research, 68(23), 1200-1209.

Liu, J. (2012). The effect of height-to-thickness ratio on the compressive strength of concrete masonry.

Liu, Z., Jiao, W., Sha, A., Gao, J., Han, Z., and Xu, W. (2017). Portland cement hydration behaviour at low temperatures: Views from calculation and experimental study. Advances in Materials Science and Engineering, 2017.

Liu, Z., Lou, B., Barbieri, D. M., Sha, A., Ye, T., and Li, Y. (2020). Effects of pre-curing treatment and chemical accelerators on Portland cement mortars at low temperature (5 °C). Construction and Building Materials, 240, 117893.

Lumantarna, R., Biggs, D. T., and Ingham, J. M. (2014). Uniaxial compressive strength and stiffness of field-extracted and laboratory-constructed masonry prisms. Journal of Materials in Civil Engineering, 26(4), 567-575.

Maliekkal, B. P., Kakkassery, J. T., and Palayoor, V. R. (2018). Efficacies of sodium nitrite and sodium citrate–zinc acetate mixture to inhibit steel rebar corrosion in simulated concrete interstitial solution contaminated with NaCl. International Journal of Industrial Chemistry, 9(2), 105-114.

Mann, W. (1982, May). Statistical evaluation of tests on masonry by potential functions. In Sixth international brick masonry conference.

Maurenbrecher, A. H. P. (1978). Use of the prism test to determine compressive strength of masonry. In NORTH AMERICAN MASONRY CONFERENCE (Vol. 1, p. 1978).

Massazza, F. (2003). Pozzolana and pozzolanic cements, w Lea's Chemistry of Cement and Concrete, PC Hewlett.

McGinley, W. M., and Greenwald, J. (2005). Hollow unit bond wrench test trials. In 10th Canadian Masonry Symposium (pp. 8-12).

Mindess, S., Young, J. F., and Darwin, D. (2003). Concrete. Pearson Education Inc., Upper Saddle River, NJ, USA, 644.

Mohamad, G., Lourenço, P. B., and Roman, H. R. (2007). Mechanics of hollow concrete block masonry prisms under compression: Review and prospects. Cement and Concrete Composites, 29(3), 181-192.

Moon, R. J., Schueneman, G. T., and Simonsen, J. (2016). Overview of cellulose nanomaterials, their capabilities and applications. Jom, 68(9), 2383-2394.

Neal, R. (2002). Problems with Concrete in Cold Weather? What's New? Hanley-Wood Press, Washington, WA, USA, 1–4.

Neville, A. (2004). The confused world of sulphate attack on concrete. Cement and Concrete research, 34(8), 1275-1296.

Neville, A. (1996). Properties of Concrete. Fourth Edition, Addision Wesley Longman, Limited, UK.

Nichols, J. M., and Holland, N. L. (2011). A Comparative Study of Balanced Bond Wrench Testing and Unbalanced Bond Wrench Testing. In Eleventh North American Masonry Conference, Minneapolis.

Nilsson J, Sargenius P. (2011). Effect of microfibrillar cellulose on concrete equivalent mortar fresh and hardened properties. Swedish Cement and Concrete Research Institute, Stockholm, Sweden.

Nmai, C. K. (1998). Cold weather concreting admixtures. Cement and Concrete Composites, 20(2-3), 121-128.

Oey, T., Stoian, J., Li, J., Vong, C., Balonis, M., Kumar, A., and Sant, G. (2015). Comparison of $Ca(NO_3)_2$ and $CaCl_2$ admixtures on reaction, setting, and strength evolutions in plain and blended cementing formulations. Journal of Materials in Civil Engineering, 27(10), 04014267.

Onuaguluchi, O., Panesar, D. K., and Sain, M. (2014). Properties of nanofibre reinforced cement composites. Construction and Building Materials, 63, 119-124.

Osong, S. H., Norgren, S., and Engstrand, P. (2016). Processing of wood-based micro fibrillated cellulose and nano fibrillated cellulose, and applications relating to papermaking: a review. Cellulose, 23(1), 93-123.

Ozyildirim, C., and Carino, N. J. (2006). Concrete strength testing. In Significance of tests and properties of concrete and concrete-making Materials. ASTM International.

Page, A. W., and Shrive, N. G. (1988). A critical assessment of compression tests for hollow block masonry. Masonry int. Masonry Int., 2(2), 64.

Peterson, K. W., Swartz, R. A., Sutter, L. L., and Van Dam, T. J. (2001). Hardened concrete air void analysis with a flatbed scanner. Transportation Research Record, 1775(1), 36-43.

Polat, R. (2016). The effect of antifreeze additives on fresh concrete subjected to freezing and thawing cycles. Cold Regions Science and Technology, 127, 10-17.

Radcliffe, M. R., Bennett, R. M., and Bryja, J. (2004). Highly cored extruded clay units: testing and design procedures. In Structures 2004: Building on the Past, Securing the Future (pp. 1-8).

Rao, K. V. M., Reddy, B. V., and Jagadish, K. S. (1996). Flexural bond strength of masonry using various blocks and mortars. Materials and structures, 29(2), 119-124.

Ratinov, V. B., and Rozenberg, T. I. (1996). Antifreezing admixtures. In Concrete admixtures handbook (pp. 740-799). William Andrew Publishing.

Ravula, M. B., and Subramaniam, K. V. (2017). Experimental investigation of compressive failure in masonry brick assemblages made with soft brick. Materials and Structures, 50(1), 1-11.

Reddy, B. V., and Gupta, A. (2005). Characteristics of cement-soil mortars. Materials and structures, 38(6), 639-650.

Reddy, B. V., and Gupta, A. (2005). Characteristics of soil-cement blocks using highly sandy soils. Materials and structures, 38(6), 651-658.

Reddy, B. V., and Vyas, C. V. U. (2008). Influence of shear bond strength on compressive strength and stress–strain characteristics of masonry. Materials and structures, 41(10), 1697-1712.

Saha, O., Boulfiza, M., and Wegner, L.D. (2019). Behaviour of masonry mortar containing a non-harmful antifreeze admixture. TMS Journal, 37(1):1-9.

Saha, O., Boulfiza, M., and Wegner, L.D. (2015a). Developing antifreeze admixtures for mortar from available off-the-shelf admixtures. In 12th North American Masonry Conference. Denver, CO. USA.

Saha, O., Boulfiza, M., and Wegner, L.D. (2015b). Characterization of the hydration products of an antifreeze treated cement paste. In CONMAT15. Whistler, BC, Canada.

Saha, O., Boulfiza, M., and Wegner, L. D. (2020). Tracking the hydration of antifreeze treated cement paste at subfreezing temperatures using the TDR technique. Construction and Building Materials, 262, 119915.

Saha, O. (2019). Cold weather admixture systems for cement-based materials applied to masonry mortar binder (Doctoral dissertation, University of Saskatchewan).

Samarasinghe, W., and Lawrence, S. J. (1992). Effect of high suction rate in low strength bricks on brick mortar bond. DBCE.

Sarangapani, G., Venkatarama Reddy, B. V., and Jagadish, K. S. (2005). Brick-mortar bond and masonry compressive strength. Journal of materials in civil engineering, 17(2), 229-237.

Scrivener, J., Zsembery, S., McNeily, T., and Lawrence, S. J. (1992). In-situ bond strength of clay brickwork. Proc., 4th Int. Seminar on Structural Masonry for Developing Countries, Madras, India, 51–55.

Senff, L., Hotza, D., Repette, W. L., Ferreira, V. M., and Labrincha, J. A. (2010). Effect of nanosilica and microsilica on microstructure and hardened properties of cement pastes and mortars. Advances in applied ceramics, 109(2), 104-110.

Senff, L., Hotza, D., Repette, W. L., Ferreira, V. M., and Labrincha, J. A. (2010). Mortars with nano-SiO_2 and micro-SiO_2 investigated by experimental design. Construction and Building Materials, 24(8), 1432-1437.

Shak, K. P. Y., Pang, Y. L., and Mah, S. K. (2018). Nanocellulose: Recent advances and its prospects in environmental remediation. Beilstein journal of nanotechnology, 9(1), 2479-2498.

Shuzhen, L., Ning, C., Zhonghua, P., Yanhua, P., and Huang, T. (2011). Preparation and properties of bacterial cellulose reinforced cement composites. China Powder Sci. Technol, 17, 57-60.

Soliman, A. M. Y. (2020). Cold weather concrete: innovative mixtures designs and protection (Doctoral dissertation, University of Manitoba).

Sonebi, M., Bassuoni, M. T., Kwasny, J., and Amanuddin, A. K. (2015). Effect of nanosilica on rheology, fresh properties, and strength of cement-based grouts. Journal of materials in Civil Engineering, 27(4), 04014145.

Song, Z. (2017). High performance and ultra high performance concrete with locally available materials from Saskatchewan (Doctoral dissertation, University of Saskatchewan).

Supit, S. W., and Nishiwaki, T. (2019). Compressive and flexural strength behaviour of ultra-high performance mortar reinforced with cellulose nano-fibres. Int. J. Adv. Sci. Eng. Inf. Technol, 9, 365-372.

Suprenant, B. A. (1992). Protecting fresh concrete from freezing weather. Concrete Construction, 37(2), 126-128.

Teklegiorgis, N. S., Pradhan, B., Prusty, J. K., and Das, J. K. (2022). Effect of Sodium Nitrite as Corrosion Inhibitor against Chloride-Induced Corrosion of Steel Rebar in Geopolymer Concrete Containing Fly Ash and GGBS. Journal of Materials in Civil Engineering, 34(4), 04022007.

Thaickavil, N. N., and Thomas, J. (2018). Behaviour and strength assessment of masonry prisms. Case Studies in Construction Materials, 8, 23-38.

Thamboo, J. A., and Dhanasekar, M. (2019). Correlation between the performance of solid masonry prisms and wallettes under compression. Journal of Building Engineering, 22, 429-438.

Thomson SL, O'Callaghan DJ, Westland JA, Su B. (2012). Method of making a fibre cement board with improved properties and the product. Patent Publication No. US8273174 B2.

Throop, D. (2005). All-Weather Masonry-Part 2. Structure Magazine, (11), Reedsburg, WI, USA, 11–14.

Weerawarna SA, O'Callaghan DJ. (2015). Internally curing cement-based materials. Patent Publication No. US9056792 B2.

Weerawarna SA, Shah HM. (2014). Fibre for fibre cement and resulting product. Patent Publication No. US8791178 B2.

Wong, H. E., and Drysdale, R. G. (1985). Compression characteristics of concrete block masonry prisms. In Masonry: Research, application, and problems. ASTM International.

Woodham, D., and Schuller, M. (2005). Masonry construction in cold weather. Concrete International, 27(11), 27-30.

Youngblood JP, Zavattieri PD, Moon RJ, Weiss WJ, Cao Y. (2016). Cellulose nanocrystal additives and improved cementious systems. Patent Publication No.US20160075601 A1.

APPENDICES

APPENDIX A – COMPRESSIVE STRENGTH VALUES WITH PAIRED SAMPLE T-TEST ANALYSIS FOR COMPRESSION TEST RESULTS BETWEEN DIFFERENT GROUPS

The compressive strength values at 28 days of all prisms that were tested are presented in this appendix, along with their corresponding standard deviations, coefficients of variation and with details of the statistical comparisons that were conducted with 95% level of confidence.

Table A.1 Compressive strengths of control prisms cured at room temperature

Force (kN)	Area(mm^2)	Compressive Strength (MPa)	Avg (MPa)	STDEV	Coefficient of Variation
316.83	13950	22.71	24.10	1.10	4.56
354.77	13950	25.43			
352.86	13950	25.29			
317.39	13950	22.75			
334.71	13950	23.99			
324.64	13950	23.27			
355.44	13950	25.48			
335.86	13950	24.08			
330.20	13950	23.67			

Table A.2 Compressive strengths of control prisms cured at -10°C

Force (kN)	Area(mm^2)	Compressive Strength (MPa)	Avg (MPa)	STDEV	Coefficient of Variation
178.15	13950	12.77	12.36	0.87	7.04
170.60	13950	12.23			
155.36	13950	11.14			
191.50	13950	13.73			
161.31	13950	11.56			
182.32	13950	13.07			
158.24	13950	11.34			
180.57	13950	12.94			
173.67	13950	12.45			

Table A.3 Compressive strengths of sodium nitrite prisms cured at room temperature

Force (kN)	Area(mm^2)	Compressive Strength (MPa)	Avg (MPa)	STDEV	Coefficient of Variation
400.67	13950	28.72	26.70	1.44	5.39
360.00	13950	25.81			
350.00	13950	25.09			
355.00	13950	25.45			
385.00	13950	27.59			
360.00	13950	25.80			
355.00	13950	25.45			
390.00	13950	27.96			
396.00	13950	28.39			

Table A.4 Compressive strengths of sodium nitrite prisms cured at -10°C

Force (kN)	Area(mm^2)	Compressive Strength (MPa)	Avg (MPa)	STDEV	Coefficient of Variation
293.00	13950	21.00	21.20	1.48	6.98
288.00	13950	20.64			
290.00	13950	20.78			
280.00	13950	20.07			
291.00	13950	20.86			
280.00	13950	20.07			
280.00	13950	20.07			
320.00	13950	22.94			
340.00	13950	24.37			

Table A.5 Compressive strengths of nanocellulose prisms cured at room temperature

Force (kN)	Area(mm^2)	Compressive Strength (MPa)	Avg (MPa)	STDEV	Coefficient of Variation
406.00	13950	29.10	27.87	1.31	4.70
400.00	13950	28.67			
360.00	13950	25.81			
404.00	13950	28.96			
390.00	13950	27.96			
365.00	13950	26.16			
375.00	13950	26.88			
390.00	13950	27.96			
410.00	13950	29.39			

Table A.6 Compressive strengths of nanocellulose prisms cured at -10°C

Force (kN)	Area(mm^2)	Compressive Strength (MPa)	Avg (MPa)	STDEV	Coefficient of Variation
160.00	13950	11.47	12.90	0.87	6.74
180.00	13950	12.90			
164.00	13950	11.76			
191.00	13950	13.69			
190.00	13950	13.62			
170.00	13950	12.19			
188.00	13950	13.48			
187.00	13950	13.41			
190.00	13950	13.62			

Table A.7 Compressive strengths of sodium nitrite and nanocellulose prisms cured at room temperature

Force (kN)	Area(mm^2)	Compressive Strength (MPa)	Avg (MPa)	STDEV	Coefficient of Variation
400.00	13950	28.67	28.10	1.35	4.80
400.00	13950	28.67			
390.00	13950	27.96			
396.00	13950	28.39			
373.00	13950	26.74			
370.00	13950	26.52			
365.00	13950	26.16			
410.00	13950	29.39			
420.00	13950	30.11			

Table A.8 Compressive strengths of sodium nitrite and nanocellulose prisms cured at -10°C

Force (kN)	**Area(mm^2)**	**Compressive Strength (MPa)**	**Avg (MPa)**	**STDEV**	**Coefficient of Variation**
304.00	13950	21.79			
290.00	13950	20.79			
310.00	13950	22.22			
290.00	13950	20.78			
298.00	13950	21.36	21.84	1.00	4.58
335.00	13950	24.01			
295.00	13950	21.15			
308.00	13950	22.08			
312.00	13950	22.36			

Table A.9 Paired samples statistics for the control groups

		Mean	N	Std. Deviation	Std. Error Mean
Pair 1	CTR23	2.40757E1	9	1.102549	.367516
	CTR10	1.23594E1	9	.871246	.290415

Table A.10 Paired samples correlations for the control groups

		N	Correlation	Sig.
Pair 1	CTR23 & CTR10	9	-.782	.013

Table A.11 Paired samples test for the control groups

		Paired Differences					t	df	Sig. (2-tailed)
		Mean	Std. Deviation	Std. Error Mean	95% Confidence Interval of the Difference				
					Lower	Upper			
Pair 1	CTR23 - CTR10	1.171629E1	1.864495	.621498	10.283110	13.149466	18.852	8	.000

Table A.12 Paired samples statistics for the sodium nitrite groups

		Mean	N	Std. Deviation	Std. Error Mean
Pair 1	SN23	2.66959E1	9	1.442507	.480836
	SN10	2.12027E1	9	1.480759	.493586

Table A.13 Paired samples correlations for the sodium nitrite groups

		N	Correlation	Sig.
Pair 1	SN23 & SN10	9	.692	.039

Table A.14 Paired samples test for the sodium nitrite groups

		Paired Differences					t	df	Sig. (2-tailed)
		Mean	Std. Deviation	Std. Error Mean	95% Confidence Interval of the Difference				
					Lower	Upper			
Pair 1	SN23 - SN10	5.493190E0	1.147350	.382450	4.611259	6.375121	14.363	8	.000

Table A.15 Paired samples statistics for the nanocellulose groups

		Mean	N	Std. Deviation	Std. Error Mean
Pair 1	NC23	2.78773E1	9	1.314706	.438235
	NC10	1.29032E1	9	.874288	.291429

Table A.16 Paired samples correlations for the nanocellulose groups

		N	Correlation	Sig.
Pair 1	NC23 & NC10	9	.360	.341

Table A.17 Paired samples test for the nanocellulose groups

		Paired Differences					t	df	Sig. (2-tailed)
		Mean	Std. Deviation	Std. Error Mean	95% Confidence Interval of the Difference				
					Lower	Upper			
Pair 1	NC23 - NC10	1.497411E1	1.290544	.430181	13.982114	15.966114	34.809	8	.000

Table A.18 Paired samples statistics for the sodium nitrite with nanocellulose groups

		Mean	N	Std. Deviation	Std. Error Mean
Pair 1	NN23	2.80685E1	9	1.347838	.449279
	NN10	2.18399E1	9	1.008055	.336018

Table A.19 Paired samples correlations for the sodium nitrite with nanocellulose groups

		N	Correlation	Sig.
Pair 1	NN23 & NN10	9	-.098	.803

Table A.20 Paired samples test for the sodium nitrite with nanocellulose groups

		Paired Differences					t	df	Sig. (2-tailed)
		Mean	Std. Deviation	Std. Error Mean	95% Confidence Interval of the Difference				
					Lower	Upper			
Pair 1	NN23 - NN10	6.228594E0	1.760088	.586696	4.875671	7.581518	10.616	8	.000

Table A.21 Paired samples statistics for the control and sodium nitrite samples cured at room temperature

		Mean	N	Std. Deviation	Std. Error Mean
Pair 1	CTR23	2.40757E1	9	1.102549	.367516
	SN23	2.66959E1	9	1.442507	.480836

Table A.22 Paired samples correlations for the control and sodium nitrite samples cured at room temperature

		N	Correlation	Sig.
Pair 1	CTR23 & SN23	9	-.477	.194

Table A.23 Paired samples test for the control and sodium nitrite samples cured at room temperature

		Paired Differences					t	df	Sig. (2-tailed)
		Mean	Std. Deviation	Std. Error Mean	95% Confidence Interval of the Difference				
					Lower	Upper			
Pair 1	CTR23 - SN23	-2.620231E0	2.194150	.731383	-4.306804	-.933658	-3.583	8	.007

Table A.24 Paired samples statistics for the control and nanocellulose samples cured at room temperature

		Mean	N	Std. Deviation	Std. Error Mean
Pair 1	CTR23	2.40757E1	9	1.102549	.367516
	NC23	2.78773E1	9	1.314706	.438235

Table A.25 Paired samples correlations for the control and nanocellulose samples cured at room temperature

		N	Correlation	Sig.
Pair 1	CTR23 & NC23	9	-.448	.227

Table A.26 Paired samples test for the control and nanocellulose samples cured at room temperature

		Paired Differences					t	df	Sig. (2-tailed)
		Mean	Std. Deviation	Std. Error Mean	95% Confidence Interval of the Difference				
					Lower	Upper			
Pair 1	CTR23 - NC23	-3.801673E0	2.059637	.686546	-5.384849	-2.218496	-5.537	8	.001

Table A.27 Paired samples statistics for the control and sodium nitrite with nanocellulose samples cured at room temperature

		Mean	N	Std. Deviation	Std. Error Mean
Pair 1	CTR23	2.40757E1	9	1.102549	.367516
	NN23	2.80685E1	9	1.347838	.449279

Table A.28 Paired samples correlations for the control and sodium nitrite with nanocellulose samples cured at room temperature

		N	Correlation	Sig.
Pair 1	CTR23 & NN23	9	-.228	.555

Table A.29 Paired samples test for the control and sodium nitrite with nanocellulose samples cured at room temperature

		Paired Differences					t	df	Sig. (2-tailed)
		Mean	Std. Deviation	Std. Error Mean	95% Confidence Interval of the Difference				
					Lower	Upper			
Pair 1	CTR23 - NN23	-3.992832E0	1.926057	.642019	-5.473330	-2.512333	-6.219	8	.000

Table A.30 Paired samples statistics for the control and sodium nitrite samples cured at freezing temperature

		Mean	N	Std. Deviation	Std. Error Mean
Pair 1	CTR10	1.23594E1	9	.871246	.290415
	SN10	2.12027E1	9	1.480759	.493586

Table A.31 Paired samples correlations for the control and sodium nitrite samples cured at freezing temperature

		N	Correlation	Sig.
Pair 1	CTR10 & SN10	9	.084	.830

Table A.32 Paired samples test for the control and sodium nitrite samples cured at freezing temperature

		Paired Differences					t	df	Sig. (2-tailed)
		Mean	Std. Deviation	Std. Error Mean	95% Confidence Interval of the Difference				
					Lower	Upper			
Pair 1	CTR10 - SN10	-8.843329E0	1.653639	.551213	-10.114429	-7.572230	-16.043	8	.000

Table A.33 Paired samples statistics for the control and nanocellulose samples cured at freezing temperature

		Mean	N	Std. Deviation	Std. Error Mean
Pair 1	CTR10	1.23594E1	9	.871246	.290415
	NC10	1.29032E1	9	.874288	.291429

Table A.34 Paired samples correlations for the control and nanocellulose samples cured at freezing temperature

		N	Correlation	Sig.
Pair 1	CTR10 & NC10	9	.096	.805

Table A.35 Paired samples test for the control and nanocellulose samples cured at freezing temperature

		Paired Differences					t	df	Sig. (2-tailed)
		Mean	Std. Deviation	Std. Error Mean	95% Confidence Interval of the Difference				
					Lower	Upper			
Pair 1	CTR10 - NC10	-.543847	1.173318	.391106	-1.445739	.358045	-1.391	8	.202

Table A.36 Paired samples statistics for the control and sodium nitrite with nanocellulose samples cured at freezing temperature

		Mean	N	Std. Deviation	Std. Error Mean
Pair 1	CTR10	1.23594E1	9	.871246	.290415
	NN10	2.18399E1	9	1.008055	.336018

Table A.37 Paired samples correlations for the control and sodium nitrite with nanocellulose samples cured at freezing temperature

		N	Correlation	Sig.
Pair 1	CTR10 & NN10	9	.146	.708

Table A.38 Paired samples test for the control and sodium nitrite with nanocellulose samples cured at freezing temperature

		Paired Differences					t	df	Sig. (2-tailed)
		Mean	Std. Deviation	Std. Error Mean	95% Confidence Interval of the Difference				
					Lower	Upper			
Pair 1	CTR10 - NN10	-9.480526E0	1.232291	.410764	-10.427748	-8.533303	-23.080	8	.000

Table A.39 Paired samples statistics for control samples cured at room temperature and sodium nitrite samples cured at freezing temperature

		Mean	N	Std. Deviation	Std. Error Mean
Pair 1	CTR23	2.40757E1	9	1.102549	.367516
	SN10	2.12027E1	9	1.480759	.493586

Table A.40 Paired samples correlations for control samples cured at room temperature and sodium nitrite samples cured at freezing temperature

		N	Correlation	Sig.
Pair 1	CTR23 & SN10	9	-.109	.780

Table A.41 Paired samples test for control samples cured at room temperature and sodium nitrite samples cured at freezing temperature

		Paired Differences					t	df	Sig. (2-tailed)
		Mean	Std. Deviation	Std. Error Mean	95% Confidence Interval of the Difference				
					Lower	Upper			
Pair 1	CTR23 - SN10	2.872959E0	1.940374	.646791	1.381456	4.364462	4.442	8	.002

Table A.42 Paired samples statistics for control samples cured at room temperature and sodium nitrite with nanocellulose samples cured at freezing temperature

		Mean	N	Std. Deviation	Std. Error Mean
Pair 1	CTR23	2.40757E1	9	1.102549	.367516
	NN10	2.18399E1	9	1.008055	.336018

Table A.43 Paired samples correlations for control samples cured at room temperature and sodium nitrite with nanocellulose samples cured at freezing temperature

		N	Correlation	Sig.
Pair 1	CTR23 & NN10	9	-.270	.483

Table A.44 Paired samples test for control samples cured at room temperature and sodium nitrite with nanocellulose samples cured at freezing temperature

		Paired Differences					t	df	Sig. (2-tailed)
		Mean	Std. Deviation	Std. Error Mean	95% Confidence Interval of the Difference				
					Lower	Upper			
Pair 1	CTR23 - NN10	2.235763E0	1.682604	.560868	.942399	3.529126	3.986	8	.004

APPENDIX B – LINEAR REGRESSION ANALYSIS FOR THE PROPOSED MODEL TO ESTIMATE THE COMPRESSIVE STRENGTH OF MASONRY BRICK PRISM

Statistical regression analysis was conducted using SPSS on 72 data sets from this study. A summary of the developed model based on regression analysis with the significant level of each parameter in the model is presented in this appendix.

Table B.1 Model summary

Model	R	R Square	Adjusted R Square	Std. Error of the Estimate
1	.962[a]	.926	.923	1.79550

Predictors: (Constant), mortar strength, brick strength

Table B.2 ANOVA

Model		Sum of Squares	df	Mean Square	F	Sig.
1	Regression	2804.686	2	1402.343	434.994	.000[a]
	Residual	225.668	70	3.224		
	Total	3030.353	72			

a. Predictors: (Constant), mortar strength, brick strength

b. Dependent Variable: *f'm*

Table B.3 Coefficients

Model		Unstandardized Coefficients		Standardized Coefficients	t	Sig.
		B	Std. Error	Beta		
1	(Constant)	-0.085	1.795		-.047	.963
	brick strength	0.330	0.047	.235	7.084	.000
	mortar strength	0.750	0.028	.891	26.863	.000

a. Dependent Variable: *f'm*

APPENDIX C – FLEXURAL BOND TEST RESULTS WITH PAIRED SAMPLE T-TEST ANALYSIS FOR COMPRESSION TEST RESULTS BETWEEN DIFFERENT GROUPS

The flexural bond strengths measured for all prisms groups are listed in this appendix, along with details of the statistical comparisons that were conducted with 95% level of confidence.

Table C.1 Flexural bond strength test results for control samples cured at the room temperature

P1 (N)	L1 (mm)	P2 (N)	L2 (mm)	t_u (mm)	P3 (N)	M (N·mm)	P (N)	S (mm^3)	Ae (mm^2)	ft (MPa)
410	380	173	92.5	45	16.67	145567.5	599.67	251250	13950	0.536386
300	380	173	92.5	45	16.67	108717.5	489.67	251250	13950	0.397605
340	380	173	92.5	45	16.67	122117.5	529.67	251250	13950	0.448071
400	380	173	92.5	45	16.67	142217.5	589.67	251250	13950	0.52377
300	380	173	92.5	45	16.67	108717.5	489.67	251250	13950	0.397605
430	380	173	92.5	45	16.67	152267.5	619.67	251250	13950	0.561619
462	380	173	92.5	45	16.67	162987.5	651.67	251250	13950	0.601992
300	380	173	92.5	45	16.67	108717.5	489.67	251250	13950	0.397605
360	380	173	92.5	45	16.67	128817.5	549.67	251250	13950	0.473304
312	380	173	92.5	45	16.67	112737.5	501.67	251250	13950	0.412744
350	380	173	92.5	45	16.67	125467.5	539.67	251250	13950	0.460687
430	380	173	92.5	45	16.67	152267.5	619.67	251250	13950	0.561619
350	380	173	92.5	45	16.67	125467.5	539.67	251250	13950	0.460687
440	380	173	92.5	45	16.67	155617.5	629.67	251250	13950	0.574235
300	380	173	92.5	45	16.67	108717.5	489.67	251250	13950	0.397605
220	380	173	92.5	45	16.67	81917.5	409.67	251250	13950	0.296673
310	380	173	92.5	45	16.67	112067.5	499.67	251250	13950	0.410221
330	380	173	92.5	45	16.67	118767.5	519.67	251250	13950	0.435454
350	380	173	92.5	45	16.67	125467.5	539.67	251250	13950	0.460687
450	380	173	92.5	45	16.67	158967.5	639.67	251250	13950	0.586852
360	380	173	92.5	45	16.67	128817.5	549.67	251250	13950	0.473304
400	380	173	92.5	45	16.67	142217.5	589.67	251250	13950	0.52377
350	380	173	92.5	45	16.67	125467.5	539.67	251250	13950	0.460687
400	380	173	92.5	45	16.67	142217.5	589.67	251250	13950	0.52377
355	380	173	92.5	45	16.67	127142.5	544.67	251250	13951	0.466998

Table C.2 Flexural bond strength test results for control samples cured at the freezing temperature

P1 (N)	L1 (mm)	P2 (N)	L2 (mm)	t_u (mm)	P3 (N)	M (N·mm)	P (N)	S (mm^3)	Ae (mm^2)	ft (MPa)
101	380	173	92.5	45	16.67	42052.5	290.67	251250	13950	0.146537
86	380	173	92.5	45	16.67	37027.5	275.67	251250	13950	0.127612
119	380	173	92.5	45	16.67	48082.5	308.67	251250	13950	0.169246
60	380	173	92.5	45	16.67	28317.5	249.67	251250	13950	0.094809
102	380	173	92.5	45	16.67	42387.5	291.67	251250	13950	0.147798
80	380	173	92.5	45	16.67	35017.5	269.67	251250	13950	0.120042
119	380	173	92.5	45	16.67	48082.5	308.67	251250	13950	0.169246
116	380	173	92.5	45	16.67	47077.5	305.67	251250	13950	0.165461
113	380	173	92.5	45	16.67	46072.5	302.67	251250	13950	0.161676
91	380	173	92.5	45	16.67	38702.5	280.67	251250	13950	0.13392
100	380	173	92.5	45	16.67	41717.5	289.67	251250	13950	0.145275
81	380	173	92.5	45	16.67	35352.5	270.67	251250	13950	0.121304
117	380	173	92.5	45	16.67	47412.5	306.67	251250	13950	0.166723
109	380	173	92.5	45	16.67	44732.5	298.67	251250	13950	0.15663
110	380	173	92.5	45	16.67	45067.5	299.67	251250	13950	0.157891
116	380	173	92.5	45	16.67	47077.5	305.67	251250	13950	0.165461
90	380	173	92.5	45	16.67	38367.5	279.67	251250	13950	0.132658
117	380	173	92.5	45	16.67	47412.5	306.67	251250	13950	0.166723
117	380	173	92.5	45	16.67	47412.5	306.67	251250	13950	0.166723
90	380	173	92.5	45	16.67	38367.5	279.67	251250	13950	0.132658
110	380	173	92.5	45	16.67	45067.5	299.67	251250	13950	0.157891
97	380	173	92.5	45	16.67	40712.5	286.67	251250	13950	0.14149
120	380	173	92.5	45	16.67	48417.5	309.67	251250	13950	0.170508
85	380	173	92.5	45	16.67	36692.5	274.67	251250	13950	0.12635
117	380	173	92.5	45	16.67	47412.5	306.67	251250	13950	0.166723

Table C.3 Flexural bond strength test results for sodium nitrite samples cured at the room temperature

P1 (N)	L1 (mm)	P2 (N)	L2 (mm)	t_u (mm)	P3 (N)	M (N·mm)	P (N)	S (mm^3)	Ae (mm^2)	ft (MPa)
374	380	173	92.5	45	16.67	133507.5	563.67	251250	13950	0.490967
368	380	173	92.5	45	16.67	131497.5	557.67	251250	13950	0.483397
260	380	173	92.5	45	16.67	95317.5	449.67	251250	13950	0.347139
293	380	173	92.5	45	16.67	106372.5	482.67	251250	13950	0.388773
270	380	173	92.5	45	16.67	98667.5	459.67	251250	13950	0.359755
400	380	173	92.5	45	16.67	142217.5	589.67	251250	13950	0.52377
252	380	173	92.5	45	16.67	92637.5	441.67	251250	13950	0.337046
260	380	173	92.5	45	16.67	95317.5	449.67	251250	13950	0.347139
280	380	173	92.5	45	16.67	102017.5	469.67	251250	13950	0.372372
390	380	173	92.5	45	16.67	138867.5	579.67	251250	13950	0.511153
360	380	173	92.5	45	16.67	128817.5	549.67	251250	13950	0.473304
351	380	173	92.5	45	16.67	125802.5	540.67	251250	13950	0.461949
300	380	173	92.5	45	16.67	108717.5	489.67	251250	13950	0.397605
271	380	173	92.5	45	16.67	99002.5	460.67	251250	13950	0.361017
250	380	173	92.5	45	16.67	91967.5	439.67	251250	13950	0.334522
260	380	173	92.5	45	16.67	95317.5	449.67	251250	13950	0.347139
260	380	173	92.5	45	16.67	95317.5	449.67	251250	13950	0.347139
360	380	173	92.5	45	16.67	128817.5	549.67	251250	13950	0.473304
324	380	173	92.5	45	16.67	116757.5	513.67	251250	13950	0.427884
371	380	173	92.5	45	16.67	132502.5	560.67	251250	13950	0.487182
286	380	173	92.5	45	16.67	104027.5	475.67	251250	13950	0.379942
277	380	173	92.5	45	16.67	101012.5	466.67	251250	13950	0.368587
275	380	173	92.5	45	16.67	100342.5	464.67	251250	13950	0.366063
280	380	173	92.5	45	16.67	102017.5	469.67	251250	13950	0.372372
300	380	173	92.5	45	16.67	108717.5	489.67	251250	13951	0.397607

Table C.4 Flexural bond strength test results for sodium nitrite samples cured at the freezing temperature

P1 (N)	L1 (mm)	P2 (N)	L2 (mm)	t_u (mm)	P3 (N)	M (N·mm)	P (N)	S (mm^3)	Ae (mm^2)	ft (MPa)
300	380	173	92.5	45	16.67	108717.5	489.67	251250	13950	0.397605
263	380	173	92.5	45	16.67	96322.5	452.67	251250	13950	0.350924
240	380	173	92.5	45	16.67	88617.5	429.67	251250	13950	0.321906
358	380	173	92.5	45	16.67	128147.5	547.67	251250	13950	0.47078
347	380	173	92.5	45	16.67	124462.5	536.67	251250	13950	0.456902
245	380	173	92.5	45	16.67	90292.5	434.67	251250	13950	0.328214
326	380	173	92.5	45	16.67	117427.5	515.67	251250	13950	0.430408
222	380	173	92.5	45	16.67	82587.5	411.67	251250	13950	0.299196
230	380	173	92.5	45	16.67	85267.5	419.67	251250	13950	0.309289
250	380	173	92.5	45	16.67	91967.5	439.67	251250	13950	0.334522
356	380	173	92.5	45	16.67	127477.5	545.67	251250	13950	0.468257
236	380	173	92.5	45	16.67	87277.5	425.67	251250	13950	0.316859
348	380	173	92.5	45	16.67	124797.5	537.67	251250	13950	0.458164
340	380	173	92.5	45	16.67	122117.5	529.67	251250	13950	0.448071
340	380	173	92.5	45	16.67	122117.5	529.67	251250	13950	0.448071
360	380	173	92.5	45	16.67	128817.5	549.67	251250	13950	0.473304
300	380	173	92.5	45	16.67	108717.5	489.67	251250	13950	0.397605
350	380	173	92.5	45	16.67	125467.5	539.67	251250	13950	0.460687
340	380	173	92.5	45	16.67	122117.5	529.67	251250	13950	0.448071
350	380	173	92.5	45	16.67	125467.5	539.67	251250	13950	0.460687
270	380	173	92.5	45	16.67	98667.5	459.67	251250	13950	0.359755
272	380	173	92.5	45	16.67	99337.5	461.67	251250	13950	0.362279
356	380	173	92.5	45	16.67	127477.5	545.67	251250	13950	0.468257
370	380	173	92.5	45	16.67	132167.5	559.67	251250	13950	0.48592
275	380	173	92.5	45	16.67	100342.5	464.67	251250	13951	0.366066

Table C.5 Flexural bond strength test results for nanocellulose samples cured at the room temperature

P1 (N)	L1 (mm)	P2 (N)	L2 (mm)	t_u (mm)	P3 (N)	M (N·mm)	P (N)	S (mm^3)	Ae (mm^2)	ft (MPa)
444	380	173	92.5	45	16.67	156957.5	633.67	251250	13950	0.579282
360	380	173	92.5	45	16.67	128817.5	549.67	251250	13950	0.473304
444	380	173	92.5	45	16.67	156957.5	633.67	251250	13950	0.579282
435	380	173	92.5	45	16.67	153942.5	624.67	251250	13950	0.567927
390	380	173	92.5	45	16.67	138867.5	579.67	251250	13950	0.511153
380	380	173	92.5	45	16.67	135517.5	569.67	251250	13950	0.498537
375	380	173	92.5	45	16.67	133842.5	564.67	251250	13950	0.492228
470	380	173	92.5	45	16.67	165667.5	659.67	251250	13950	0.612085
370	380	173	92.5	45	16.67	132167.5	559.67	251250	13950	0.48592
400	380	173	92.5	45	16.67	142217.5	589.67	251250	13950	0.52377
500	380	173	92.5	45	16.67	175717.5	689.67	251250	13950	0.649934
476	380	173	92.5	45	16.67	167677.5	665.67	251250	13950	0.619655
482	380	173	92.5	45	16.67	169687.5	671.67	251250	13950	0.627225
370	380	173	92.5	45	16.67	132167.5	559.67	251250	13950	0.48592
400	380	173	92.5	45	16.67	142217.5	589.67	251250	13950	0.52377
423	380	173	92.5	45	16.67	149922.5	612.67	251250	13950	0.552787
350	380	173	92.5	45	16.67	125467.5	539.67	251250	13950	0.460687
330	380	173	92.5	45	16.67	118767.5	519.67	251250	13950	0.435454
354	380	173	92.5	45	16.67	126807.5	543.67	251250	13950	0.465734
380	380	173	92.5	45	16.67	135517.5	569.67	251250	13950	0.498537
400	380	173	92.5	45	16.67	142217.5	589.67	251250	13950	0.52377
440	380	173	92.5	45	16.67	155617.5	629.67	251250	13950	0.574235
390	380	173	92.5	45	16.67	138867.5	579.67	251250	13951	0.511156
410	380	173	92.5	45	16.67	145567.5	599.67	251250	13952	0.536392
402	380	173	92.5	45	16.67	142887.5	591.67	251250	13953	0.526302

Table C.6 Flexural bond strength test results for nanocellulose samples cured at the freezing temperature

P1 (N)	L1 (mm)	P2 (N)	L2 (mm)	t_u (mm)	P3 (N)	M (N·mm)	P (N)	S (mm^3)	Ae (mm^2)	ft (MPa)
110	380	173	92.5	45	16.67	45067.5	299.67	251250	13950	0.157891
115	380	173	92.5	45	16.67	46742.5	304.67	251250	13950	0.1642
112	380	173	92.5	45	16.67	45737.5	301.67	251250	13950	0.160415
116	380	173	92.5	45	16.67	47077.5	305.67	251250	13950	0.165461
100	380	173	92.5	45	16.67	41717.5	289.67	251250	13950	0.145275
102	380	173	92.5	45	16.67	42387.5	291.67	251250	13950	0.147798
120	380	173	92.5	45	16.67	48417.5	309.67	251250	13950	0.170508
110	380	173	92.5	45	16.67	45067.5	299.67	251250	13950	0.157891
95	380	173	92.5	45	16.67	40042.5	284.67	251250	13950	0.138967
93	380	173	92.5	45	16.67	39372.5	282.67	251250	13950	0.136443
120	380	173	92.5	45	16.67	48417.5	309.67	251250	13950	0.170508
120	380	173	92.5	45	16.67	48417.5	309.67	251250	13950	0.170508
130	380	173	92.5	45	16.67	51767.5	319.67	251250	13950	0.183124
112	380	173	92.5	45	16.67	45737.5	301.67	251250	13950	0.160415
80	380	173	92.5	45	16.67	35017.5	269.67	251250	13950	0.120042
82	380	173	92.5	45	16.67	35687.5	271.67	251250	13950	0.122565
80	380	173	92.5	45	16.67	35017.5	269.67	251250	13950	0.120042
80	380	173	92.5	45	16.67	35017.5	269.67	251250	13950	0.120042
120	380	173	92.5	45	16.67	48417.5	309.67	251250	13950	0.170508
110	380	173	92.5	45	16.67	45067.5	299.67	251250	13950	0.157891
90	380	173	92.5	45	16.67	38367.5	279.67	251250	13950	0.132658
120	380	173	92.5	45	16.67	48417.5	309.67	251250	13950	0.170508
70	380	173	92.5	45	16.67	31667.5	259.67	251250	13950	0.107425
120	380	173	92.5	45	16.67	48417.5	309.67	251250	13950	0.170508
70	380	173	92.5	45	16.67	31667.5	259.67	251250	13950	0.107425

Table C.7 Flexural bond strength test results for sodium nitrite with nanocellulose samples cured at the room temperature

P1 (N)	L1 (mm)	P2 (N)	L2 (mm)	t_u (mm)	P3 (N)	M (N·mm)	P (N)	S (mm^3)	Ae (mm^2)	ft (MPa)
490	380	173	92.5	45	16.67	172367.5	679.67	251250	13950	0.637318
450	380	173	92.5	45	16.67	158967.5	639.67	251250	13950	0.586852
400	380	173	92.5	45	16.67	142217.5	589.67	251250	13950	0.52377
500	380	173	92.5	45	16.67	175717.5	689.67	251250	13950	0.649934
400	380	173	92.5	45	16.67	142217.5	589.67	251250	13950	0.52377
400	380	173	92.5	45	16.67	142217.5	589.67	251250	13950	0.52377
400	380	173	92.5	45	16.67	142217.5	589.67	251250	13950	0.52377
480	380	173	92.5	45	16.67	169017.5	669.67	251250	13950	0.624701
400	380	173	92.5	45	16.67	142217.5	589.67	251250	13950	0.52377
430	380	173	92.5	45	16.67	152267.5	619.67	251250	13950	0.561619
400	380	173	92.5	45	16.67	142217.5	589.67	251250	13950	0.52377
370	380	173	92.5	45	16.67	132167.5	559.67	251250	13950	0.48592
380	380	173	92.5	45	16.67	135517.5	569.67	251250	13950	0.498537
400	380	173	92.5	45	16.67	142217.5	589.67	251250	13950	0.52377
500	380	173	92.5	45	16.67	175717.5	689.67	251250	13950	0.649934
480	380	173	92.5	45	16.67	169017.5	669.67	251250	13950	0.624701
390	380	173	92.5	45	16.67	138867.5	579.67	251250	13950	0.511153
375	380	173	92.5	45	16.67	133842.5	564.67	251250	13950	0.492228
360	380	173	92.5	45	16.67	128817.5	549.67	251250	13950	0.473304
350	380	173	92.5	45	16.67	125467.5	539.67	251250	13950	0.460687
370	380	173	92.5	45	16.67	132167.5	559.67	251250	13950	0.48592
400	380	173	92.5	45	16.67	142217.5	589.67	251250	13950	0.52377
360	380	173	92.5	45	16.67	128817.5	549.67	251250	13950	0.473304
390	380	173	92.5	45	16.67	138867.5	579.67	251250	13950	0.511153
420	380	173	92.5	45	16.67	148917.5	609.67	251250	13950	0.549003

Table C.8 Flexural bond strength test results for sodium nitrite with nanocellulose samples cured at the freezing temperature

P1 (N)	L1 (mm)	P2 (N)	L2 (mm)	t_u (mm)	P3 (N)	M (N·mm)	P (N)	S (mm^3)	Ae (mm^2)	ft (MPa)
370	380	173	92.5	45	16.67	132167.5	559.67	251250	13950	0.48592
380	380	173	92.5	45	16.67	135517.5	569.67	251250	13950	0.498537
450	380	173	92.5	45	16.67	158967.5	639.67	251250	13950	0.586852
400	380	173	92.5	45	16.67	142217.5	589.67	251250	13950	0.52377
400	380	173	92.5	45	16.67	142217.5	589.67	251250	13950	0.52377
500	380	173	92.5	45	16.67	175717.5	689.67	251250	13950	0.649934
320	380	173	92.5	45	16.67	115417.5	509.67	251250	13950	0.422838
380	380	173	92.5	45	16.67	135517.5	569.67	251250	13950	0.498537
440	380	173	92.5	45	16.67	155617.5	629.67	251250	13950	0.574235
420	380	173	92.5	45	16.67	148917.5	609.67	251250	13950	0.549003
430	380	173	92.5	45	16.67	152267.5	619.67	251250	13950	0.561619
440	380	173	92.5	45	16.67	155617.5	629.67	251250	13950	0.574235
500	380	173	92.5	45	16.67	175717.5	689.67	251250	13950	0.649934
450	380	173	92.5	45	16.67	158967.5	639.67	251250	13950	0.586852
380	380	173	92.5	45	16.67	135517.5	569.67	251250	13950	0.498537
320	380	173	92.5	45	16.67	115417.5	509.67	251250	13950	0.422838
320	380	173	92.5	45	16.67	115417.5	509.67	251250	13950	0.422838
360	380	173	92.5	45	16.67	128817.5	549.67	251250	13950	0.473304
330	380	173	92.5	45	16.67	118767.5	519.67	251250	13950	0.435454
400	380	173	92.5	45	16.67	142217.5	589.67	251250	13950	0.52377
370	380	173	92.5	45	16.67	132167.5	559.67	251250	13950	0.48592
390	380	173	92.5	45	16.67	138867.5	579.67	251250	13950	0.511153
340	380	173	92.5	45	16.67	122117.5	529.67	251250	13950	0.448071
330	380	173	92.5	45	16.67	118767.5	519.67	251250	13950	0.435454
350	380	173	92.5	45	16.67	125467.5	539.67	251250	13950	0.460687

Table C.9 Paired samples statistics for the control groups

		Mean	N	Std. Deviation	Std. Error Mean
Pair 1	CTR23	.471739	25	.0837258	.0167452
	CTR10	.148959	25	.0243554	.0048711

Table C.10 Paired samples correlations for the control groups

		N	Correlation	Sig.
Pair 1	CTR23 & CTR10	25	-.354	.083

Table C.11 Paired samples test for the control groups

		Paired Differences					t	df	Sig. (2-tailed)
		Mean	Std. Deviation	Std. Error Mean	95% Confidence Interval of the Difference				
					Lower	Upper			
Pair 1	CTR23 - CTR10	.3227803	.0951086	.0190217	.2835214	.3620392	16.969	24	.000

Table C.12 Paired samples statistics for the sodium nitrite groups

		Mean	N	Std. Deviation	Std. Error Mean
Pair 1	SN23	.405730	25	.0835702	.0167140
	SN10	.404266	25	.0814370	.0162874

Table C.13 Paired samples correlations for the sodium nitrite groups

		N	Correlation	Sig.
Pair 1	SN23 & SN10	25	-.260	.209

Table C.14 Paired samples test for the sodium nitrite groups

	Paired Differences					t	df	Sig. (2-tailed)
	Mean	Std. Deviation	Std. Error Mean	95% Confidence Interval of the Difference				
				Lower	Upper			
Pair 1 SN23 - SN10	.0014635	.1309892	.0261978	-.0526062	.0555332	.056	24	.956

Table C.15 Paired samples statistics for the nanocellulose groups

		Mean	N	Std. Deviation	Std. Error Mean
Pair 1	NC23	.532602	25	.0564496	.0112899
	NC10	.149312	25	.0298405	.0059681

Table C.16 Paired samples correlations for the nanocellulose groups

		N	Correlation	Sig.
Pair 1	NC23 & NC10	25	.456	.022

Table C.17 Paired samples test for the nanocellulose groups

	Paired Differences					t	df	Sig. (2-tailed)
	Mean	Std. Deviation	Std. Error Mean	95% Confidence Interval of the Difference				
				Lower	Upper			
Pair 1 NC23 - NC10	.3832896	.0504136	.0100827	.3624799	.4040993	38.015	24	.000

Table C.18 Paired samples statistics for the sodium nitrite with nanocellulose groups

		Mean	N	Std. Deviation	Std. Error Mean
Pair 1	NN23	.538405	25	.0669021	.0133804
	NN10	.512162	25	.0667522	.0133504

Table C.19 Paired samples correlations for the sodium nitrite with nanocellulose groups

		N	Correlation	Sig.
Pair 1	NN23 & NN10	25	-.138	.511

Table C.20 Paired samples test for the sodium nitrite with nanocellulose groups

	Paired Differences					t	df	Sig. (2-tailed)
	Mean	Std. Deviation	Std. Error Mean	95% Confidence Interval of the Difference				
				Lower	Upper			
Pair 1 NN23 - NN10	.0262423	.1008116	.0201623	-.0153707	.0678553	1.302	24	.205

Table C.21 Paired samples statistics for control samples cured at room temperature and sodium nitrite samples cured at freezing temperature

		Mean	N	Std. Deviation	Std. Error Mean
Pair 1	CTR23	.471739	25	.0837258	.0167452
	SN10	.404266	25	.0814370	.0162874

Table C.22 Paired samples correlations for control samples cured at room temperature and sodium nitrite samples cured at freezing temperature

		N	Correlation	Sig.
Pair 1	CTR23 & SN10	25	.068	.748

Table C.23 Paired samples test for control samples cured at room temperature and sodium nitrite samples cured at freezing temperature

	Paired Differences					t	df	Sig. (2-tailed)
				95% Confidence Interval of the Difference				
	Mean	Std. Deviation	Std. Error Mean	Lower	Upper			
Pair 1 CTR23 - SN10	.0674730	.1127772	.0225554	.0209209	.1140251	2.991	24	.006

Table C.24 Paired samples statistics for control samples cured at room temperature and sodium nitrite with nanocellulose samples cured at freezing temperature

		Mean	N	Std. Deviation	Std. Error Mean
Pair 1	CTR23	.471739	25	.0837258	.0167452
	NN10	.512162	25	.0667522	.0133504

Table C.25 Paired samples correlations for control samples cured at room temperature and sodium nitrite with nanocellulose samples cured at freezing temperature

		N	Correlation	Sig.
Pair 1	CTR23 & NN10	25	.213	.307

Table C.26 Paired samples test for control samples cured at room temperature and sodium nitrite with nanocellulose samples cured at freezing temperature

	Paired Differences					t	df	Sig. (2-tailed)
				95% Confidence Interval of the Difference				
	Mean	Std. Deviation	Std. Error Mean	Lower	Upper			
Pair 1 CTR23 - NN10	-4.0423114E-2	.0953182	.0190636	-.0797685	-.0010777	-2.120	24	.044

APPENDIX D – ASTM C140 ABSORPTION TEST RESULTS

Five brick specimens from each pallet were chosen randomly to perform the water absorption test. The received mass of each specimen was recorded in kg as W_r. Then, the test specimens were immersed in water at room temperature of 25±2°C for 24 hours. After 24 hours of immersion, the specimens were weighed while suspended by the metal wire while they were completely submerged in water and the immersed mass was recorded in kg as W_i. Subsequently, bricks were removed from the water and drained for 60±5 s, then they were weighed and their mass recorded as W_s. After that, all specimens were dried in the ventilated dry oven located in the Geotechnical Engineering Lab at 105°C for 24 hours, after which they were weighed and mass recorded as W_d. Detailed results are presented in Table D.1.

Table D.1 ASTM C140 absorption test results

Sample	W_r **(kg)**	W_i **(kg)**	W_s **(kg)**	W_d **(kg)**	**Absorption kg/m^3**	**Absorption%**
1-1	1.7060	0.970	1.753	1.658	121.258	5.7
1-2	1.7395	0.980	1.771	1.673	123.893	5.9
1-3	1.7359	0.990	1.769	1.673	122.919	5.7
1-4	1.6989	0.950	1.738	1.638	126.903	6.1
1-5	1.7513	0.990	1.787	1.683	130.982	6.2
2-1	1.7130	0.964	1.748	1.660	112.245	5.3
2-2	1.6780	0.943	1.723	1.636	111.538	5.3
2-3	1.6890	0.937	1.731	1.643	110.831	5.4
2-4	1.6490	0.923	1.696	1.608	113.842	5.5
2-5	1.6500	0.923	1.693	1.610	107.792	5.2

APPENDIX E – INITIAL RATE OF ABSORPTION TEST RESULTS

The IRA for the bricks was measured using bricks that had been oven-dried for 24 hours at 105°C using the ventilated dry oven located in the Geotechnical Engineering Lab. Five full-size specimens were tested per pallet as required by ASTM C67. The results were reported in grams of water gained per cm^2 when the brick was soaked in 3 mm of water for 1 min. Detailed results are presented in Table E.1.

Table E.1 Initial rate of absorption test results

Sample	Length (cm)	Width (cm)	Void fraction	Dry Weight (g)	Wet Weight (g)	IRA ($g/cm^2/min$)	Average IRA
IR1-1	19.05	9.065	0.1883	1580	1584	0.0285	0.0328
IR1-2	19.05	9.038	0.1883	1640	1645	0.0357	
IR1-3	19.05	9.034	0.1883	1641	1645	0.0286	
IR1-4	19.05	9.038	0.1883	1627	1632	0.0357	
IR1-5	19.05	9.050	0.1883	1625	1630	0.0357	
IR2-1	18.95	9.000	0.1883	1709	1713	0.0289	0.0289
IR2-2	18.95	8.950	0.1883	1630	1634	0.0291	
IR2-3	19.00	8.950	0.1883	1717	1721	0.0290	
IR2-4	19.00	8.950	0.1883	1730	1734	0.0290	
IR2-5	19.00	9.000	0.1883	1711	1715	0.0288	

APPENDIX F – COMPRESSIVE STRENGTH OF STANDARD CONCRETE MASONRY BRICKS

Seven standard concrete bricks were randomly selected from each pallet and tested in compression as described in Chapter 3. using a 200-tonne capacity Amsler Beam Bender machine in the structural engineering lab at the University of Saskatchewan. The brick surface dimensions were measured by the use of a digital caliper. The calculation of the compressive strength was performed by dividing the ultimate load by the net area of the brick. Table F.1 presents the compressive strength of the standard concrete bricks.

Table F.1 Compressive strength of standard concrete masonry bricks

Pallet no.	Sample no.	Area (mm^2)	Ultimate Load (kN)	Compressive Strength (MPa)	Average (MPa)	Standard deviation (MPa)	COV (=St. Deviation /Average) (%)
First Pallet	1	13950	590	42.3	39.3	3.6	9.1
	2	13950	590	42.3			
	3	13950	520	37.3			
	4	13950	570	40.9			
	5	13950	571	40.9			
	6	13950	450	32.3			
	7	13950	550	39.4			
Second Pallet	1	13950	565	40.5	39.5	3.3	8.3
	2	13950	558	40.0			
	3	13950	453	32.5			
	4	13950	552	39.6			
	5	13950	570	40.9			
	6	13950	555	39.8			
	7	13950	600	43.0			